REPORT SERIES IN AEROSOL SCIENCE
N:o 223 (2019)

ON OBSERVATIONS OF NEWLY FORMED NANOPARTICLES: THEIR DETECTION, CHARACTERIZATION AND ABUNDANCE IN VARIOUS ENVIRONMENTS

LAURI AHONEN

Institute for Atmospheric and Earth System Research / Physics
Faculty of Science
University of Helsinki
Helsinki, Finland

Academic dissertation

To be presented, with the permission of the Faculty of Science of the University of Helsinki, for public criticism in Exactum auditorium B123, Pietari Kalmin katu 5, on November 8th, 2019, at 14 o'clock.

Helsinki 2019

Author's Address: INAR – Institute for Atmospheric and Earth
P.O Box 64
00014 University of Helsinki
lauri.r.ahonen@helsinki.fi

Supervisors: Professor Tuukka Petäjä Ph.D.
Institute for Atmospheric and Earth System Research / Physics
Faculty of Science, University of Helsinki, Finland

Academician, Professor Markku Kulmala Ph.D.
Institute for Atmospheric and Earth System Research / Physics
Faculty of Science, University of Helsinki, Finland

Assoc. Prof. Katrianne Lehtipalo Ph.D.
Institute for Atmospheric and Earth System Research / Physics
Faculty of Science, University of Helsinki, Finland
Finnish Meteorological Institute

Docent Juha Kangasluoma Ph.D.
Institute for Atmospheric and Earth System Research / Physics
Faculty of Science, University of Helsinki, Finland

Reviewers: Professor Jian Wang, Ph.D.
Center for Aerosol Science and Engineering, Department of Energy Environmental and Chemical Engineering, Washington University in St. Louis, Missouri, USA

Docent Jorma Joutsensaari, Ph.D.
Department of Applied Physics
University of Eastern Finland, Kuopio, Finland

Opponent: Assoc. Prof. Ph.D. Adam Kristensson
Division of Nuclear Physics
Lund University

ISBN 978-952-7276-28-0 (printed version)
ISSN 0784-3496
Helsinki 2019
Unigrafia Oy

ISBN 978-952-7276-29-7 (pdf version)
http://www.atm.helsinki.fi/FAAR
Helsinki 2019

Acknowledgements

The research for this thesis was carried out in the Institute for Atmospheric and Earth System Research (INAR), Department of Physics of the University of Helsinki and Department of Mechanical Engineering of the University of Minnesota. I would like to thank all the institutions for providing the instruments and the infrastructure making the research possible. I am grateful for the Prof. Markku Kulmala, the head of the institute for all the opportunities in the group, and the atmosphere and working culture you have created. I would like to thank all my co-workers and co-authors. A special thanks for professor Jian Wang and Docent Jorma Joutsensaari for reviewing this thesis.

I am grateful for all my supervisors for giving the support and guidance when it was needed. I would like to thank prof. Tuukka Petäjä for being a wealth of knowledge on aerosol instrumentation. I am also thankful for the valuable advices while preparing the thesis, especially at final steps of process. I would like to thank Assoc. Prof. Katrianne Lehtipalo for the guidance, especially in the process of writing scientific articles. Conversations with person having such an eye for both technical and scientific aspects the of discipline has been reassuring and confidence-inspiring. I am thankful for Juha Kangasluoma for all the hands on the guidance in the laboratory since the beginning, and for the can-do attitude that you have been expressing.

I would like to thank Prof. Chris Hogan for the opportunity to visit his research group and the entire group for making me feel welcome while being there. I am grateful for all the expertise that was shared with me, without withholding any knowledge. It was a great learning period broadening the scope of my expertise, building on top of work that I had already practiced here in Helsinki. I also would like to express my gratitude for prof. Hanna Vehkamäki for giving the chance to do this research visit abroad.

I would like to thank the technical staff here in Helsinki and Hyytiälä for a good cooperation with setting up and maintaining the instruments, as well as for the patience with the somewhat temperamental devices. A special thanks for Frans Korhonen and Erkki Siivola for all the hardware and software produced for the measurement. These were extensively used in many of studies included in the thesis.

I would like to thank my office mates in B407 and B414 for all the small chats in the midst of the day lightening up work and giving much needed breaks. Also, for the informal events lifting the spirits.

I am also grateful for my friends outside the working community. It has been refreshing and recovering to have discussion and activities that are not in any way related to the ongoing work.

I am thankful for my family for the support and keeping my feet tightly on the ground. I am thankful for my Anu being there with me and being understanding during the process. It has been important do this with someone who understands what kind of thoughts there are going on during this venture.

On observations of newly formed nanoparticles: their detection, characterization and abundance in various environments

Lauri Reino Antero Ahonen
University of Helsinki, 2019

Abstract
New particle formation (NPF) is a dominant source for atmospheric aerosol particles in terms of their number concentration, and a major contributor to the number of cloud condensation nuclei globally. Atmospheric aerosol particles have impact on Earth's climate *via* direct and indirect effects. In addition to climate, aerosol particles have impact on human health. In polluted environments, airborne pollutants, especially particulate matter, shorten the lifetime expectancy by several years. Understanding the processes of NPF is in a key role, for example, while identifying the most effective acts to improve the air quality in megacities or assessing the role of anthropogenic emissions in climate change.

A NPF event consists of formation of molecular clusters and their subsequent growth into larger particle sizes by condensable vapors and/or coagulation In order to quantify NPF events, measurements of particle number size distribution close to the size where gas-to-particle conversion takes place are necessary. The gas-to-particle conversion takes place in the 1-2 nm size range, where there exist electrically charged and neutral molecular clusters. On one hand, in most of the environments such clusters are present also in the absence of NPF events. The growth of the small clusters to the 2-3 nm size range is, on the other hand, indicative of a NPF event. In this thesis, we gather knowledge on the concentration of sub-3 nm aerosol particles by conducting both long-term and campaign-like measurements with particle size magnifier (PSM; Airmodus Ltd.). Our results were compared with the other available PSM data, from sites around the world, and presented in compilation study. In all the sites the sub-3 nm particle concentration had a daytime maximum. Generally, the highest concentrations were observed at the sites with the highest anthropogenic influence. In this thesis, we also conducted a campaign to observe particle formation in a cleanroom environment, where PSM was used for the first time to monitor concentration of nanoparticles in such an environment. The results showed that sub-2 nm clusters were observed to be always present in this clean room in relatively small concentrations. Short periods of high concentrations were observed during active manufacturing processes in the clean room.

Instrumental development was one important aspect of this thesis. We experimented with the possibility of using two commercial condensation particle counters (CPCs), with nominal lower limit close to 10 nm, for the detection of sub-3 nm particles. Optimized operating temperatures and flow rates were tested in laboratory conditions and by using simulation tools. We showed that commercially-available CPCs can be optimized down to sub-3 nm detection. In addition, a differential mobility particle sizer (DMPS) was specially built to measure particle number size distributions in the sub-10 nm size range using PSM and half-mini differential mobility analyzer (DMA). Due to the improved overall transmission of our system, the counting uncertainty compared to a harmonized DMPS was reduced to a half in the sub-10 nm size range.

An ion mobility-mass spectrometry was utilized to investigate the structures and hydration of iodine pentoxide iodic acid clusters, similar to ones observed during coastal nucleation events. The number of water molecules in hydrated clusters was sufficient to convert iodine pentoxide into iodic acid but the water sorption beyond this amount was limited.

Keywords: sub-3 nm, particle size magnifier, iodine, particle counter, DMA

Contents

List of publications

This thesis consists of an introductory review, followed by five research articles. In the introductory part, the papers are cited according to their roman numerals. **Paper II** is reprinted under the Creative Commons license, **Paper I** and **IV** with permission from Taylor & Francis and **Paper V** with a permission of American Chemical Society. Paper **III** is reprinted with a permission from Elsevier.

I Kangasluoma, J., Ahonen, L., Attoui, M., Vuollekoski, H., Kulmala, M., and Petäjä, T. (2015). Sub-3 nm particle detection with commercial TSI 3772 and Airmodus A20 fine Condensation Particle Counters. Aerosol Science and Technology, 49(8), 674-681. doi:10.1080/02786826.2015.105848

II Kontkanen, J., Lehtipalo, K., Ahonen, L., Kangasluoma, J., Manninen, H. E., Hakala, J., Rose, C., Sellegri, K., Xiao, S., Wang, L., Qi, X., Nie, W., Ding, A., Yu, H., Lee, S., Kerminen, V.-M., Petäjä, T., and Kulmala, M. (2017). Measurements of sub-3 nm particles using a particle size magnifier in different environments: from clean mountain top to polluted megacities. Atmospheric Chemistry and Physics, 17(3), 2163-2187. doi:10.5194/acp-17-2163-2017

III Kangasluoma, J., Ahonen, L. R., Laurila, T. M., Cai, R., Enroth, J., Mazon, S. B., Korhonen, F., Aalto, P. P., Kulmala, M., Attoui, M., and Petäjä, T. (2018). Laboratory verification of a new high flow differential mobility particle sizer, and field measurements in Hyytiälä. Journal of Aerosol Science, 124, 1-9. doi:10.1016/j.jaerosci.2018.06.009

IV Ahonen, L. R., Kangasluoma, J., Lammi, J., Lehtipalo, K., Hämeri, K., Petäjä, T., and Kulmala, M. (2017). First measurements of the number size distribution of 1 – 2 nm aerosol particles released from manufacturing processes in a cleanroom environment. Aerosol Science and Technology, 51(6). doi:10.1080/02786826.2017.1292347

V Ahonen, L., Li, C., Kubečka, J., Iyer, S., Vehkamäki, H., Petäjä, T., Kulmala, M., & Hogan Jr, C. J. (2019). Ion mobility-mass spectrometry of iodine pentoxide–iodic acid hybrid cluster anions in dry and humidified atmospheres. The Journal of Physical Chemistry Letters, 1935-1941. doi:10.1021/acs.jpclett.9b00453

Abbreviations and nomenclature

		unit
A10	Particle size magnifier, Airmodus Ltd.	
A11	nCNC; A20 CPC and A11 PSM	
A20	CPC; Airmodus Ltd.	
ABC	Artificial bee colony	
AIS	Air ion spectrometer	
API	Atmospheric pressure interface	
CPC	Condensation particle counter	
CSS	collision cross section	($Å^2$)
DFT	Density functional theory	
DHSS	Diffusive hard sphere scattering	
DMA	Differential mobility analyzer	
DMA-MS	Differential mobility analysis mass spectrometry	
DMPS	Differential mobility particle sizer	
dp_{50}	cut-off diameter	(nm)
EHSS	Elastic hard sphere scattering	
GR	Growth rate	(nm/h)
IMoS	Ion spectrometry suite	
J_{dp}	Formation rate at size d_p	($cm^{-3}s^{-1}$)
MS	mass spectrometer	
NAIS	Neutral cluster and Air Ion Spectrometer	
PSM	Particle Size Magnifier	
Q_a	Aerosol sample flowrate in the DMA	(l/min)
Q_{act}	activation flow in PSM	(l/min)
Q_{sh}	Volumetric flowrate of sheath air in the DMA	(l/min)
R	Resolving power of the analyzer, i.e., resolution	
TOF	time-of-flight	

1 Introduction

An aerosol is an umbrella term covering several concepts that may be more familiar to us. For example, mist, clouds, fog, dust and smoke, all of them are aerosols. By definition, aerosol is a mixture of liquid or solid particles suspended in a gas medium. Aerosol particles may be formed in many processes such as abrasion, combustion, resuspension and photochemically, and even biological entities like viruses, fungal spores and pollen are considered aerosol particles. Due to their diverse origin aerosol particles can vary greatly in their shape, size, concentration and chemical composition but they are practically all the time present in the surrounding air.

The size of the particles spans approximately from 1 nm to 10-100 μm. The smallest aerosol particles approach the size of surrounding gas molecules containing only a few molecules and they are sometimes referred as molecular clusters. For atmospheric aerosol particles, there is a division into primary and secondary particles which both have natural and anthropogenic sources. Primary particles are released/emitted directly in particle phase (liquid or solid), whereas secondary particles are formed in the atmosphere from the reaction products of gaseous emissions *via* gas-to-particle conversion. Term nucleation might also be used for the formation of secondary aerosol particles, but it has more specific meaning as a process including energy barrier (Vehkamäki and Riipinen, 2012). A new particle formation (NPF) process includes the formation of molecular clusters and their subsequent growth into larger aerosol particles (Kulmala and Kerminen, 2008; Kulmala et al., 2014). It has been observed to be a global phenomenon and to occur in almost all kinds of locations where measurements have been performed (Kulmala et al., 2004b; Nieminen et al., 2018).

Aerosol particles have significant impact on our planet's climate directly and indirectly (Boucher et al., 2013), and further via different feedback processes (e.g. Kulmala et al., 2004a). As an example, they have an important role in the formation of clouds (e.g. Pruppacher, 2010) where, outside the most extreme conditions, droplets require a seed particle in order to be formed. Aerosol particles that are large enough in diameter, around 100 nm, can act as a seed for cloud droplets and are called Cloud Condensation Nuclei (CCN). Particles can also act as an ice nucleus in ice clouds. The number concentration of CCNs influences the Earth's radiation balance by changing the cloud reflectivity for the shortwave radiation, termed the albedo effect (Twomey et al., 1984), as well as the life time of clouds (Albrecht, 1989). In addition to aerosol-cloud interactions, aerosol particles interact directly with the sun light by scattering back part of the incoming light. The total radiative forcing from the atmospheric aerosol particles is composed of these aerosol-radiation interactions and aerosol-cloud interactions, both of which still contain a number of uncertainties (Boucher et al., 2013). Based on simulations, atmospheric new particle formation has a strong influence on the climate forcing (Wang and Penner, 2009; Makkonen et al., 2012), since many of the atmospheric aerosol particles originate from atmospheric new particle formation. During a NPF event newly formed particles can grow to CCN-sized particles and this growth can take place during one day (Kulmala, 2003), thus contributing to the CCN

budget (Kulmala et al., 2004b). The importance of NPF varies between different types of environments, but it has been estimated using large-scale models that the majority of atmospheric aerosol particles in terms of their total number concentration (Spracklen et al., 2006; Yu and Luo, 2009) and around half of the global CCN budget (e.g. Merikanto et al., 2009) originate from NPF.

To understand the process of atmospheric new particle formation, it is important to be able to directly measure newly formed particles, as well as their precursors, in the size range where gas-to-particle conversion takes place (e.g. Kulmala et al., 2012; Kulmala et al., 2013). There are several methods for the detection and sizing of aerosol particles based on their different properties, such as inertia, aerodynamics, movement in medium and interaction with electromagnetic radiation (see e.g. Kulkarni et al., 2011). However, only a handful of these methods are applicable for ultrafine particles, i.e. particles with diameters smaller than 100 nm, whereas for sub-3 nm particles there are even fewer methods and none of those are without some limitations. The 1 nm to 3 nm size range, in which NPF occurs, lies between particles with bulk properties and non-sticky gas molecules and has proven to be difficult to measure. Ions, molecular clusters, and large molecules coexist in this size range (e.g. McMurry et al., 2011). Ion spectrometers were the first instruments to cover this size range (Tammet, 2006; Mirme et al., 2007) and later on the ion spectrometers were further developed to measure neutral clusters as well (Kulmala et al., 2007). Instruments are based on a mobility analyzer (Knutson and Whitby, 1975) and an electrostatic detector (e.g. Flagan, 1998). Their drawback is the relatively high limit of detection due to their detector. Other approach has been modifying and developing condensation particles counters that had a lower limit of 3 nm for a long time, which was accomplished with the original ultrafine condensation particle counter (Stolzenburg and McMurry, 1991).

The instrumental development during the past decade has provided means for a direct measurement of neutral clusters and molecules in addition to charged particles (Manninen, 2009; Junninen et al., 2010; Jiang et al., 2011; Vanhanen et al., 2011; Jokinen et al., 2012; C. Kuang et al., 2012). Now there is, for example, a possibility to study the role of neutral clusters in the process of atmospheric new particle formation. In spite of this, there are still many improvements to be made on implementing these methods in a robust and reproducible way. There is an increasing amount of ambient data on NPF measured using instruments capable of detecting sub-3 nm aerosol particles, both in remote sites as well as in sites with a strong anthropogenic influence (Mirme et al., 2010; Rose et al., 2015; Xiao et al., 2015; Bianchi et al., 2016; Debevec et al., 2018; Yan et al., 2018; Chu et al., 2019; Leino et al., 2019).

Iodine-containing compounds from biogenic sources are recognized to be a source of secondary particles in coastal regions (Hoffmann et al., 2001; Mäkelä et al., 2002; O'Dowd et al., 2002; O'Dowd and Hoffmann, 2005; McFiggans et al., 2010). These marine aerosol particles has been proposed to consist of iodic acid (Sunder and Vikis, 1987) and iodine pentoxide (Saiz-Lopez and Plane, 2004). Sipilä et al. (2016) showed a direct molecular evidence that sequential addition of iodic acid molecules could explain the rapid NPF observed in coastal areas. In other environments, such as boreal forest or urban areas, the NPF process

is more complex due to more diverse emissions (Kulmala et al., 2016). In this kind of multicomponent system, some of the compounds have synergies enhancing the particle formation while others may suppress it (Lehtipalo et al., 2018), making the system nonlinear in nature. In order to understand this kind of system, having reliable experimental data is vital.

Nanoparticles have also negative health effects when entering the human body (e.g. Alenius et al., 2014). Every day a vast amount of air is passing through our respiratory system and some of the aerosol particles that we inhale are deposited along the respiratory track. These inhaled particles, both outdoors and indoors, are a threat for the human health due to the harmful materials in these particles and due to the potentially toxic nature of nanoparticles inside the body (Oberdörster et al., 2004). Not least for this, the measurement of nanometer sized clusters has gained interests also outside the new particle formation community. Emerging awareness of the potential toxicity of nanoclusters has raised an interest in measuring sub-3 nm particles in the context of urban air quality as well as in emission assessment. There has been emission studies, including sub-3 nm particle measurements in a laboratory conditions (Alanen et al., 2015; Alanen et al., 2017) and in urban roads with a mobile platform (Rönkkö et al., 2017). For example, Rönkkö et al. (2017) showed that traffic is a major source for the sub-3 nm particles, and in urban areas there can be high concentrations of molecular clusters also in the absence of new particle formation.

This thesis comprises work for improving the instrumentation and optimizing their operation for the detection of newly formed aerosol particles (**Paper I** and **III**) as well as performing measurements. We measured sub-3 nm particle number concentrations in both remote (Hyytiälä) and urban (Helsinki) site using a particle size magnifier (Vanhanen et al., 2011), and compared these results with other data sets from around the world (**Paper II**). In addition, we performed a measurement campaign to investigate the existence of sub-2 nm particles and their concentrations in a facility with clean rooms that is also an occupational environment (**Paper IV**). In **Paper V** we focused on studying the physical properties of iodine pentoxide iodic acid clusters such as their structure and mobility and collision cross section together with their hydration, with the help of computational methods.

The aims / objectives of this thesis are:

(i) To explore the properties of iodine-containing clusters in the sub-3 nm size range, including their size, composition and structure, and to examine adsorption of water molecules onto these clusters, which can be pertinent either to their detection or to the mechanisms behind new particle formation.

(ii) To gain information on vapor-to-aerosol particle transformation in the atmosphere and in the laboratory while developing methods and practices for measuring sub-3 nm aerosol particle concentration.

(iii) Performing sub-3 nm particle concentration measurements with particle size magnifiers using the current best knowledge and know-how available.

(iv) To broaden the applications of the particle size magnifier from atmospheric studies to other uses, such as to characterization of nanocluster emissions during a manufacturing process.

2 Experimental methods / Instrumentation

Several instruments and methods were used in the thesis. The most important ones are introduced here, and their operation is explained in a general level. At the beginning, there are a few concepts explained to set the basis and make following sections easier to follow.

Saturation vapor pressure and supersaturation

A *saturation vapor pressure* describes the vapor pressure over a flat liquid surface in an equilibrium, where there is no net flux of molecules through the surface. On average, molecules escape from liquid the same rate as they condense back. The saturation vapor pressure $p_{i,s}(T, x_i)$ for a compound i is a function of temperature T and molar fraction x_i of the compound in the liquid (see e.g. Vehkamäki, 2006). A *saturation ratio* is defined as ratio of partial pressure p_i and the saturation vapor pressure.

$$S_i = \frac{p_i}{p_{i,\mathrm{sat}}(x_i, T)}. \tag{1}$$

When the saturation ratio exceeds unity, the vapor is *supersaturated* and respectively *subsaturated* below this.

Over a curved surface the vapor pressure $p_{d_p,\mathrm{sat}}$ required for equilibrium is higher than over a flat surface $p_{\infty,\mathrm{sat}}$, a phenomenon referred as *Kelvin effect*. The equation describing the ratio of saturation vapor pressure over curved surface to a flat surface, is called *Kelvin equation*. The ratio is a function of droplet diameter d_p, temperature T and the liquid properties.

$$\frac{p_{d_p,\mathrm{sat}}}{p_{\infty,\mathrm{sat}}} = \exp\left(\frac{4v\sigma_{\mathrm{g,l}}}{k_B T d_{\mathrm{p}}}\right) \tag{2}$$

In the equation, $\sigma_{\mathrm{g,l}}$ is the surface tension in the gas-to-liquid surface, v is the molecular volume of the liquid and $k_B$is the Boltzmann constant (Pruppacher, 2010).

When the vapor is supersaturated and there is no existing liquid surface to condense onto, the vapor can stay in metastable state due to the energy required in the formation of gas-to-liquid surface. This energy barrier is inhibiting the formation of stable molecular clusters that are more likely to grow than shrink away. *Nucleation* is an initial stage in the phase transition, the formation of small clusters or embryos of stable phase, inside the metastable mother phase (e.g. Vehkamäki, 2006). *Homogenous nucleation* refers to the formation of stable clusters in the absence of an existing surface. *Heterogenous nucleation*, in turn, refers to the process in the presence of existing surface, e.g. aerosol particles, on top of which clusters are formed. Heterogenous nucleation is energetically more favorable and requires smaller supersaturation to take place (e.g. Fletcher, 1958).

2.1 Condensation Particle Counter

A condensation particle counter (CPC) is an instrument that measures the particle number concentration by growing aerosol particles with a supersaturated vapor and by counting the grown particles with an optical detector. The process of heterogenous nucleation and irreversible growth into droplets in the condenser of CPC is referred as *activation* in this context, analogous to the activation in the Köhler theory for cloud droplets (Köhler, 1936).

CPCs are the most common type of an instrument for the measurement of ultrafine aerosol particle number concentration (McMurry, 2000). They are used in variety of applications due to their sensitivity, i.e. the low limit of detection (LOD) compared to electrostatic methods, and the wide size and concentration range over which they can operate. Additionally, CPCs are used as a stand-alone instrument and a part of combined measurement systems such as mobility size spectrometers (Wiedensohler et al., 2012). The concentration range that a CPC can measure is governed by the undiluted sample flow rate passing through instrument optics as well as other instrumental factors such as the signal acquisition hardware. The lower end of concentration range is limited by decreasing counting statistics and the upper end by too frequently arriving particles coinciding in the counting region. When the concentration is small enough for the CPC to resolve pulses from the individual particles, it is operating in a *single counting mode*. With a proper calibration, CPCs can measure higher concentrations using total scattering/attenuation correction or similar means to expand the concentration range upwards (Zhang and Liu, 1990). *Live-time counting* is also used in CPCs to correct counting error from the coincidence. A live-time is the time when instrument can actually trigger from incoming particles. The live-time is obtained by removing the accumulated *dead-time* from the integration time. A dead-time is the time when signal is above triggering level, and the instrument is not ready to count additional particles. In the *cloud* or *photometric mode*, where the concentration is determined from light extinction, the measured concentration is not as accurate and instrument is more sensitive to factors such as accumulation of contaminants in the optics, which may cause the calibration to drift. CPCs were used in **papers I**, **II**, **III**, and **IV**.

The main characterizing parameter of the CPC is called cut-off diameter dp50 and it is defined to be the diameter resulting in 50% detection efficiency (Zhang and Liu, 1990) The total detection efficiency η_{CPC} is governed by multiple processes and, similar way as in Stolzenburg and McMurry (1991), it can be expressed in a factorized form. This yields a following equation

$$\eta_{\mathrm{CPC}}(d_{\mathrm{p}}) = \eta_{\mathrm{sam}}(d_{\mathrm{p}}) \cdot \eta_{\mathrm{act}}(d_{\mathrm{p}}) \cdot \eta_{\mathrm{det}}(d_{\mathrm{p}}), \tag{3}$$

were d_{p} is particle diameter, η_{sam} is the penetration efficiency for particles to pass from the inlet to the detector. η_{act} is the probability that particle entering to the condenser are activated/grown and η_{det} the probability that grown particles are detected in the optical system. All the factors are size dependent and decreases towards smaller diameter. The cut-off diameter and the steepness of detection efficiency curve are affected by all of these. For large

particles with diameters larger than about 1 micrometer, the detection efficiency again starts to decrease (Yli-Ojanperä et al., 2012; Järvinen et al., 2018) as large aerosol particles start to have considerable inertial losses (e.g. Pui et al., 1987).

A common way to produce super saturation in the CPC is *via* diffusion in a laminar flow. In this type of design, the sample air is passed through a saturator which have surfaces that are wetted with a working fluid, and often heated to increase the vapor concentration. Here, the sample air attains a vapor concentration close to a saturation vapor pressure. After the saturator, there is a condenser at a different temperature, typically in a lower temperature, creating a gradient both in the vapor concentration and temperature. This induces a diffusion of mass and heat and depending on the differences in the thermal and mass diffusivities, one or the other moves quicker. Depending on these rates, the supersaturation is achieved either by heating or cooling the flow (Zhang and Liu, 1990; Hering and Stolzenburg, 2005). In a common use, the temperature difference and the selected working fluid governs the super-saturation, but also the carrier gas affects the transfer rates. Normally the carrier gas is air or nitrogen which have very similar properties considering heat and mass transfer but the carrier gas can also be used to change the performance of the CPC by using different back-ground gas (Thomas et al., 2018).

A variation of the diffusion-based CPC has a sheathed design, in which a separate flow is saturated and taken into condenser forming most of the flow in the condenser (Wilson et al., 1983). The actual sample is taken directly into the condenser where it is introduced at the center line of the stream. This increases the sampling efficiency $\eta_{\mathrm{sam}}(dp)$ but introduces an additional dilution since most of the flow through the optics consist a particle free sheath air. The sheathed design is used for example in the ultrafine CPC (Stolzenburg and McMurry, 1991) and its successors. Some of these approaches are depicted in the Figure 1.

Alternatively, the supersaturation can be induced, e.g. by adiabatic expansion (Aitken, 1888; Kurten et al., 2005) or mixing (Kousaka et al., 1982). These approaches are not as widely used but have their own advantages. The mixing method allows fast changes to supersaturation due to the fast response in supersaturation upon changes in the flow rates while the expansion method yields well defined supersaturation values with a downside of discontinuous sample flow (for more information see e.g. Cheng, 2011).

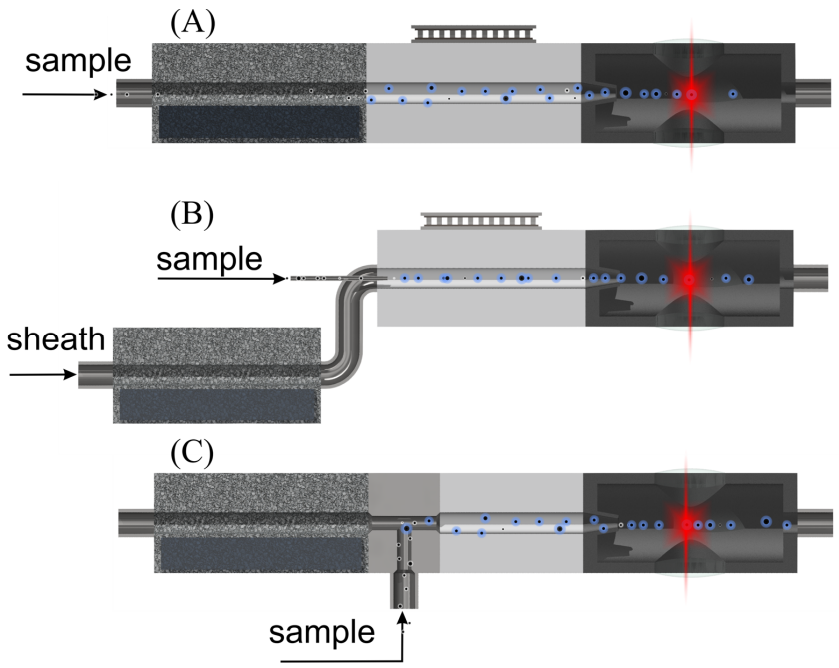

Figure 1. A Schematic figure of differences in the CPC designs: (A) the Laminar flow diffusion type, (B) a sheathed CPC and (C) a mixing type CPC.

2.2 Particle size magnifier (PSM)

The growth of aerosol particles can be accommodated in more than one stage. An additional unit placed in front of the CPC providing an initial growth stage is often called particle size magnifier, PSM (Fuchs and Sutugin, 1965; Okuyama et al., 1984), or sometimes referred as booster (Iida et al., 2009). The purpose of the additional stage is to increase the activation efficiency of the combined system and to expand the capability of the CPC towards smaller particles. A higher activation efficiency can be accomplished in a combined instrument with a likely drawback of larger internal losses and more complex system.

A10 PSM (Airmodus Ltd.) is a continuous flow mixing type particle size magnifier using diethylene glycol (DEG) as the working fluid. The sample air is mixed turbulently with heated and saturated flow and the subsequently cooled down in a growth tube, i.e., condenser (Figure 2). Particles that activate in the PSM grow up to a size around 90 nm (Vanhanen et al., 2011). The instrument is based on prior work with particle size magnifiers (Okuyama et al., 1984; Gamero-Castaño and Fernández de la Mora, 2000; Sgro and Fernández de la Mora, 2004). The construction of this PSM is very similar to a mixing type CPC but the supersaturation can be achieved either *via* adiabatic mixing and/or laminar flow diffusion depending on the configuration of the instrument (Kangasluoma et al., 2016b). Together with Airmodus A20 CPC it is called A11 nCNC but for simplicity combined instrument is referred now in the text as the PSM. The PSM is able to detect particles starting from around

1 nm diameter (Vanhanen et al., 2011). This commercial PSM has been stable and robust enough for field deployments even in quite challenging locations, which is its main merit compared to the previous designs. The PSM is used in **papers I, II, III** and **IV.** Recently there have been other developments with particle size magnifiers, such as a commercial DEG based Nano Enhancer by TSI (Kangasluoma et al., 2017) and a miniaturized design based on microelectromechanical systems MEMS (Kwon et al., 2018).

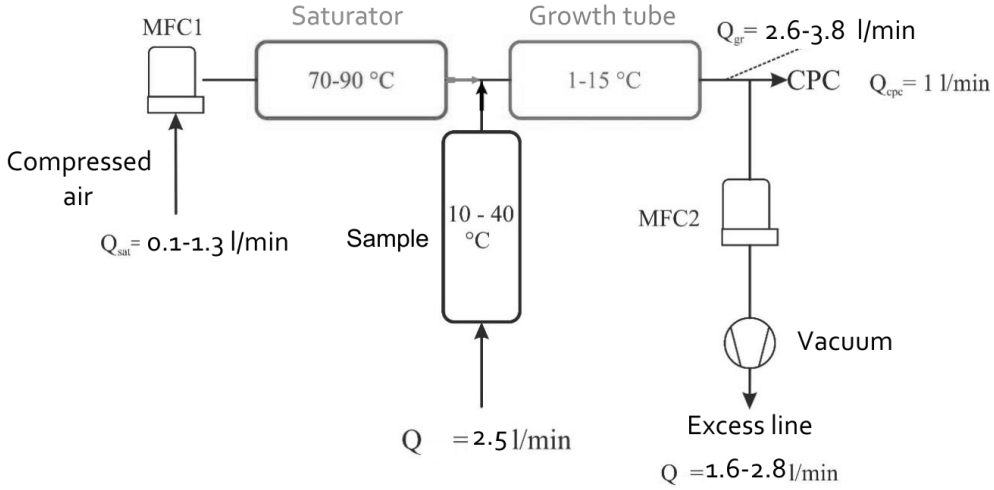

Figure 2. Schematic figure of the PSM as a flow diagram. Flows in the PSM are controlled by two mass flow controllers and the CPC.

The volumetric flow rate through the saturator is referred simply as the *saturator flow*. Other flows and components of the PSM are named in Figure 2. PSM can be used in a mode where saturator flow is ramped up and down periodically, referred as a *scanning mode*, differentiating from *fixed mode* with constant saturator flow. Ramping the saturator flow results in a fast response in the supersaturation of diethylene glycol and changes the smallest detectable particle size accordingly. When the relationship between the saturator flowrate and the smallest detectable particle diameter is available via calibrations, a number size distribution can be inverted from measurements (Lehtipalo et al., 2014; Cai et al., 2018b). The particle number size distribution can be measured in the size range where the detection efficiency is dependent on the saturation flow rate. This size range is roughly between 1 and 3 nm, but it is dependent on the specific instrumental settings. For example, if the settings are optimized for the smallest clusters, the upper size limit might be smaller, and conversely if the settings are optimized for larger clusters. The detection efficiency of the PSM is affected by the particle composition and the charge state. Charged particles are activated with smaller saturator flows compared to a neutral cluster with similar diameter (Kangasluoma et al., 2016c). Clusters formed from the oxidation of monoterpenes are activated with higher saturator flows compared to clusters consisting of e.g. ammonium bisulfates or tungsten oxides (Kangasluoma et al., 2014).

2.2.1 Calibration

The calibration of the instrument is one of the first things to consider when preparing measurements. Operations to measure the PSM's cut-off diameter as a function of saturator flow and the maximum detection efficiency as a function of particle size is referred to as calibration in this context, even though these quantities are not connected to traceable standards. PSM can be calibrated with particles produced by variety of different methods (e.g. Kangasluoma et al., 2013; 2014). The selection of a calibration method is important as it is shown that the activation of the particles in the PSM is affected by the chemical composition (and charge state) of the particles (Jiang et al., 2011; Kangasluoma et al., 2014; Kangasluoma et al., 2016c) which is the case for other condensation-based instruments as well (e.g. O'Dowd et al., 2004).

When preparing the PSM for the field measurements, decision on the calibration approach needs to be made because there are at least two approaches. Firstly, when there exists a knowledge on the expected particle composition, instrument can be calibrated using particles of similar chemical composition. The knowledge may come from complementary measurements or/and knowledge of their precursors. In addition to this information, calibration requires a reliable and reproducible method to produce such particles with large enough concentration. For some chemical systems, such as the one including oxidation products of monoterpenes, this can be challenging due to the flow tube setup which can be tricky to operate. The other approach is to use the same standard procedure for all the instruments and be more focused on the comparability of instruments. This is usually the only way to go when there is no knowledge on the particle properties or when the studied chemical system varies a lot like often in ambient measurements. For our permanent measurements at SMEAR (I)*, II and III (**Paper II**), this approach was used. In the case of the measurements during the cleanroom campaign (**Paper IV**), we did a site-specific calibration since the conditions were more controlled and we had a good idea on the possible precursors (This will be explained in more detail in section 3.3.1).

The calibration setup that was used in a **Paper IV** is depicted in Figure 3. A comparable setup was used also in **Paper II** and **III**. This setup consists of a method to produce aerosol particles of known composition, a tube furnace and glowing wire generator for **Paper I** and **III**, a high-resolution DMA (section 2.1.1) and a reference for the concentration. A modified Vienna type Herrmann DMA (Cylindrical) (Kangasluoma et al., 2016a) or Half-mini DMA from SEADM (Fernández de la Mora and Kozlowski, 2013), both capable for resolving power more than 20, was used as a DMA. Concentrations were compared to those obtained using a faraday cup electrometer (FCE, see e.g. Flagan (1998)). The FCE is a good reference due to its high detection efficiency for small particles if internal losses are small. The FCE's collection efficiency follows filtration theory and increases towards small particle sizes. Even though, it has a relatively high limit of detection, it is usually not a problem in the

* Data was not yet available for the **Paper II.**

laboratory where the concentration of the produced particles is high enough for decent signal-to-noise ratio. The CPC counts the number of particles, but FCE counts the number of charges that accumulate onto a filter with the particles. When the particle population is singly charged, both numbers are the same. The probability for an aerosol particle to carry more than one charge in the sub-10 nm range is extremely low (Wiedensohler, 1988), which means that the concentration reading by FCE is not affected by multiply-charged particles. This is the case when the sample is close to a charge equilibrium, which does not hold while using electrospray ionization without neutralizer. This kind of setup can be used to calibrate other instruments in sub-10 nm size range, not just the PSM. When performing concentration calibration for CPCs with larger particles, the fraction of multiply charged particles can be significant. Then a reference CPC, a separately calibrated CPC, or single charged aerosol reference (SCAR) type setup (Yli-Ojanpera et al., 2010) should be used.

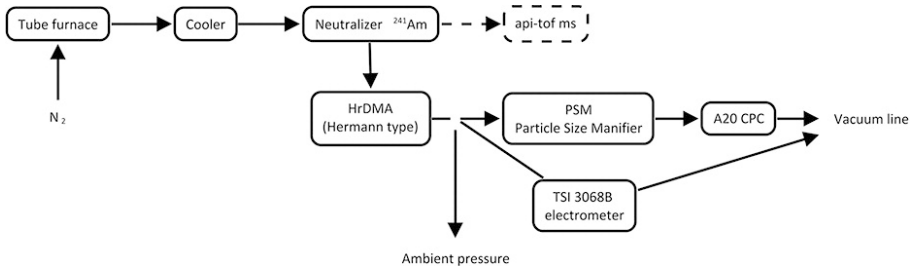

Figure 3. Calibration setup for PSM calibration that was used in **Paper IV**. Before connecting the DMA, the tube furnace was connected to the API-tof-MS to investigate the chemical composition of the produced particles. (adopted from **Paper IV**)

The total detection efficiency of the PSM system can be expressed in a similar way as for the CPC (Equation 3), even if it is a combination of two instruments. The sampling efficiency involves now internal losses in both instruments and in the line between them. Particles that are activated in the PSM are much larger than the cut-off diameter of the CPC, so the activation efficiency of CPC can be assumed to be unity and the combined activation efficiency to be governed just by the PSM. The counting efficiency of the optics is the same as for a simple CPC. Before performing the PSM calibration, operation of the CPC needs to be verified. The exact cut-off diameter of the CPC is not very important, since it is always much smaller than the size of the activated particles after the PSM. It is preferable to decrease the temperature difference in the CPC, if it is known that the particular CPC will be coupled to a PSM. This will ensure that CPC does not activate particles in the size range where PSM is scanning. In addition, a lower saturation temperature decreases the vapor concentration and butanol consumption, while a higher condenser temperature decreases condensation of water and DEG that make it to the CPC. Concentration calibration of the CPC, on the other hand, is important and the response of the instrument should be linear in the expected concentration range. In many locations, the sub-3 nm number concentration is quite high (e.g. **Paper II**) and the CPC behind the PSM is operating in the cloud mode. This means that the optics need to be clean and the correction are parameters correct.

The actual calibration procedure is quite simple once the preferred particle source and the calibration setup has been set up. Particles with a certain diameter are selected with the DMA and the detection efficiency is measured over a few cycles in the scanning mode. This is then repeated as many times as needed to cover the diameter range, where detection efficiency is dependent on the saturator flow rate. This provides a detection efficiency as function of saturator flow for each particle size. The two parameters that are needed for the inversion can be obtained from the data with a fit or by interpolation. An example is shown in Figure 4. The activation flow rate ($Q_{\text{activation}}$) is the saturator flow rate that gives the half from the maximum activation efficiency for a certain particle size whereas maximum detection efficiency ($\eta_{\text{det,max}}$) is the highest detection efficiency for the same particle size. When presented as functions of particle diameter, these give the two curves that are needed for the inversion and can be considered as a product of the calibration. PSMs used in **paper II** and **IV** were scanned between 0.1-1 lpm saturator flow range within a period of 240 s. Newer firmware's allows scanning up to 1.3 lpm.

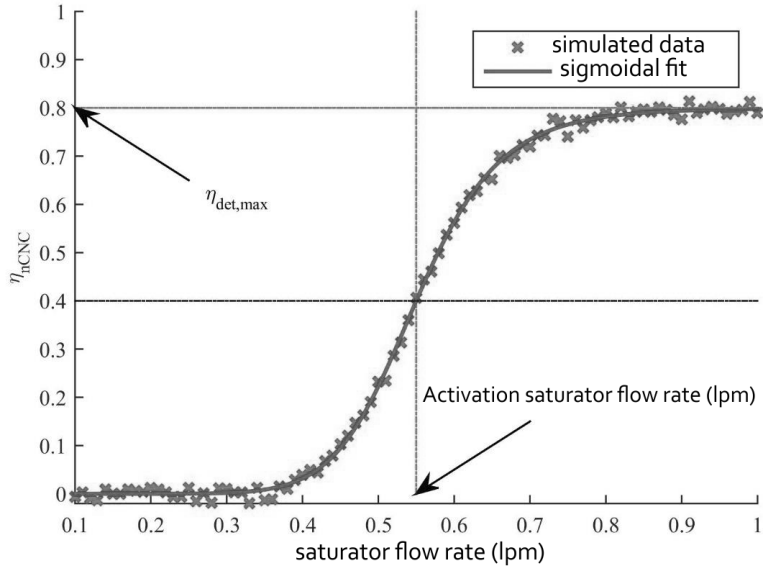

Figure 4. An example on how to determine parameters from the PSM calibration data.

2.2.2 Setting up a PSM for a field measurement

The sampling is probably the most important thing to consider when measuring concentration of sub-3 nm particles in any condition. This is true for the PSM as well. While measuring the total number concentration with a stand-alone CPC, correcting the size dependent losses is not possible, if the particle number size distribution is not known. In e.g. urban locations with high number concentrations, there might be a need for controlled dilution to keep the measured concentration within the capabilities of the CPC. In all applications, size dependent losses are still unwanted since these can skew the results and are hard to correct.

When the CPC is used in mobility size spectrometers, there is a possibility for correcting size-dependent losses. However, the signal for the smallest particles in the CPC is already limited by the charging probability (Wiedensohler, 1988) and the transmission of the DMA as well as the detection efficiency of the CPC, and thereby any additional factors lowering the signal-to-noise ratio need to be avoided.

In order to minimize the sampling losses in the atmospheric measurements, **Paper II** and **III**, a core sampling inlet was used to minimize diffusional losses before the instrument. In this kind of an inlet, a large flow is drawn through the main inlet line and the actual sample flow for the instrument is sampled from the middle of this larger flow (Figure 5). In the middle of the stream the radial concentration gradient is not as steep as near the walls. The sampling efficiency of similar design is shown in Kangasluoma et al. (2016b) and further analysis on the method is presented in Fu et al. (2019). Further, our permanent PSM measurements in SMEAR stations, used in **Paper II** (SMEAR II (2014, 2015) and SMEAR III (2015)), have a more complete sampling system with automated zero and background measurements.

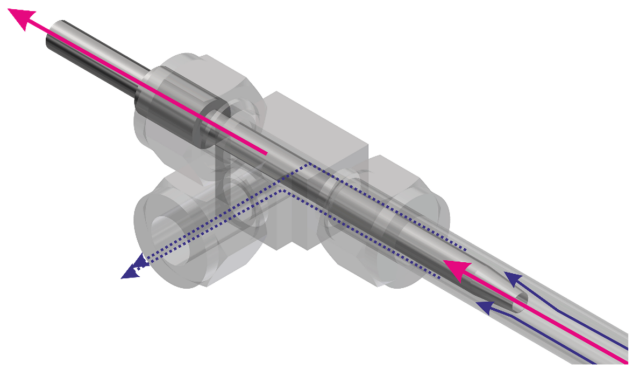

Figure 5. An illustration of the geometry in the core sampling inlet. The blue path shows the additional bypass flow and the magenta actual sample that is taken from the middle of the stream to the CPC or PSM (compressed markup).

The PSM data that I provided to the **Paper II** were measured by tuning the instruments to the edge of homogenous nucleation and slightly past it. The instruments were tuned to have a small amount of background counts originating from homogenous nucleation, as a tracer for the performance. The background counts were measured automatically several times per day and removed from the data before further analysis. The settings of the instrument were changed accordingly in order to keep the magnitude of background counts similar when environmental conditions changed. It has been observed that increased water concentration improves the activation efficiency of the PSM (Kangasluoma et al., 2013), so tuning the settings was done to mitigate this effect. Diurnal changes can be considered negligible but seasonal changes in the water content can be expected to have large impact and should be dealt in some way. Tuning the settings based on the homogenous background is based on the assumption that the heterogenous nucleation probability follows the homogenous nucleation probability. We recognize that there are problems with this kind of approach, but there

is, at the moment, no proven explicit way to deal with the environmental conditions altering the calibration. Drying the sample air, like it is done for harmonized DMPS/SMPS measurements (Wiedensohler et al., 2012), is not a viable solution due to the additional sampling losses that would be introduced in this sub-3 nm size range. For the smallest particles, the losses can be more than 70 % when using diffusion dryer (e.g. Tuch et al., 2009)

In a long-term operation of a PSM, there are several parameters that should be monitored to recognize occurring problems timely. Different problems of both instrumental and environmental origin are part of field measurements. Being aware of these problems helps operators to intervene before they affect data quality or at least keep the data gaps as short as possible via early discovery of errors. For example, large suspended particles such as dust and pollen and even insects may end up in the narrow mixing section partially blocking the line. This kind of a problem can be diagnosed by the measurement of inlet flows or monitoring the pressure drop in the PSM. Since the homogenous background measurement is used as a proxy for the activation efficiency, we need to be sure that the measured background consists of signal only from the homogenous nucleation and not from other factors such as leaks or excess liquid accumulating at PSM's outlet. The later of these is usually easy to recognize because the background signal that it produces is independent of the saturator flow. However, the number of background counts should not be too substantial, in order to keep the size distribution measurements reliable. The number of background counts that are tolerable in the data analysis depends on the ambient concentration levels that are measured.

2.3 Detection of sub-3 nm particles with laminar flow CPCs

In **Paper I,** we experimented with a possibility of using typical butanol CPCs, TSI 3772 and A20 Airmodus Ltd., to measure concentration of sub-3 nm particles. Both are common laminar flow diffusion CPCs, and with factory settings they have a nominal cut-off diameter close to 10 nm. The idea was to see whether these simple and less expensive instruments could be utilized for sub-3 nm particle detection by adjusting the instrument parameters. There is already similar work with other CPC models (Mertes et al., 1995; Russell et al., 1996; Wiedensohler et al., 1997; Petäjä et al., 2006; Sipilä et al., 2009; C. A. Kuang et al., 2012).

In **Paper I**, the instruments were optimized for the detection of sub-10 nm particles by adjusting the temperature difference, obtaining the highest possible detection efficiency without introducing a background signal from homogenous nucleation. Additionally, their performance was tested in a situation, where a small amount of background signal was accepted. The A20 was also tested with different inlet flow rates to optimize the sampling efficiency and thus to further increase the detection efficiency. These CPCs where then compared against instruments specifically designed for the detection of small particles: a TSI 3776 ultrafine CPC and Airmodus A11 nCNC system. TSI 3776 is based on the original ultrafine CPC (Stolzenburg and McMurry, 1991) having a sheathed inflow design. Details of the PSM are discussed in the section 2.2.

2.3.1 CFD model for A20 CPC

If the supersaturation and temperatures inside the CPC are known, the activation and growth of the particles inside the CPC can be modelled based on condensation and nucleation theories. Typically, some computational flow model is required to acquire temperature, concentration of vapor molecules and flow fields but in some cases an analytical solution can be also found (e.g. Hering and Stolzenburg, 2005). There exist several computational fluid dynamic methods such as finite volume (FVM) and finite element method (FEM) of which FEM is used in **Paper I** with Comsol Multiphysics software.

For **Paper I** a simple computational fluid dynamics CFD model was constructed to estimate the supersaturations achieved with the tuned settings. Heat and mass transfer were modelled in a laminar incompressible flow using COMSOL Multiphysics. The supersaturation field of butanol was calculated from the simulated temperature and vapor concentration that was used to calculate activation efficiency based on the classical nucleation theory, following the approach in Winkler et al. (2008) supplementary information. Separate growth model for the droplet was not made but we assumed that all the activated particles grow large enough to be detected in the optical detector.

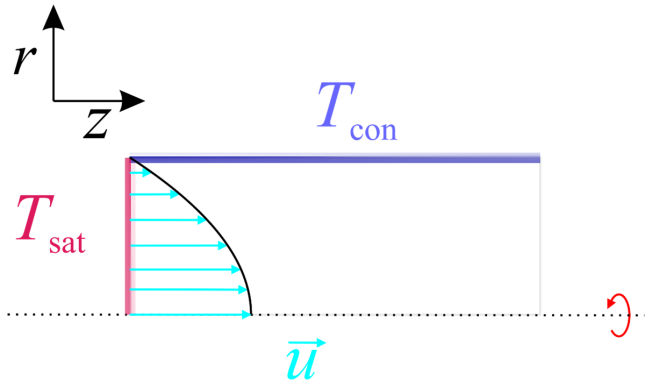

Figure 6. Simulation domain for the CPC model.

The condenser of the CPC was modelled assuming a fully saturated flow entering an axisymmetric simulation domain (Figure 6). The walls of the condenser were assumed to be fully wetted and at the set point temperature. Boundary conditions and the specifics of the model are presented in the paper. CPC's size dependent internal losses were taken into account by calculating diffusional losses in a laminar flow in a tube with effective length based on the equations from Gormley and Kennedy (1949). The losses were calculated for a tube, the length of which was adjusted to get the best match with experimental results. This can be connected to the factorized form of the CPC's detection efficiency (Equation 3). Here, we model the activation probability, assume the counting efficiency to be unity and adjust the sampling efficiency. For determining the final droplet size or accurate internal losses, more sophisticate model should have been used instead.

The total activation efficiency was calculated by assuming a uniformly distributed particle concentration entering the condenser. The flux-averaged total concertation was calculated based on the axial activation efficiency and the parabolic flow profile in similar way as in (Giechaskiel et al., 2011). This takes into account that particles travelling in the middle of the tube, and encounter higher supersaturation, contribute more to the total flux of particles. By repeating this, through the size range of interest, gives the activation efficiency curve used to calculate total detection efficiency as function of particles size.

2.4 Ion mobility spectrometry

The work in this thesis relies on the basic definitions governing the motion of aerosol particles in a medium. The most important ones for mobility classification are introduced here.

An *electrical mobility* Z is defined based on how charged particles move in the background gas while electric field is applied, and it is the ratio of drift velocity in gas v_d and the strength of the electric field E (e.g. Hinds, 1999).

$$Z = \frac{v_d}{E} \tag{4}$$

In small electric fields, ions do not gain substantial velocity between collisions with background gas molecules, compared to a thermal movement of the gas molecules. While this is true, diffusion coefficient D relates to the electrical mobility and mechanical mobility with Einstein relation and electrical mobility is independent on the electric field (Mason et al., 1975):

$$D = \frac{k_\mathrm{B} T Z}{q} = k_\mathrm{B} T B, \quad q = ne \tag{5}$$

Here, k_B is Boltzmann constant, q the charge in the particle, n number of elementary charges e and T temperature of the background gas and B is mechanical mobility of the particle. These three attributes, B, Z and D are equivalent attributes to describe the movement of the particle in the background gas (Tammet, 1995). If Z is measured in the linear regime, where it is independent on the electric field, the mobility analysis method is referred as *linear*, in contrast to *nonlinear* methods (Gabelica et al., 2019).

The electrical mobility is also related to the concept of Collision Cross Section *CCS*, describing momentum transfer between the charged particle and the background gas, which it can be expressed through Mason-Schamp equation (Eiceman et al., 2013):

$$Z = \frac{3q}{8\rho_\mathrm{gas}} \sqrt{\left(\frac{\pi}{2\mu k_\mathrm{B} T}\right)} \frac{(1+\alpha)}{\Omega} \tag{6}$$

where ρ_{gas} is the mass density of the background gas, μ is reduced mass of the ion and gas molecules, and α is a higher-order correction factor that is typically assumed to be negligible (McDaniel and Viehland, 1984). The parameter Ω is the collision cross section, an orientationally averaged first collision integral.

The electrical mobility is convertible to a particle diameter d_p with certain assumptions. For a spherical particle in Stokes regime, the relation can be written with an equation

$$Z = \frac{qC_c(\mathrm{Kn})}{3\pi\eta d_\mathrm{p}}, \tag{7}$$

where η is viscosity of the background gas and C_c a Cunningham slip correction factor that takes into account non-continuum effect in the transition regime. The correction factor is expressed with a dimensionless Knudsen number Kn and empirical constants α, β and γ as follows (Flagan, 2011):

$$C_c = 1 + \mathrm{Kn}\left(\alpha + \beta \exp\left(-\frac{\gamma}{\mathrm{Kn}}\right)\right), \qquad \mathrm{Kn} = \frac{2\lambda}{d_p} \tag{8}$$

Here λ is the mean free path of the background gas. The diameter that results from the Stokes-Millikan relation in the equation 7 is called the electrical mobility equivalent diameter. In this study, we refer to this diameter definition, if not otherwise specified. While comparing electrical mobility diameter to other diameter definitions, it is important to remember that the electrical mobility equivalent diameter is based on the steady state drift velocity which is independent on the particle mass and does not contain information on the inertia of the particle, unlike for example aerodynamic diameter.

2.1.1. Differential Mobility Analyzer

A differential mobility analyzer (DMA) is an instrument, in which charged particles are pulled through the gas with electrostatic force in a particle free air sheath flow via electrophoretic migration. There are several different DMA designs and two of those, planar design and cylindrical, are used in this thesis. Both designs have a particle free sheath flow perpendicular to the electric field (Figure 7). The charged particles are introduced into the sheath flow from an inlet slit at the one side of the stream and collected from an outlet slit at the other electrode downstream of the inlet. Depending on the sheath flow velocity U, applied voltage V_{DMA} and the distance between plates and the axial distance d between the inlet and the outlet L, ions with specific mobility are transmitted from inlet to outlet.

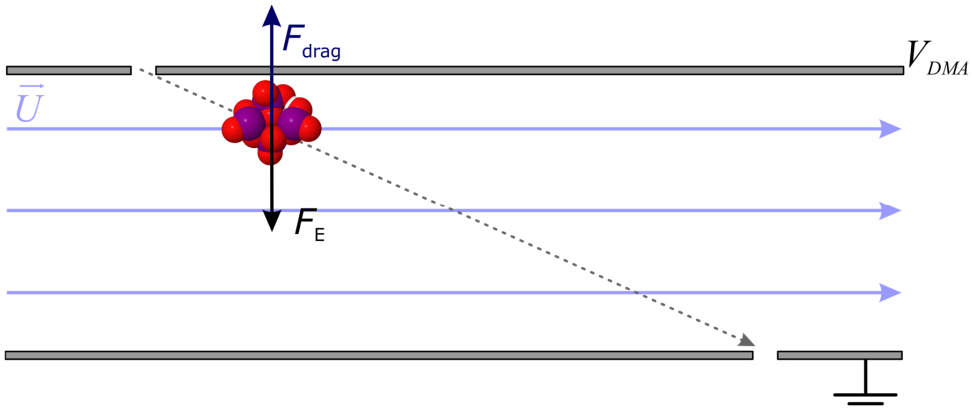

Figure 7. A schematic presentation of parallel plate DMA. Particles are drawn across the particle free sheath air stream with an electrostatic force.

The mean mobility Z^* of the transmitted ions can be written with an equation in the planar DMA as follows (e.g. Fernández de la Mora et al., 2006):

$$Z^* = \frac{Ud^2}{LV_{\mathrm{DMA}}} \tag{9}$$

For the balanced cylindrical DMA, the relation can be written following the form derived in Knutson and Whitby (1975):

$$Z^* = \frac{Q_{sh} \ln \frac{R_1}{R_2}}{2\pi V_{\mathrm{DMA}} L'}, \tag{10}$$

where Q_{sh} is the volumetric flow rate of sheath, and R_1 and R_2 are the radius of the inner and outer electrode, respectively. In our DMA setups, the sheath flow is usually too large to be measured accurately with common flow meters. Therefore, the inverse relation between DMA voltage and mean mobility of transmitted particles

$$Z^* \propto \frac{1}{V_{\mathrm{DMA}}} \tag{11}$$

is calibrated using ions of a known mobility, i.e. mobility standards, for example tetraheptylammonium bromide (THABr) molecular clusters from electrospray ionization (Ude and de la Mora, 2005).

The transfer function of the DMA has a finite width. By studying the streamlines starting from the inlet slit and streamlines leading to outlet slit in the DMAs sizing region, it can be found that also slightly less mobile and slightly more mobile particles, compared to Z^*, will be transmitted through the DMA with a probability having a triangular shape, when diffu-

sion is excluded (Knutson and Whitby, 1975). The width depends on the ratio between aerosol and sheath flows. The resolving power R of the DMA is defined as a ratio of mean mobility and the full width half maximum (FWHM) of the transfer function ΔZ_{fwhm}

$$R = \frac{Z^*}{\Delta Z_{\mathrm{fwhm}}} = \frac{Q_{\mathrm{sh}}}{Q_{\mathrm{sample}}} \tag{12}$$

R is governed by the ratio of sample flow rate Q_{sample} and the volumetric sheath flow rate. In the case of the smallest ions, the path of will deviate from their straight line trajectories due to random Brownian motion broadening the transfer function further (Tammet, 1970; Stolzenburg, 1988). The transfer function considering diffusional broadening was introduced in the thesis of Stolzenburg (1988) and computationally less expensive approximation in the Stolzenburg and McMurry (2008).

In DMAs the electric field is relatively small and the traverse speed of charged particles is small compared to the mean thermal velocity of the background gas molecules. Therefore, in a typical configuration the DMA can be considered as a linear method for measuring electrical mobility (Hogan and de la Mora, 2009).

2.1.2. Time-of-flight (TOF) Mass Spectrometers TOF-MS

We discuss here briefly the principles of time-of-flight mass spectrometers. Even if this instrument is not directly related to the ion mobility spectrometry, it is often used in a conjunction with mobility analyzer of some sort. There exists a variety of mass spectrometry (MS) methods to measure the mass-to-charge ratio (m/z) and time-of-flight is one of the earliest methods (e.g. Griffiths, 2008). In the TOF-MS, an ion beam is accelerated in pulses with electric field and collected with an ion detector in vacuum. The time difference between the acceleration pulse and the detection of ions, *flight time*, is recorded and it is dependent on the mass-to-charge ratio of ions. The entire mass spectrum is recorded for each acceleration pulse unlike for example in a quadrupole-MS (Wiley and McLaren, 1955). The time-of-flight measurement is performed in high vacuum to prevent collisions of the ions with the background gas. A conversion between the drift time and the mass of an ion can be calibrated with identified peaks of known m/z, sometimes referred as lock masses.

In this work, two TOF-MS instrument were used: An Atmospheric Pressure Interface Time of Flight Mass Spectrometer (APi-TOF, Tofwerk AG) (Junninen et al., 2010) in the **Paper IV** and QSTAR XL (AB Sciex, Concord, ON, Canada) in the **Paper V**. Both instruments are based on the orthogonal acceleration time-of-flight mass spectrometry with reflecting mass analyzer. In this type, a packet of ions is accelerated with electric field perpendicular to the initial direction of a collimated ion beam (Figure 8). The flight path is steered back to a microchannel plate (MCP) detector with reflectors along v- or w-shaped path (Guilhaus et al., 2000).

There is an atmospheric pressure interface (API) preceding the TOF-region where pressure is pumped sequentially in three stages from ambient pressure before the first pinhole to high

vacuum (around 10^{-6} mbar) in the TOF chamber. This enables sampling directly from an ambient pressure. Air is pumped with a scroll pump as roughing/fore pump and turbo molecular pumps at the consecutive stages. In the ion beam line, in first two stages, there is quadrupole to guide ions into next stage with good transmission. In the Q-star XL, there is an additional third quadrupole for MS-MS measurement, but the instrument was used just as a TOF-MS. There is acceleration and deceleration of ions due to the fluid flow through the pinholes and electric fields that are there to guide the ions, which induce fragmentation. The extent of fragmentation is depended on the specifics of the design, pressures and the settings applied as well as the binding energies in the clusters (Lopez-Hilfiker et al., 2016; Passananti et al., 2019; Zapadinsky et al., 2019).

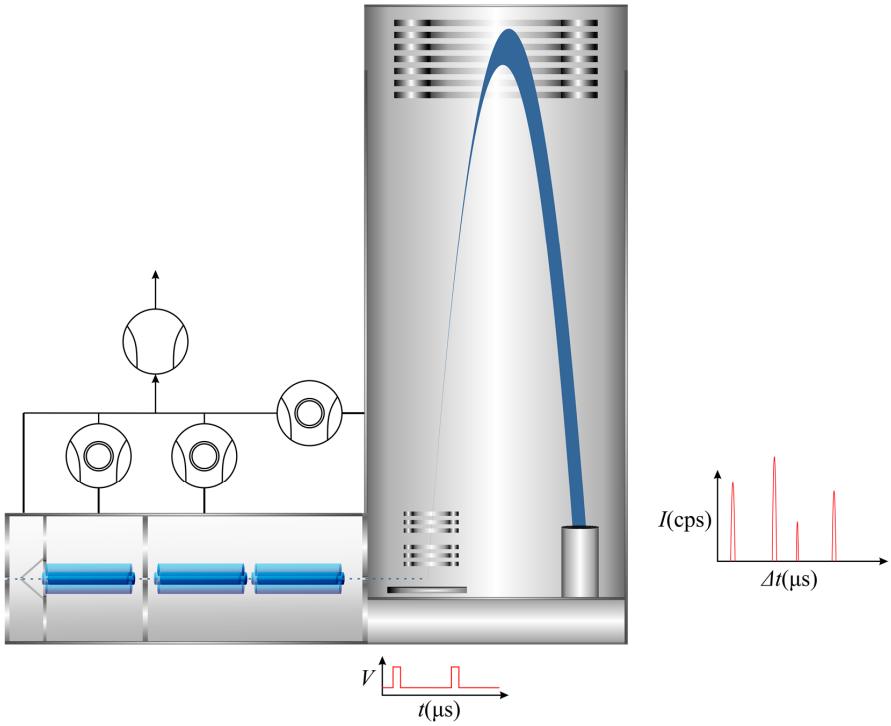

Figure 8. Schematics of the TOF-MS with an API inlet following loosely the design of QSTAR XL. Pressure is pumped down in sequentially with turbomolecular pump and a separate fore pump. Ions are guided and collimated into a beam before ion extraction region where they are accelerated in pulses to the direction that is orthogonal to their initial direction of travel. The time, from the extraction pulse to the detection of ions in MCP after they traverse through the TOF region, is recorded and converted into a mass of ion in the later analysis.

2.1.3. Differential mobility analysis Mass Spectrometry DMA-MS

Combining the mobility and mass measurement of ions adds an additional dimension to the data. Even though both quantities correlate, they are derived from different properties. The mobility spectrum carries information on size and shape, together with interactions with the background gas, and the mass spectrum on the mass and the charge state of the ion. The mobility analysis can be performed with for example a drift tube (IMS-MS; see e.g. Krechmer et al. (2016)) or differential mobility analyzer like in the **paper V**. Highly charged clusters are a feature of electrospray ionization making the mobility spectrum often difficult to interpret without some additional information. DMA-MS enables accurate mobility measurement of large ions without the need of charge reduction (Ude et al., 2004; Fernández de la Mora et al., 2006). Additionally, an information on the fragmentation of ions in the API interface is also derivable based on the additional data dimension (e.g. Hogan and de la Mora, 2010; Passananti et al., 2019).

In the DMA-MS system we used, a parallel plate DMA (model P5, SEADM, Boecillo, Spain) is coupled with a time-of-flight mass spectrometer (QSTAR XL, AB Sciex, Concord, ON, Canada) in a way that DMAs outlet slit is the first pinhole to the mass spectrometer. Details of this system is presented in Rus et al. (2010). In the DMA, laminarization screens preceding a converging section where flow is accelerated just before the sizing region and highly polished surface allows high flow velocities still maintaining turbulent free flow in supercritical Reynolds numbers. This converts into high resolving power up to 50, and even up to 100 with special care and some modifications (Amo-González and Pérez, 2018). The high voltage (DMA voltage) is applied to the front plate of the DMA and the back plate is grounded. The electrospray liquid is floated 1-2 kV above the front plate to produce a stable Taylor cone (Gomez and Deng, 2011). This configuration without a need of potential transition past the size classification and direct coupling to MS gives rise to the high transmission efficiency. The system together with the humidification equipment for the sheath air presented are in the Figure 9. The purpose of the humidification equipment is explained later (section 3.5.3).

Measurements were conducted operating the DMA in a closed-loop configuration, recirculating the gas in the sheath loop (Jokinen and Mäkelä, 1997). An additional flow, referred here as a compensation flow, was connected to the sheath loop to compensate the flow exiting from the DMA into the MS. This was adjusted to be slightly larger than the MS's sample flow, inducing a small counter flow against the ions entering into DMAs sizing region. While operating in a counter flow mode, the ions are drawn into DMA electrostatically which prevents large droplets and most of the solvent from entering into DMA resulting in a cleaner mass spectrum.

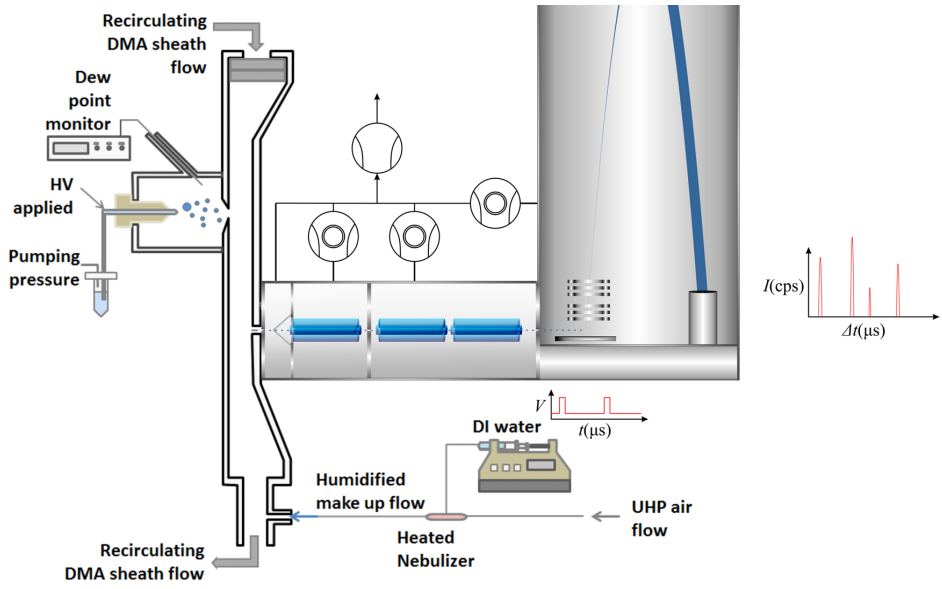

Figure 9. An illustration of DMA-MS with an electrospray source and a system for humidifying the compensation flow, similar to the one used in **Paper V**.

2.5 Differential mobility particle sizer (DMPS) for sub-10 nm size distribution measurement

A Differential mobility particle sizer (DMPS) consists a DMA, CPC and aerosol charger, and it is used to measure particle number concentration (e.g. Tenbrink et al., 1983; Winklmayr et al., 1991). A Scanning Mobility Particles Sizer SMPS (Wang and Flagan, 1990) is very similar instrument having continuous ramping of DMA voltage instead of discreate steps. Typically, both of these systems operate in 10 to 800 nm size range, sometimes starting from 3 nm when using ultrafine CPC as a detector (Aalto et al., 2001). There exists well-established guidelines for the design of the instrument as well as for the operation and data analysis (Wiedensohler et al., 2012). In a harmonized DMPS system, there is a pre-impactor and dryer in the sampling line. The impactor at the beginning of the sampling line is there to remove particles that are larger than the upper size limit of the instrument, which is important for the data inversion. The dryer is there to decrease the humidity of sample to a level that is below 40% relative humidity. Drying is done to mitigate effect of hygroscopic growth which can alter the size of particles significantly (Swietlicki et al., 2008). Additionally, it is recommended to have complementary sensors such as temperature, pressure and relative humidity (RH) to ensure harmonized size distribution measurements around the world.

As discussed in the introduction, there is a demand for concentration and size distribution data close to the size where first steps of new particles formation take place. There are already different approaches to expand the size distribution measurements towards smaller sizes (e.g. Manninen, 2009; Jiang et al., 2011; Stolzenburg et al., 2017). In the **Paper III** we build a DMPS system that was optimized for the sub-10 nm size range, which had a moderate resolving power, portable size and good transmission.

The instrument in **Paper III** is referred as high flow differential mobility particle sizer HFDMPS. This was achieved using Half-mini DMA (Fernández de la Mora and Kozlowski, 2013) and PSM (section 2.2) as a detector together with optimized sampling. The design of the Half-mini DMA allows it to operate at high Reynolds number maintaining laminar flow. The high sheath flow velocity converts into short residence time minimizing the resolution decrease due to the diffusion broadening. This makes it very suitable for sub-2 nm mobility analysis, although only moderate flowrates were used in this study. The system was thoroughly characterized in the laboratory and then set up in Hyytiälä for intercomparison measurements. The size range where is operates is 3-10 nm, the upper end of which is limited by the DMA voltage of 5kV that the instrument withstands. After this study, an improved aerosol injection slit has been developed for the Half-mini DMA making it more suitable for atmospheric measurements with reduced flow rates (Cai et al., 2018a).

2.6 Parameters quantifying the new particle formation event

The intensity of new particle events can be characterized based on parameters such as formation rate and growth rate. The formation rate J_{dp} is a flux of particles through a specific particle size and the growth rate GR is the time evolution of the mean size of the growing particle mode (Kerminen et al., 2018 and references therein). The growth rate is affected by the growth of individual aerosol particles, self-coagulation and scavenging. Self-coagulation involves collisions between particles within a particle mode, resulting in an increase of the mean particle size in this mode. Scavenging involves collisions with larger particles, which removes particles from the smaller mode and increases the size of the larger particles by a factor that is unnoticeable. The scavenging efficiency is the highest for the smallest particles in the mode, due to faster Brownian motion, affecting the mean diameter.

The formation rate can be written with the time derivative of the number concentration and loss terms which are from processes such as coagulation and growth out of the size bin:

$$J_{d_p} = \frac{dN_{d_p}}{dt} + \mathrm{Coag}S_{d_p} \cdot N_{d_p} + \frac{\mathrm{GR}}{\Delta d_p} \cdot N_{d_p} + S_{losses}\,, \quad \mathrm{GR} = \frac{dd_p}{dt} \tag{13}$$

Here $N_{d\mathrm{p}}$ is the number concentration in the size bin with diameter d_p as the lower limit, CoagS_{dp} size dependent coagulation sink and S_{losses} term includes additional loss processes, e.g. dilution. (e.g. Kulmala et al., 2012).

The formation rate can be scaled to the different size via revised Kerminen-Kulmala (KK) equation (Kerminen and Kulmala, 2002) using growth rate and coagulation sink (Lehtinen et al., 2007):

$$J_{d_\mathrm{p}} = J^* \exp\left\{-\gamma d^* \frac{\mathrm{Coag}S(d^*)}{\mathrm{GR}}\right\}, \gamma = \frac{1}{m+1}\left[\left(\frac{d_p}{d^*}\right)^{m+1} - 1\right] \tag{14}$$

Here J^* is the measured formation rate at the diameter d^*, J_{d_p} the scaled formation rate at new diameter d_p, and m is a parameter related to the size dependency of the coagulation sink which value is dependent on the background aerosol population (see Lehtinen et al., 2007). Equation 14 describes the proportionality between formation rates at different sizes as a function of the ratio between growth rate and coagulation sink, competition between the flux of particles into the size range and the removal of those via scavenging. A constant growth rate over the diameter range that is scaled is assumed and the effect from self-coagulation presumed negligible, in the derivation of the equation.

3 Results and discussion

3.1 Sub-3 nm particles were detected with laminar flow CPCs

In **Paper I** the detection efficiency of two commercial CPC was tested in the sub-10 nm size range (see section 2.3). Based on the experiments, we can conclude that a conventional laminar flow diffusion CPC using butanol can be boosted from nominal settings to be suitable for sub-10 nm and even for sub-3 nm particles, as shown in Figure 10. However, the instruments, such as Airmodus A11 and TSI ultrafine CPC (3776), that are designed from the beginning to measure small particles, perform still better having a higher detection efficiency and steeper ascend of the detection curve.

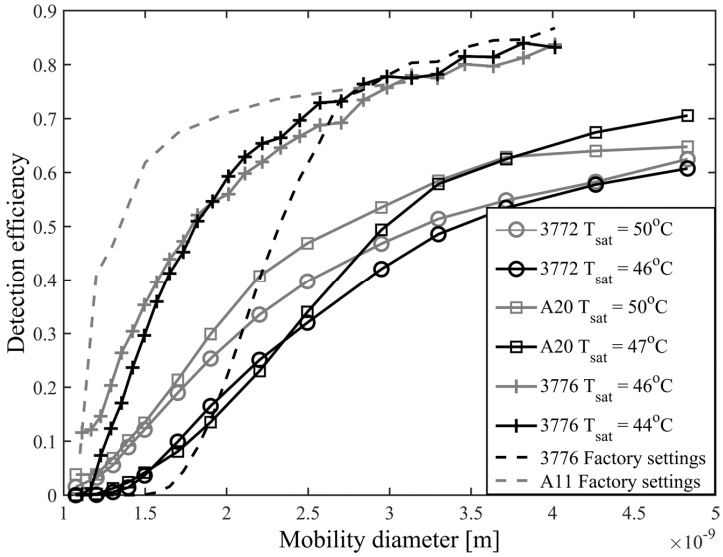

Figure 10. Detection efficiency curves for the A20, 3772, 3776(ultrafine) and A11 with factory settings and boosted settings (adopted and modified from **Paper I**).

Computational fluid dynamic (CFD) model was used to support the experimental work and to calculate theoretical predictions for the detection efficiency curves with new optimized settings obtained. The flow profile, vapor concentration and temperature fields were obtained from the CFD model (Figure 11), while the activation probability was solved based on these. Assuming that particles follow streamlines, the activation probability for the particles traveling along a certain radial path was calculated. The highest value was stored for each radial location. Aerosol particles in these sizes follow streamlines without being affected by their inertia. However, they will deviate from their path due to random Brownian motion. There are different schemes for simulating the diffusion of particles in a fluid flow, such as continuous or discrete random walk models (se e.g. Bocksell and Loth, 2001). However, these were not applied in the simple model. In a more advanced simulations these should be applied together with full instrument geometry.

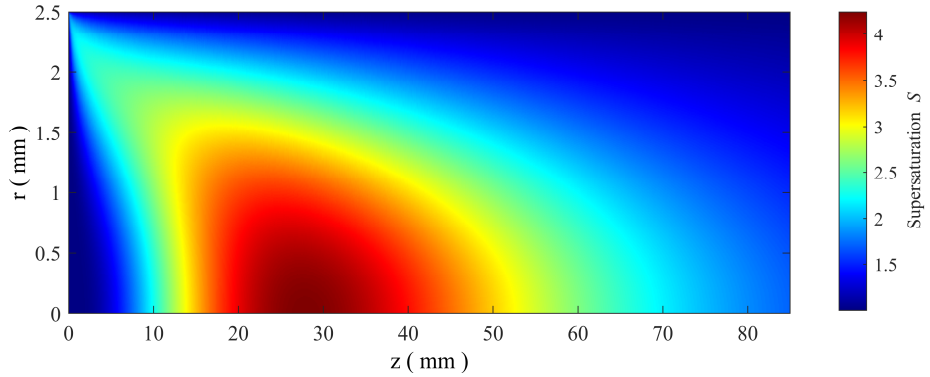

Figure 11. Modelled supersaturation field of A20 CPC with settings at $T_{condenser}$ = 10°C and $T_{saturator}$ = 45°C. (adopted and modified from **Paper I**).

The modelled detection efficiency curves suggested that the activation efficiency was not the limiting factor for the CPC's detection efficiency (Figure 12), but rather the losses due to diffusion and unoptimized design of the optics and nozzle would need revisions for the boosted settings. For example, a higher temperature difference between saturator and the condenser will lead to a higher vapor concentration and larger final droplet size with different aerodynamic properties. This changes, for example, the performance of the nozzle that is supposed to collimate the particle trajectories, before detection with the laser beam, without introducing additional losses.

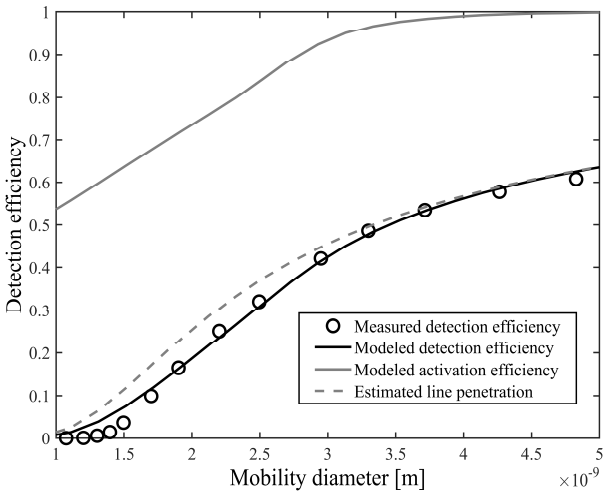

Figure 12. Comparison of measured and modeled A20 detection efficiency at the brink of homogeneous nucleation. (adopted and modified from **Paper I**)

3.2 Aerosol formation in the atmosphere

The new particle formation process includes the formation of molecular clusters and their subsequent growth into aerosol particles (Kulmala et al., 2013). The initial formation of molecular clusters, charged and neutral, seems to be more general process happening all the time, while the production of a growing mode of particles, that is referred as new particle formation NPF event, needs more specific conditions to occur (Kulmala et al., 2014). The concentration of molecular clusters is often related to NPF, but an elevated sub-3 nm particle concentration does not always lead to new particle formation (Yu et al., 2014; Yu et al., 2016). There is a competition between the formation of cluster from gaseous precursors and the removal processes for the growing clusters and precursor gases (McMurry and Friedlander, 1979; Kulmala et al., 2004b).

When new particle formation is a regional event occurring homogenously over a wide area, the evolution of a growing particle population (Figure 13) can be followed at a stationary measurement station (Mäkelä et al., 1997). Based on the evolving particle number size distribution, both particle growth rate and formation rate can be obtained (section 2.6). The procedures and analysis for these kinds of regional NPF events is presented as a protocol in Kulmala et al. (2012).

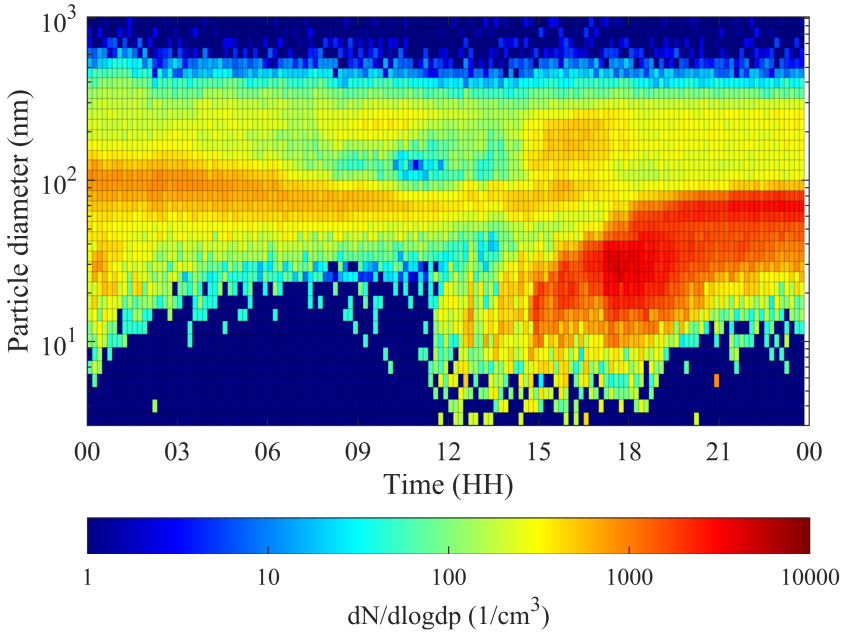

Figure 13. An example NPF event shown as a contour plot observed at Hyytiälä, Finland (Permission granted for the use of example data).

The formation rate can be scaled to a diameter that is different from the measured one using the KK equation or its revised version (equation 14; section 2.6). This is useful when comparing formation rates that are measured at different sizes, or when scaling the value of J

for sizes where particle concentration is not measured due to instrumental limitations. The latter is not anymore as pressing issue as it was a decade ago. However, in many measurement sites sub-3 nm particle concentrations are still not measured. Furthermore, the growth in the smallest sizes is dependent on the particle diameter, contradicting the assumptions in KK-equation, and the volatilities of the condensable vapors have effects on which particles they can condense on (Tröstl et al., 2016). For this reason, the measurement of newly formed particles, close to the size where gas-to-particle conversion takes place, is important for understanding and quantifying the process of new particle formation. For measuring reliable formation rates and growth rate, size resolved concentration measurements in the sub-10 nm size range, and preferably in the sub-3 nm size range, are needed.

3.2.1 Concentrations of sub-3 nm atmospheric clusters

Using the data from continuous PSM measurements in SMEAR II and III, and the other sub-3 nm number concentration data that were available for the **Paper II,** we were able to compare median diurnal variations in the number concentrations between several different measurement sites. In general, the daytime concentrations were higher than nighttime concentration (Figure 14). As a summary, the highest cluster concentrations were measured in the locations that had strong anthropogenic influence, Nanjing, Shanghai, San Pietro Capofiume and Helsinki, compared to more remote locations such as Hyytiälä. The observed daytime maxima indicate photochemical production of low-volatile precursors from a gaseous emission from biogenic and anthropogenic origin (e.g. Ehn et al., 2014; Tröstl et al., 2016; Pye et al., 2019). However, also emissions from sources such as traffic and other anthropogenic activities that have a diurnal variation contribute to the variation in cluster concentration in the urban measurement sites. For example, traffic emits particles in a wide size range with large emissions of sub-3 nm particles (Rönkkö et al., 2017).

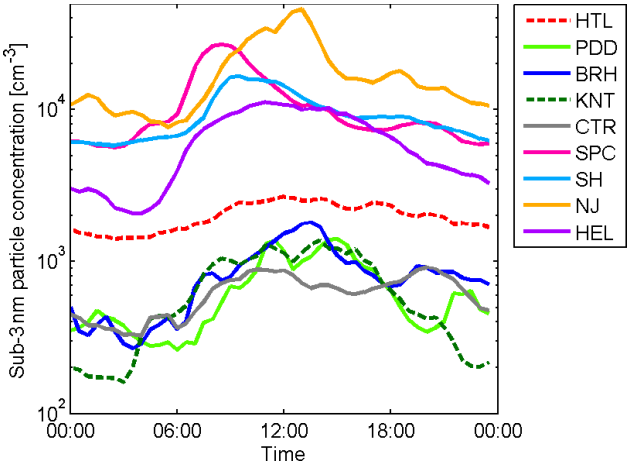

Figure 14. Diurnal median number concentrations of sub-3 nm particles. (HTL = Hyytiälä, PDD = Puy de Dôme, BRH = Brookhaven, KNT = Kent, CTR = Centreville, SPC = San Pietro Capofiume, SH = Shanghai, NJ = Nanjing and HEL = Helsinki) (adopted from **Paper II**)

Two longer data sets from SMEAR II (HTL) and SMEAR III (HEL) were grouped seasonally, into spring (March-May), summer (June-August), autumn (September-November) and winter (December-February). The seasonal differences in the diurnal patterns were compared in each size bin (Figure 15). In Hyytiälä the daytime maximum was the strongest during spring and visible also during the summer. In Helsinki the daytime maximum was almost equally prominent in all seasons. This suggest that the sub-3 nm concentration in Helsinki is affected by anthropogenic sources of precursors, which is expected. In Hyytiälä the concentration in the smallest sizes was the highest during summer months, whereas the concentration in 2-3 nm was the highest during spring. The ratio between the concentration in the 1.2-2 nm and 2-3 nm size ranges was three to four times higher during summer and autumn compared to other seasons. This suggests that the production of the clusters is higher during these months, and that further growth was not as efficient compared to the growth during the springtime or during winter. Elevated concentrations in the 2-3 nm size bin are more indicative of NFP events than elevated concentrations in smaller size bins. Several studies have already shown that the frequency of NPF events in Hyytiälä is the highest during springtime (see e.g. Nieminen et al., 2018).

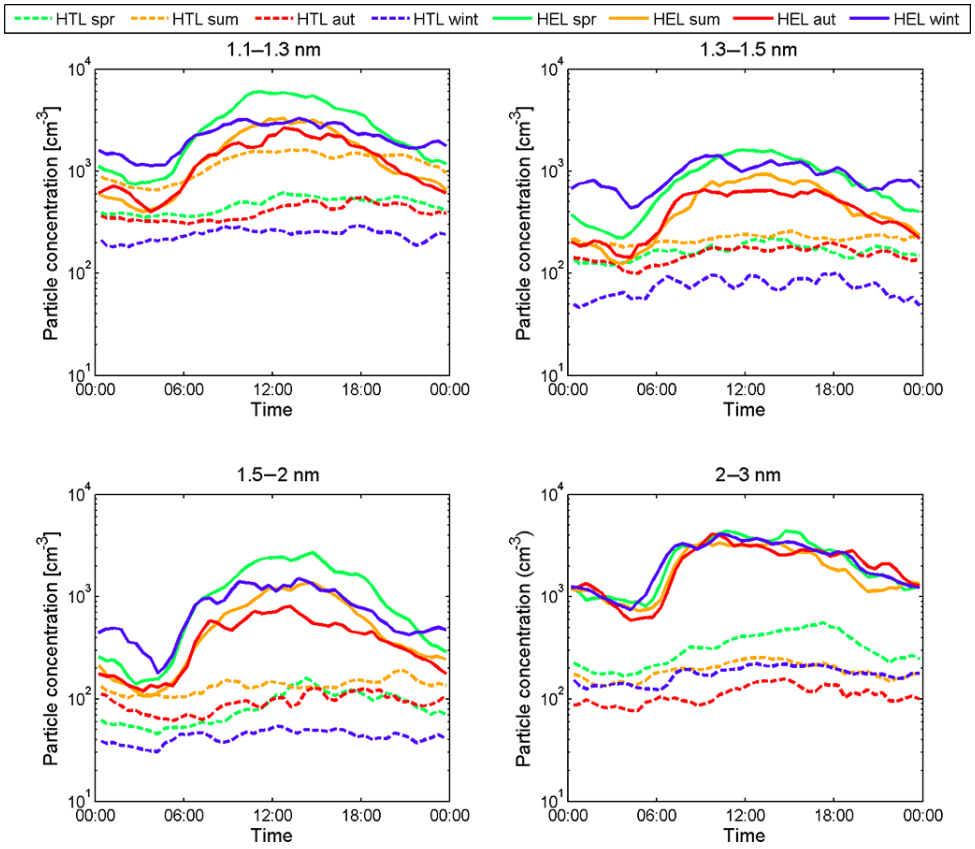

Figure 15. Diurnal median concentrations from Hyytiälä (HTL) and Helsinki (HEL) in different seasons (spr = spring, smr = summer, aut = autumn and wint = winter). Concentration in different size ranges is plotted separately. (adopted from **Paper II**)

For the sites with complementary ion spectrometer NAIS/AIS (Mirme et al., 2007; Manninen, 2009) data, a comparison was made to derive a fraction of charged particles to the sum of the clusters. A PSM measures the total concentration counting for both charged and neutral clusters, whereas an ion spectrometer in the ion mode counts only charged particles. Dividing the total number of clusters with the ion concentration gives a fraction of ions to the total particle concentration in sub-3 nm concentration. Certainly, there are uncertainties in the comparison of two instruments with a different operation principle. Even though a PSM is calibrated using mobility diameter, it is ultimately classifying particles based on their activation properties. NAIS and AIS, on the other hand, are measuring the mobility of ions with multichannel DMA having variable diameter inner electrode and an outer electrode constructed from ring-shaped electrometers. About uncertainties related to NAIS and AIS, see Wagner et al. (2016). However, based on the comparison, there seems to be a larger ratio of electrically neutral clusters over charged ones in polluted environments compared to remote sites. Additionally, it was observed that in some occasions the fraction exceeded unity in Hyytiälä which suggest that some of the ions were not activated in the PSM.

3.2.2 Verifying the operation of the HFDMPS in SMEAR II

The HFDMPS (section 2.5) was used in the SMEAR II station during a short intercomparison campaign. During the atmospheric measurements it was compared against the twin DMPS system optimized to cover the whole 3 to 1000 nm range. The system is presented in Aalto et al. (2001). The HFDMPS was located around 20 m away from it. There were some differences compared to harmonized DMPS measurements in how the instrument was set up for ambient measurements. Some of the recommendations are not pertinent or suitable for the detection sub-10 nm particles. For example, a dryer in the sampling line induces additional sampling losses that are relatively small above 10 nm but increase rapidly when going below that (Tuch et al., 2009). Therefore, sampling was done without a pre-impactor and dryer in the sampling line. The sampling line was kept as short as possible and free of bends which causes extra losses (Wang et al., 2002). A similar core-sampling inlet to the one described in section 2.2.2 and depicted in Figure 5, was used to further increase the sampling efficiency.

The HFDMPS showed on average 1.8 times higher concentration than the other DMPS for the 3-10 nm size range. The disagreement was larger in the smallest size bins, and at the 10 nm size the instruments agreed already rather well. A more important outcome was that the HFDMPS counts 4-9 times higher raw counts depending on the particle size, thus cutting the counting uncertainties in half. This is accomplished by a higher total penetration efficiency, which is due to the good transmission in the DMA and sampling lines but also due to the PSM that has larger undiluted flow through the optics. Like the name implies, the twin DMPS has two DMPS systems having partially overlapping size ranges. The one dedicated for small sizes has a TSI ultrafine as a detector, which is suitable for activating particles down to 3 nm and below as seen in **Paper I**. It has also smaller internal losses than non-

sheathed CPCs whose activation efficiency is boosted from nominal performance. The difference here is that the dilution from the sheathed design starts to affect counting statistics when the overall efficiency of the system is quite low even at the best, as seen in **Paper III.**

We found that the HFDMPS was not really able to detect sub-3 nm particles in the SMEAR II (Hyytiälä) site that is strongly affected by biogenic emissions. However, in the laboratory calibrations PSM's d_{50} was measured to be 1.4 nm with molecular clusters from CrO_3 and 2 nm with THABr, respectively. The fact that the HFDMPS was not detecting sub-3 nm particles suggest that DEG might not be suitable for activating clusters formed from low-volatile organic compounds (Ehn et al., 2014; Jokinen et al., 2017; Bianchi et al., 2019) when background counts cannot be tolerated.

Based on the results we can conclude that applying the HFDMPS to field use was a good opening to improve size distribution measurements in the 3 to 10 nm size range. However, there are still several improvements to be made. For the mobility analyzer, there is already better hardware available, which improves the shape of the transfer function when a Half-mini DMA is used with reduced flowrates. It would be also simpler to have a detector that is contained in a single unit, unlike the PSM, still reaching a high activation efficiency. Based on **Paper I,** increasing the sample flow rate could be a viable approach to increase the detection efficiency. This also improves the counting statistics of the DMPS if flow rate through the optics also increases. This requires a hardware specially build for high flowrates.

One aim for the new system was to measure particle number size distribution also below 3 nm in Hyytiälä, but that was not a success. It proved to be difficult to detect particles smaller than 2 nm of organic composition while at the same time maintaining almost zero background which is necessary for a DMPS application. This could maybe be improved by experimenting with different working fluids that are less composition dependent. In addition, there might still be room for improvements by further optimizing the instrument for better activation without homogenous nucleation occurring inside the detector.

There has been work in this field towards making the performance assessment of different types of instruments more comparable. A detailed comparison between different size distribution instruments for the sub-3 nm size range was recently made by Cai et al. (2019), also deriving Π parameter as a proposed indicator for the performance of electrical mobility spectrometers. The parameter Π takes into account the overall efficiency, integration time, undiluted aerosol flowrate and the resolution of the mobility analyzer. It can be used to estimate the number of raw counts, in each size bin, based on a given particle number size distribution, but also to compare instruments with different operation principles such as FCE based size spectrometers and scanning PSM with more conventional DMPS systems having a CPC as the detector.

3.3 Cluster measurements in a cleanroom

As a simple description, cleanrooms are spaces were the level of airborne particulate matter is kept very low. The particle concentration is controlled to a level that is required for the intended use of the space, and depending on the aimed cleanliness, different actions are required. For example, compared to a typical indoor space, in the cleanroom the ventilation rate is faster, operators use specialized outfits and materials to prevent release of particles from the operators, and the airflow in the space is optimized to avoid contaminating sensitive products and processes. An ISO numbering system is used to classify cleanrooms based on the maximum particles concentration that is accepted in the space. The maximum number concentration for a specific ISO class is a function of particle size. The requirements and instructions together with recommended practices for contamination control and monitoring in cleanrooms that are stated in the ISO 14644-1 standard (ANSI/IEST/ISO, 1999).

The regulation of the cleanrooms leads to a very small aerosol number concentration, especially for particles larger than 100 nm, which is the lower size limit for current contamination control in the cleanrooms. In the context of new particle formation and its dynamics, this means that the sinks for the precursor vapors and for newly formed clusters are very small due to the absence of background aerosol particles. Other sinks are deposition to wall surfaces and dilution due to the ventilation. Generally speaking, there is a competition between the formation of clusters from gaseous precursors and the removal processes for the growing clusters and precursor gases (McMurry and Friedlander, 1979; Kulmala et al., 2004b). With a similar precursor source rates, the reduced sinks can yield fast particle formation via gas-to-particle formation, if suitable vapors are present or emitted.

In **Paper IV** we wanted to explore the concentration of molecular clusters in a cleanroom environment and to find out, if new particle formation takes place in cleanrooms. Another aspect was to take an instrument that was previously used to study NFP, in laboratory and atmospheric environments and use it to extend the monitoring in cleanroom to sub-2 nm particles. This was not done prior to this study. Measurements were carried out during autumn 2014 (29 September to 7 December 2014) in a production facility operating in a suite of cleanrooms with different requirements for the particle number concentration (ISO Class 4–6). Airmodus A11 and a separate A20 CPC was used to measure number concentrations above 1 nm and 7.5 nm as well as the size distribution of clusters in the 1-2 nm size range. Details of the three sites inside the cleanroom facility are described in more detail in **Paper IV**. However, in brief, one of the sites was Atomic Layer Deposition (ALD) processing space that was occupied by around 30 machines, two-thirds these in thin film production use and the rest in research and development use (R&D). In the production machines, precursors such as solid phase manganese, zinc, titanium chlorides, gaseous ammonia, hydrogen sulfide, nitrogen, and liquid/gaseous trimethylaluminum (TMA) were used. The specifics of the R&D machines were a trade secret. The second measurement location was Indium Tin Oxide (ITO)-sputtering space where glass surfaces was coated with physical vapor deposition using a commercial machine and the last site, lithography site, accommodated self-built production line for coating the glass substrates.

3.3.1 PSM calibration with metal chlorides

During the cleanroom measurements (**Paper IV**), we had a good idea on the expected chemical composition of the aerosol particles in the measurement space where the highest concentrations were observed. Therefore, we preformed specific PSM calibration for these cleanroom clusters. The maximum number concentration was detected in the vicinity of Atomic Layer Deposition (ALD) processing. The highest peak concentrations were observed during weekday mornings, when the previous day production runs were completed, and the machines opened for maintenance and change of ALD-precursors. This was the likely source for the highest concentrations and the reason behind the decision to calibrate the PSM with similar precursors that are used in the ALD processes.

The calibration setup followed typical principles for the CPC calibration setup in the sub-3 nm size range, as explained in the section 2.2.1 (Figure 3). Manganese, zinc and aluminum chloride were heated in a tube furnace in a nitrogen atmosphere and passed through americium-241 neutralizer. An API-TOF-MS was used to measure the chemical composition of the particles formed in the furnace (Figure 16). After identifying that the sample was clean enough and consisted of large enough clusters, the particle source was connected to the DMA setup for the actual PSM calibration.

From the calibration results, we saw that the particles consisting of products from manganese chloride or zinc chloride particles had different detection efficiency curves compare to particles consisting aluminum chloride (Figure 16). However, the reason for the difference was not identified in this study. In the end, the calibration curves with $MnCl_2$ particles were used in the inversion of PSM data from the cleanroom because it was the middle curve between the other two calibration curves. Furthermore, the exact particle composition in the cleanroom was not known as it was not measured. Most likely it was a mixture of different compounds. Also, it is likely that the composition of the clusters formed during the particle/vapor emission episodes, times with the highest peak concentrations, differ from the ones observed in the absence of those. The size distribution measurements with the PSM depend on the inversion that rely on assumed detection efficiency curves. Therefore, the variability in the cluster chemical composition will lead to some uncertainty in the sizing accuracy of the instrument as well as to the inverted concentrations, but it should not alter the main findings of the study. The calibration results with manganese, zinc and aluminum chloride is presented in more detail in **Paper IV.**

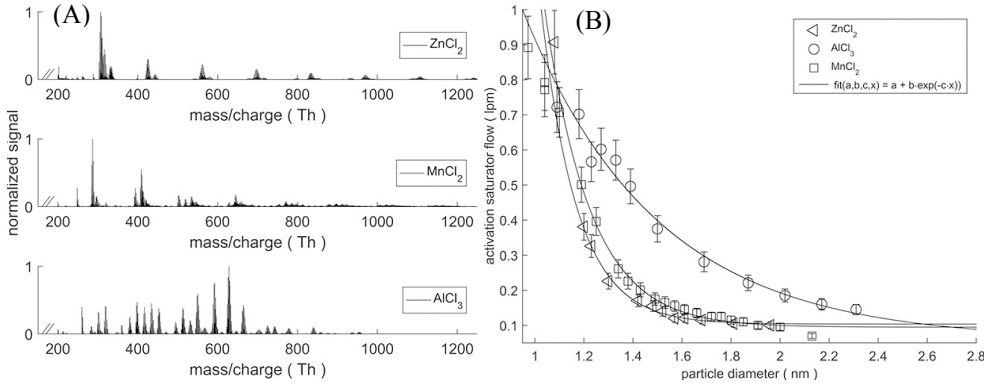

Figure 16. PSM's size calibration with particles produced from manganese, zinc and aluminum chloride. (A) The mass spectrum of the produced clusters was measured with API-TOF-MS (Tofwerk AG) prior to connecting the particles source to the calibration setup. (B) $Q_{activation}$ as function of particle diameter for all of the clusters which is the size calibration for the PSM. (adopted from **Paper IV**)

3.3.2 Concentration sub-2 nm clusters in the cleanroom

In **Paper IV**, we showed that there are sub-2 nm clusters present all the time also in the cleanroom environments where the measurements were carried out (Figure 17). The observed concentrations are likely to be influenced by characteristics of the specific cleanroom. There was no obvious diurnal pattern for the concentration of the smallest clusters, so the source is unlikely to be directly related to the activities in the space. In the ambient conditions, the concentration of cluster ions (ions < 1.8 nm) is known to be strongly dependent on the condensation sink, CS (Hirsikko et al., 2007b) and this should hold also for neutral particles. During our measurements, the sinks can be considered to be rather constant because the background aerosol concentration outside emission episodes (explained later next subsection) was really low, lower than 0.1 cm^{-3}, and the other sinks, namely deposition to clean room surfaces and dilution due to ventilation, did not change over time. Since the sinks and the observed concentrations were rather constant, the production rate of these sub-2 nm particles should have been quite stable.

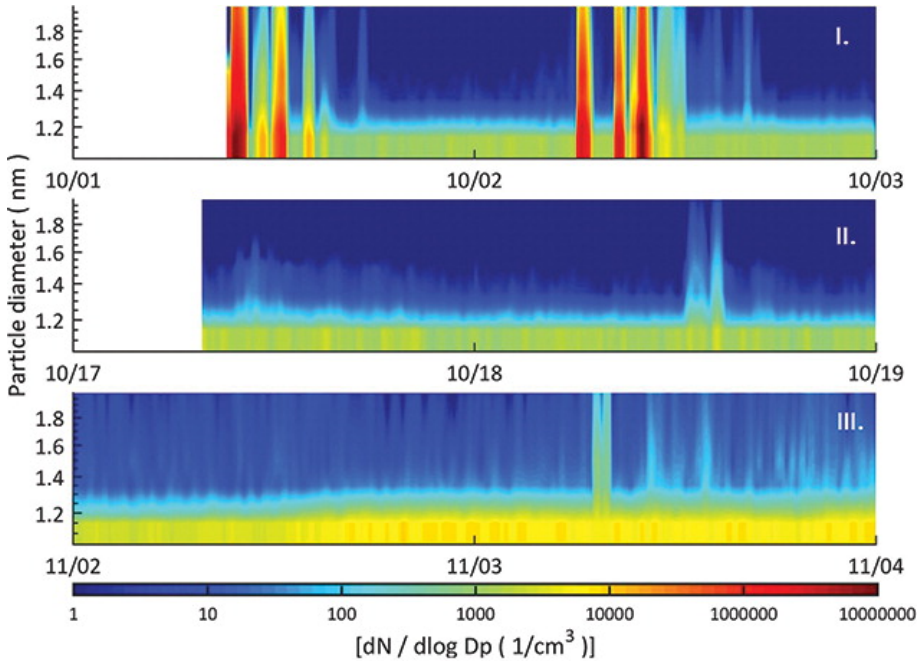

Figure 17. A particle size distribution at each of the three sampling sites as a two-day example: (I) ALD, (II) ITO-sputtering, and (III) lithography site. Clusters in the smallest size bins we observed in all the sampling sites. (adopted from **Paper IV**)

During the measurement we did not have the means to determine the charging state of clusters because the PSM used in the study did not have an ion filter attached and therefore the measured concentration was the total concentration of clusters, including both the charged and the neutral particles. We assumed that the observed particles and molecular clusters were formed inside the cleanroom via both gas-to-particle conversion and via ion pair production due to natural radioactivity and galactic cosmic rays and natural radioactivity of earth which are factors for ionization close to earth's surface (Harrison and Tammet, 2008). The production rate of ion pairs in a unit volume were estimated to be on the order of 4 to 8 $cm^{-3}s^{-1}$ which is a typical ionization rate at a continental surface level (Hirsikko et al., 2007a). Around 2 $cm^{-3}s^{-1}$ of the total ion pair production rate can be caused by cosmic rays. The ionization rate caused by radon can be much larger when radon gas accumulates due to limited ventilation or meteorological conditions, which is not the case in the cleanroom.

Other possible sources for the nanoparticles in the cleanroom could be infiltration from outside into the cleanroom (e.g. through entrances) or through a ventilation system, if the filtration efficiency is not good enough. First, if the clusters were to be infiltrated into the space, it is unlikely that there would not be any daily cycle observed. The use of clean rooms and thus the use of entrances and passages were limited to working hours and weekdays. We did not perceive any clear difference in the concentration of clusters between a weekday and weekend. Second, the filtration efficiency should increase towards the smaller more mobile particles that are more likely to collide with the fibers in the filter due to their high

diffusivity. Typically, the minimum of the filtration efficiency curve as a function of particles size lies somewhere in the range of a few hundreds of nanometers in the area between effective capture by diffusion (small particles) and the effective capture by impaction and interception (see for example Lee and Liu, 1982). However, there is a non-confirmed hypothesis that there might be a decrease of filtration efficiency for the small particles due to phenomenon called thermal rebound. The probability of aerosol particles to be captured upon a collision with the surface, is assumed to be unity in classical filtration theory. It was proposed by Dahneke (1971) that a particle with a sufficient kinetic energy can rebound from the surface. Wang and Kasper (1991) developed a model for the filtration efficiency incorporating particle rebound due to their thermal velocity. This model suggest that rebound of particles from the filter media may decrease the filtration efficiency in a size range of 1 to 10 nm, depending on the adhesion energies and temperature. Although there are some conflicting results on this matter (Givehchi and Tan, 2014), no solid experimental proof is shown at room temperatures. It is possible, for semi-volatile gases once captured into the filters, that they evaporate back into the gas phase (e.g. Volckens and Leith, 2003), and this way get inside the cleanroom. However, it would be unlikely that there was no diurnal variation if the precursors for clusters in the cleanroom if there were gases of outdoor origin. Considering these, we conclude that the observed clusters were most probably formed inside the cleanroom.

3.3.3 Occupational health aspect in cleanroom

A person inhales 10 000 liters of air per day on average and our respiratory track, upper and lower airways, forms the largest epithelial surface that is exposed to surroundings (Alenius et al., 2014). When measuring in the environment where people spend extended periods, such as in workplaces, there is always a human health aspect to be considered. Dust and inhaled aerosol particles are known to pose health risks once inhaled (e.g. Brunekreef and Holgate, 2002; Pope et al., 2009). The community have started for some time ago to be more concerned about number concentrations of ultrafine particles in addition to particulate mass concentrations (PM10 and PM2.5) implemented to air quality monitoring already earlier. Several studies have shown that ultrafine particles (Oberdorster et al., 2005; Elsaesser and Howard, 2012; Meng et al., 2013; Pawar and Kaul, 2014), as well as the elevated particulate mass concentrations (von Klot et al., 2005; Strak et al., 2012), may have harmful health effects. In a human respiratory system, aerosol particles are deposited onto different parts based on their size and inertia. Similarly, as in many other pathways, e.g. fiber filters, sampling lines etc., particle transmission is determined by familiar deposition mechanisms: diffusion, interception, impaction and gravitational settling (also electrostatic).

It has been known that particles of a certain size can reach alveolar region and cross cell boundaries and thus enter to blood stream through air-blood barrier (e.g. Oberdörster et al., 2004). In addition to particles that breach the pulmonary air-blood barrier, small aerosol particles can also enter human body *via* nasal olfactory route and be transported into the brain without crossing the strict blood-brain (e.g. Hopkins et al., 2018). In the top of the nasal cavity, the distance from the olfactory epithelia to olfactory bulb located in the frontal

lobe is just a few millimeters and small nanometer sized particles can be transported via the olfactory tract in to various parts of the brain (Alenius et al., 2014). This can be used for advantage in brain targeted drug delivery, but it also raises a concern whether this is a pathway for harmful contaminants from air. The small nanometer sized aerosol particles that readily deposit onto the nasal passage due to their rapid diffusion, can be directly adsorbed into the brain (Dong et al., 2018). Traditionally, it has been thought that the particles need to penetrate all the way down into the deepest parts of the respiratory system to enter our body or otherwise they are cleared by physiological removal processes such as mucociliary clearance (See e.g. Bustamante-Marin and Ostrowski, 2017).

During the cleanroom measurements we observed time periods when the particle number concentration above 1 nm was more than 10^5 cm^{-3} and in some occasions almost 10^6 cm^{-3}. During these peaks, concentrations of particles larger than 10 nm were higher than 10^4 cm^{-3} (Figure 18). These can be considered remarkably high concentrations in a working environment. The duration of the highest concentrations was short, at maximum a few tens of minutes, which kept the overall exposure for the operators relatively small, from around ($2 \cdot 10^4$ - $4 \cdot 10^4$) cm^{-3} at the highest (8-hour time-weighted average concentration). Although, in von Klot et al. (2005) cardiac readmissions increased already by 1 % per increase of 10^4 cm^{-3} in the particle number concentration. Expanding the routine particle monitoring to cover also the smallest particles should be encouraged, since it is known that the smallest particles may breach the physiological barriers and the health risk that the pose is not accurately known (Alenius et al., 2014). These high concentrations were observed only in one of the measurement rooms. More detailed comparison between the spaces and description of the measurement locations is presented in **Paper IV.**

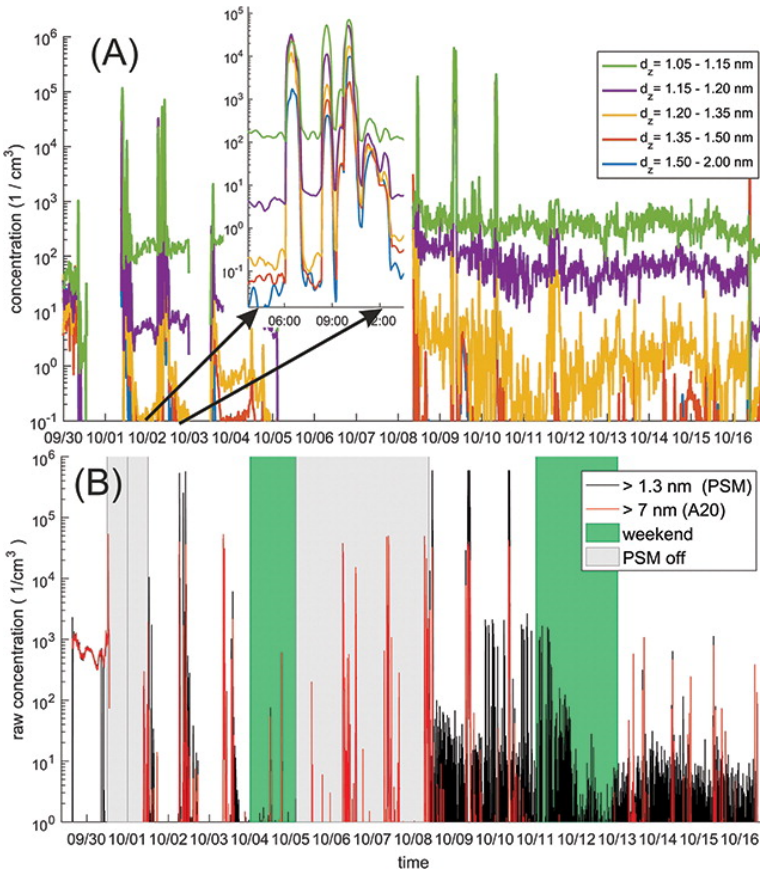

Figure 18. Time series of the number concentration measured at the ALD site. (a) Number concentration in different size classes in 1–2 nm size range. (b) Number concentration for particles above 7 nm measured with the A20 CPC and with the nCNC with a 1.4 nm cut-off diameter. The periods when the A11 was offline, are marked in the figure with light gray. (adopted from **Paper IV**)

3.5 Physical properties of laboratory generated Iodine pentoxide-iodic acid clusters

Biogenic emissions of iodine containing vapors have been linked to rapid new particle formation in coastal regions (Hoffmann et al., 2001; Mäkelä et al., 2002; O'Dowd et al., 2002; O'Dowd and Hoffmann, 2005; McFiggans et al., 2010). These gaseous iodine compounds are known to be emitted into the atmosphere by micro and macro algae in coastal regions but also from open ocean (e.g. Giese et al., 1999; Laturnus et al., 2000). In the studies reporting rapid nucleation bursts, the emissions were connected to the exposure of sea floor biota to atmospheric conditions during low-tide episodes (Mäkelä et al., 2002).

It has been proposed that coastal marine aerosol consists of oxidized iodine compounds, such as iodine pentoxide I_2O_5 (Saiz-Lopez and Plane, 2004), and supporting findings have been made in laboratory experiments conducted in a dry atmosphere (Saunders, 2006; Saunders, 2010). The reactions of gaseous iodine I_2 in the presence of O_3 and water leads to the formation of HIO_3 (Sunder and Vikis, 1987). Sipilä et al. (2016) showed via online mass spectrometry that HIO_3 forms fast-growing molecular clusters by a sequential addition of this molecule, showing a linear dependency with the cluster number concentration. Based on their measurements, gas-phase I_2O_5 concentration was low and not sufficiently high to explain the observed growth of the clusters. In the particle phase, hydration of clusters may affect, since hydration/dehydration converts HIO_3 and I_2O_5 into each other (Smith et al., 2017). In **Paper V** we contributed into this open question by measuring anions of iodine pentoxide–iodic acid hybrid clusters with ion mobility spectrometry methods.

3.5.1 Studying iodine pentoxide iodic acid clusters with ion mobility spectrometry

In **Paper V** we used DMA-MS measurements (see section 0) to study iodine pentoxide-iodic acid clusters in laboratory conditions. The clusters were produced via electrospray ionization in a carbon dioxide atmosphere to ensure stable electrospray conditions and to prevent arcing while using pure water as a solvent. We were able to measure singly charged anions up to a cluster containing seven iodine pentoxide molecules, corresponding to 2511 Dalton in mass. Clusters of the same composition were observed in Mace Head Atmospheric Research Station, in Ireland, during new particle formation events (Sipilä et al., 2016).

Figure 19a depicts a typical data obtained with the DMA-MS system. The ion signal is presented as a function of DMA voltage and mass-to-charge ratio where the signal intensity is shown in color scale. The clusters with different charge state form separate “line segments” that can be easily identified. However, if there is a lot of fragmentation, segments might become harder to distinguish from each other. When the ion signals corresponding to identified compounds is plotted, we get mass selected mobility spectrum (Figure 19b). This can be used to obtain corresponding mobilities and investigate the fragmentation of ions post mobility classification (in API). During the data analysis of this study (**Paper V**), we discarded multiply charged clusters from detailed analysis since they are a feature specific to

the electrospray ionization in this size range and plausibly do not reflect the atmospheric clustering.

We observed more than one mobility peak for all the specific compounds depicted here. First of the consecutive peaks corresponds to the cluster itself, the parent ion, and consequent peaks originate from the fragmentation of the larger less mobile clusters. When the larger ions of certain mobility fragment, we observe the corresponding ion signal at lower mass. This kind of fragmentation, taking place after the mobility analysis and before the mass measurement, produces coinciding peaks that align horizontally in the plot (Figure 19a). Depending on the application this can be either wanted or unwanted behavior. Nonetheless, it produces additional information on the parent ion which can be useful when identifying unknown compounds.

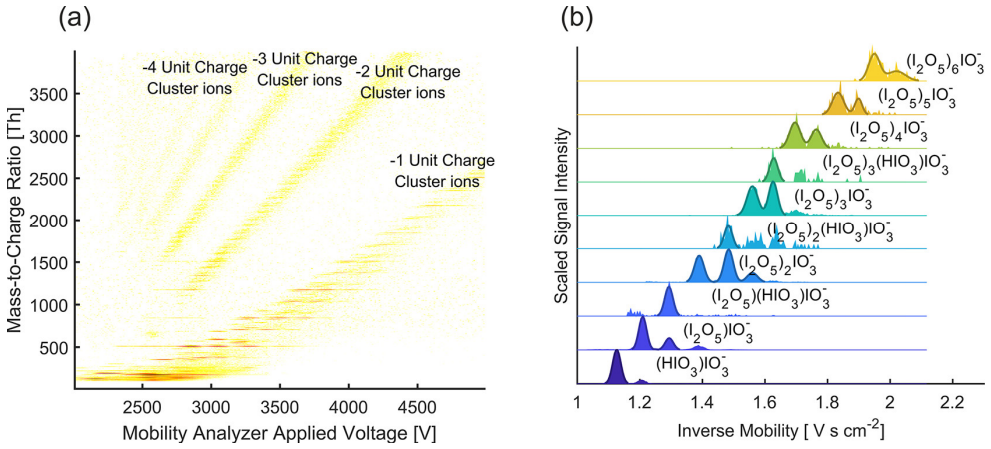

Figure 19. (a) Ion signal as a function of DMA voltage and mass-to-charge ratio m/z. (b) A mobility resolved mass spectrum were DMA voltage is converted to inverse mobility. Depicting signal for the identified clusters as a function of inverse mobility shows that there is more than one mobility peak corresponding to each mass. First peak corresponds to a unfragmented ion and the consequent peak that coincide with the larger clusters is a mark of the cluster fragmentation post the mobility classification. (adopted from Paper V)

Using the 2d-data we were able to measure the mobilities accurately for the identified clusters even when there was signal from other ions with a similar mobility or the signal was small. The relation between the mobility and applied DMA voltage (equation 11) was fixed with tetraheptylammonium$^+$ ion that has a known mobility in CO_2 (Fernández de la Mora et al., 2012). Experimental mobility values of identified clusters are reported in **Paper V** in a form of collision cross sections, CCS. Additionally, we were able to derive qualitative information on the cluster stability with respect to the clusters from sulfuric acid dimethyl amine system and alkali metal iodine cluster by comparing results to prior experiments that had used a similar experimental setup. Fragmentation of iodine pentoxide iodic acid cluster was observed to be much less pronounced than in prior studies with clusters of different

chemical composition. Even if the fragmentation in the API-interface is phenomenon specific to these types of instruments, it provides some information on how strongly molecules in the clusters are bound to each other. Therefore, we conclude that clusters from this chemical system seem to be quite stable (**Paper V**), which may be a contributor in the rapid new particle formation events reported in the coastal regions (Sipilä et al., 2016).

3.5.2 Comparison between computationally derived CCS to experimental results

In addition to measuring the collision cross section of iodine pentoxide iodic acid clusters in **Paper V,** we calculated computationally-derived collision cross sections for the same compounds. We utilized a configurational sampling based on a 'build-up approach' to generate candidate cluster structures (Jensen, 2007).

First, a large number of structures were generated and optimized using a computationally fast, low-level theory. Configurational sampling was performed by principles of molecular mechanics (intermolecular interactions were defined by CHARMM force field (Halgren, 1996a; 1996b; 1996c; Halgren and Nachbar, 1996; Vanommeslaeghe et al., 2010; Yu et al., 2012)). Subsequently, the energetically lowest structures were optimized at a high level of theory.

Since quantum chemistry calculations of clusters containing even a few iodine atoms start to be computationally expensive, we treated configurational sampling in two different ways. For the smallest clusters $(HIO_3)IO_3^-$, $(I_2O_5)IO_3^-$, and $(I_2O_5)(HIO_3)IO_3^-$, the structures were optimized using a density functional theory (DFT) at the ωB97xD//aug-cc-pVTZ-PP level. Larger clusters containing more than two iodine atoms and hydrated molecular clusters were treated with computationally less expensive method. This is described in detail in the supporting information of **Paper V**.

We used Ion Mobility Spectrometry Suite (IMoS) 1.08 (Larriba and Hogan, 2013b; Shrivastav et al., 2017) which is a MATLAB based software package to calculate collision cross section from all-atom models. The method is described in detail in Larriba and Hogan (2013a). We used IMoS to compute CCSs considering ion induced dipole potential with two scattering models: elastic hard-sphere scattering (EHSS) and diffused hard-sphere scattering (DHSS), in which gas molecules are re-emitted in a random diffused angle with a velocity sample from the Maxwell−Boltzmann distribution.

A comparison between the experimental and computationally-derived values of CSS is shown in Figure 19. The DHSS model showed a good agreement with experimental values. If there were multiple good, energetically low-lying, configurations found among the optimized structures, the CCS was simulated for all the these. We observed that the selection of scattering model makes larger difference to the CCS than the small changes in the cluster configuration. Together with the previous studies (Oberreit et al., 2015; Rawat et al., 2015), this enforces the idea that the simulated collision cross sections can be used in calculations,

when there are no experimental values available. This is particularly relevant when estimating the collision cross sections for the clusters in the specific hydration state for which the experimental data is typically not available.

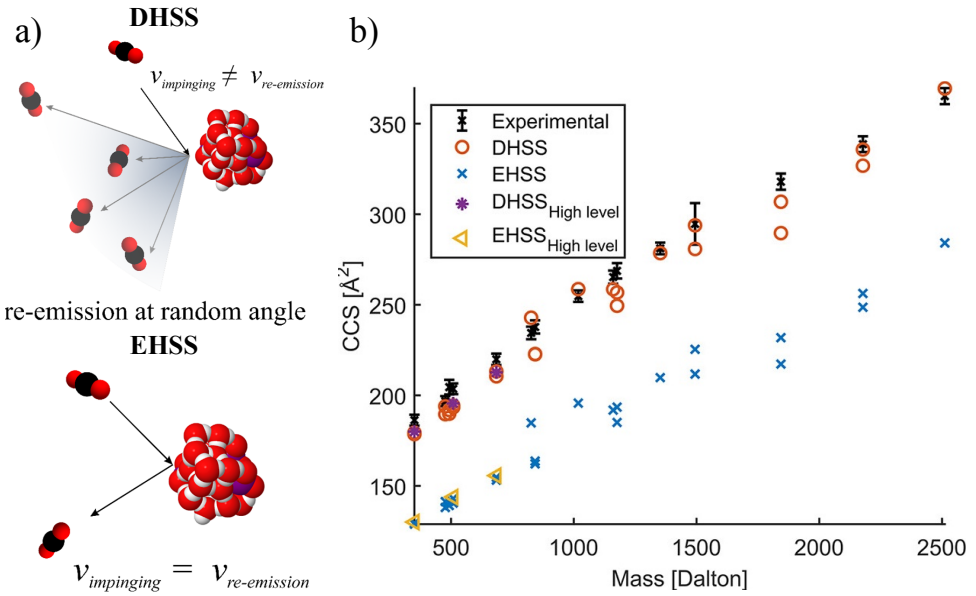

Figure 20. a) The main difference in the scattering models (will be re drawn with similar information). b) Comparison between measured *CCS* and computationally derived values. The diffuse scattering model give a good agreement with the experimental collision cross sections. (Right panel adopted from **Paper V**).

3.5.3 Hydration of iodine pentoxide clusters

Hydration of iodine pentoxide clusters was studied by adding water vapor into the background gas and performing the DMA-MS analysis to the clusters with a variable mixing ratio of water vapor. In practice, the compensation flow into the DMA was humidified with a self-built heated nebulizer. Thereby, ions were produced and analyzed in a background gas, which was a mixture of water and carbon dioxide molecules. The gas-phase water concentration was calculated based on the flow rate of CO_2 and liquid flow rate that was federated by a syringe pump. This was compared against a reading from a chilled mirror dew point meter (Figure 9). The setup is explained in more detail in the supporting information of **Paper V**. If water molecules attach to the iodine clusters, even for momentarily, there is a shift in the mobility, which is measurable even if water is dissociated in the mass spectrometer API-interface.

In **Paper V**, the CSS was measured as a function of saturation ratio between 0 and 0.65, and we observed a slight but measurable change in the CSS, around 10% at maximum. From the measured shift in CCS, we cannot directly deduce how many water molecules there have been, but additional information is needed. This is because we measured an average *CCS* of

the whole population having certain iodine containing clusters together with different number $g = 1,2,3, \ldots$ of water molecules. Each of the clusters will have their own specific CCS_g depending on the amount of water associated with the cluster and influenced by the internal configuration of the cluster.

The observed CCS is the mean of all the CCS_g weighted by their prominence, i.e., a probability P_g of having such a number of water molecules bound into the cluster. The probability is dependent on factors such as humidity, temperature and cluster composition. In addition, the amount of water in each cluster is not static either and there is adsorption and desorption happening along the path as the clusters traverse through the DMA (Figure 20). In the supplementary of **Paper V**, there is a detailed derivation of how the measured change in the CCS relates to P_g and g when taking into account the mixture of gases as a background gas.

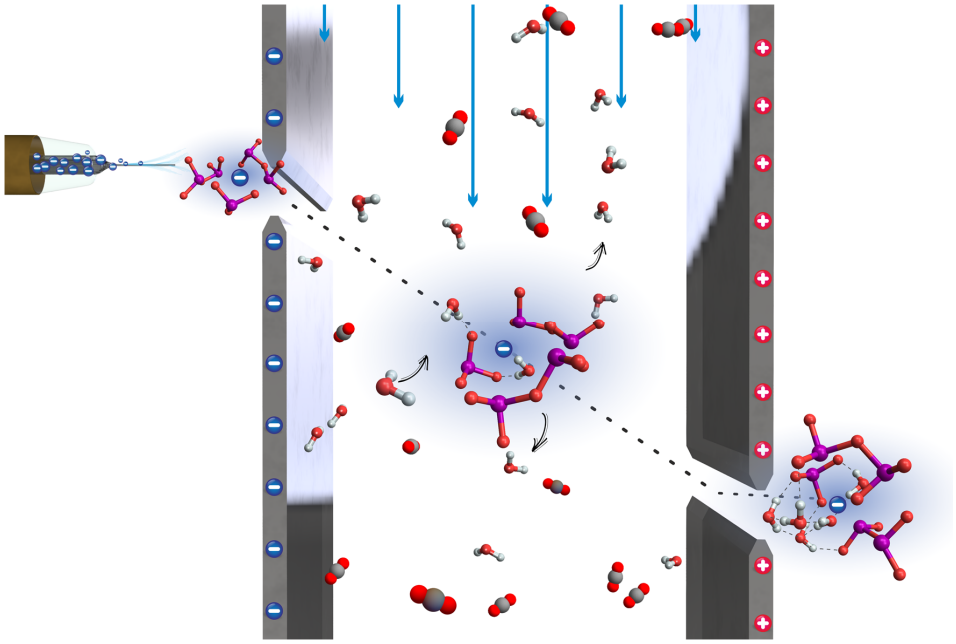

Figure 21 An illustration of clusters traversing through the DMA when sheath air is conditioned with water vapor.

We used computationally-derived CCS values to estimate the amount of change in the CCS that the addition of certain amount g of water molecules induce. This was verified against data from unhydrated molecular clusters. Structures for iodine pentoxide clusters containing from zero to 20 molecules was build up and optimized using a computationally less expensive method utilizing Artificial Bee Colony (ABC) algorithm. The $CCS_{g,i}$ (i=H_2O,CO_2) was simulated again with IMoS using both CO_2 and water as a background gas, as the measurements were carried out in a mixture of CO_2 and water. The collision cross sections in CO_2 and H_2O, were treated in additive manner following Blanc's law (Revercomb and Mason, 1975).

By looking at the change in the modelled collision cross sections as function of water molecules bound, we were able to roughly estimate how many water molecules is needed to explain the observed ~10% shift. A Languir-like model (Rawat et al., 2015; Li and Hogan, 2017) was used to get quantitative information on the of hydration using a best fit method. Based on the data presented in **Paper V**, we concluded that the iodic acid clusters were only mildly hydrated when the saturation ratio of water was less than 0.65. The number of water molecules in the clusters did not exceed greatly the amount needed to facilitate the conversion from I_2O_5 into HIO_3.

The results of **Paper V** gave insight into the properties of iodine pentoxide−iodic acid hybrid clusters that are also encountered in coastal regions during new particle formation events. The clusters where observed to be rather stable, qualitatively, against fragmenting in the mass spectrometers API interface indicating that they are likely to be stable also in ambient conditions.

These clusters were observed to be hydrated enough to facilitate the conversion from I_2O_5 into HIO_3, however the sorption of water molecules beyond this point was not prominent in relative humidifies smaller than 65 %. Upon the hydration the CCS shifted maximum of around 10%. The good agreement with modelled CCSs and experimental values suggests that the computational method can capture the global features in the clusters, even when computationally less expensive method that needs to be used for large iodine containing clusters. This could be used to study also uptake other vapor, e.g. amines, onto large iodine containing clusters that are computationally demanding.

4 Review of papers and the author's contribution

Paper I shows how two commercial condensation particle counters, TSI 3772 and Airmodus A20, can be set up to detect aerosol particles with diameters smaller than 3 nm. Especially TSI 3772 is a commonly used detector in a variety of applications, such as Electrical Mobility Spectrometers. The operating temperatures were set up to maximize the detection efficiency for small particles yet maintaining small number of false counts from homogenous nucleation. Further, in the case of A20 the effect of sample flow rate was also investigated. A Computational Fluid Dynamic (CFD) simulation was conducted to support the study. Theoretical estimation for the detection efficiency was calculated based on the supersaturation field and expected instruments internal losses due to diffusion. I performed the simulation with CFD model run with COMSOL Multiphysics, that was used in this article and performed the nucleation calculations. I participated in writing and data interpretation.

Paper II shows a comparison of atmospheric sub-3 nm aerosol particle concentration measurements conducted with PSM from nine sites located worldwide. The diurnal variation of sub-3 nm particle concentration was presented from all the locations, and the influences of environmental conditions, such as sulfuric acid concentration derived from a proxy, were studied. Additionally, the relative fractions of sub-3 nm ions and total particles were reported from the sites where ion spectrometer data were available. Seasonal changes in the diurnal cycles were investigated at SMEAR II (Hyytiälä) and SMEAR III (Helsinki) stations, where data coverage was adequate. I was the responsible person taking care of our permanent Particle Size Magnifier measurements in SMEAR II (2014, 2015) and SMEAR III (2015). I contributed to the pre-treatment of the data, especially for the instruments with automatic background measurement inlet and participated in the data interpretation and commented on the manuscript.

Paper III presents a Differential Mobility Particles Sizer (DMPS) system optimized for sub-10 nm aerosol particles. The article presents a laboratory characterization of the mobility analyzer with respect to its resolving power and transmission, detection efficiency of the A10 with suitable settings for DMPS use and the total transmission of the combined instrument. The instrument was taken to the SMEAR III field station (Hyytiälä) for comparison measurements against a long-term DMPS system with a more typical design. The comparison yielded a result that the DMPS system optimized for sub-10 nm particles showed twice the concentration of 3 nm particles compared to the standard DMPS, and that this discrepancy decreased towards larger particles, almost disappearing close to the 10 nm size. I participated in the development and early tests of the instrument, participated in the operating and monitoring the instrument in the field measurements, and commented on the manuscript.

Paper IV investigates the formation or/and release of aerosol particles in a cleanroom. We measured the total number concentrations of aerosol particles larger than about 1 nm and 10 nm in diameter during a measurement campaign in a production facility with cleanrooms of different size and cleanliness. Additionally, a particle number size distribution was obtained

in the 1-2 nm size range. Later, the particle size magnifier was calibrated in a laboratory with particles produced from similar starting materials that were used in the machines suspected to be a source observed particle emissions. I operated the instruments during the measurement campaign and was responsible for the data analysis. In addition, I performed the laboratory calibrations for the PSM and wrote most of the article.

Paper V examines iodine pentoxide – iodic acid clusters, their mobility, hydration and their stability qualitatively. In the study we produced iodine pentoxide – iodic acid cluster via electrospray ionization, measured their mobility resolved mass spectrum and calculated collision cross section (CSS) for the identified clusters in a carbon dioxide atmosphere. Furthermore, we measured the hydration of these clusters using the experimental data and computational methods. To estimate the state of hydration we deployed density functional theory (DFT) calculations and configuration sampling via Artificial Bee Colony (ABC) algorithm to obtain energetically low-lying structures for the clusters containing varying amount of water. The CSS was calculated for computationally these structures using Ion Spectrometry Suite (IMoS) with two different scattering models. Computationally-derived CCS values were compared against experimental values in the case of unhydrated clusters. Once validated by the comparison, these were used to estimated change in the CSS due to water molecules adsorbed to the clusters. I performed the experiments, conducted the data-analysis based on the experimental data and computationally modelled cluster structures that was calculated by other authors, and participated in writing the article.

5 Conclusions and outlook

We showed in **Paper I** that 3772 and A20 CPCs can be used to detect sub-3 nm particles by using temperature settings higher than nominal temperature difference between the saturator and condenser. These two studied instruments are more affordable and simpler than instruments purposely built for the detection of sub-3 nm particles. With optimized sample flowrate and allowing a small number of background counts, the detection efficiency can be enhanced even further. This can be utilized in applications where a few false counts are tolerable, such as CPC batteries which can measure rudimentary size distribution without prior mobility analysis. For these CPCs, internal losses proved to be more of a limiting factor compared to the activation efficiency for detection of sub-3 nm particles (*objective ii*).

Long-term measurements with the PSM were established in SMEAR II and SMEAR III stations and performed with the best knowledge available at the time, based on experience and prior laboratory work (Kangasluoma et al., 2013; 2014; 2015; 2016b) (*objective iii*). These data were utilized in comparison with other available PSM data sets from varying locations. The concentrations of sub-3 nm particles were observed to vary greatly between different types of measurement locations. From the nine sites, the highest concentrations were observed in locations with the highest anthropogenic influence. The concentration of particles smaller than 3 nm was found to be the highest during daytime at all the sites. Higher daytime particle concentrations are likely linked with the photochemical production of low-volatile precursor gases. Relatively high nighttime particle concentrations, observed in many of the sites, indicate that the sub-3 nm particles were also formed in the absence of sun light. Longer data sets from the SMEAR stations enabled seasonal comparison in Hyytiälä and Helsinki. The particle concentrations varied considerably between the seasons in Hyytiälä (SMEAR II). In the smallest sizes, concentrations were the highest during summer and autumn when biogenic emissions are also the highest (Rantala et al., 2015). On the other hand, the ratio between the 2-3 nm particles above 1-2 nm particles, as well as the 2-3 nm number concentration, were the highest during the springtime which is also, on average, the season with the highest frequency of new particle formation events in Hyytiälä (Nieminen et al., 2018). In Helsinki, influenced less by biogenic emissions, the seasonal differences were less noticeable (*objective ii*).

The new DMPS system, specially designed to measure sub-10 nm particle number size distribution, was characterized and set up into comparison measurement in the field station (**Paper III)**. The benefits compared to the more traditional harmonized DMPS system were identified, but also improvements for further revisions was found (*objective ii*). Due to the optimized overall transmission, the amount of raw counts was four to nine times more than in the typical DMPS device, decreasing the counting uncertainty to a half. Larger undiluted sample flowrate was also recognized to be factor contributing to the improved sensitivity in 3 to 10 nm size range. On average, the current HFDMPS system measured 1.8 times higher particle concentrations than the compared DMPS system in this size range. Based on the results, we can argue that a CPC with large sample flow that is optimized for detection of

sub-3 nm particle would be a great detector for the sub-10 nm size fraction of a DMPS/SMPS.

In **Paper II**, the fraction of charged particles in the sub-3 nm size range was investigated from the comparison of PSM data and ion concentrations from AIS/NAIS. Occasionally, the ion fraction appeared to exceed unity in Hyytiälä, which means that the PSM was most likely underestimating the total particle concentration below 3 nm. This is an aspect that should be further investigated and considered if the measurement procedure could be further improved. For example, the PSM should be tuned to the higher operating settings in sites where particles are mainly composed of oxidation products of monoterpenes. A repeatable and reproducible method for producing particles composed of oxidized organics, is needed in PSM calibrations, in order to have representative calibration for these types of environments. Additionally, *in situ* calibrations that would be conducted at the measurement sites, should be considered. The HFDMPS presented in **Paper III** is portable and capable of a high resolving power. In conjunction with an additional concentration reference and a particle source, it could be used also as a field calibration unit.

We studied the existence and formation of sub-3 nm particles in cleanroom environments with the PSM and a CPC. Based on **Paper IV**, small clusters are present in cleanroom environment even when there was no clear emission or particle release episode taking place. Particle formation bursts, with concentrations more than 10^5 cm^{-3}, were observed in the midst of the manufacturing machines. These were most likely related to the maintenance cycles of the production machines. The rapid particle formation was probably caused by combinations of supersaturated vapors released from machines and the very low condensation sink caused by the absence of accumulation and coarse mode particles. During these short periods, the particle number concentration was extremely high, but due to the short duration the overall exposure for the workers can be expected to be rather small. Anyhow, expanding the monitoring to sub-3 nm particles is important, since health risks posed by nanometer sized particles are poorly known. The PSM proved to be suitable for monitoring the number concentration also in the cleanroom, extending the size range down around 1 nm (**Paper IV**). Even if the PSM has typically a higher background signal compared to a bare CPC, it is still sufficiently sensitive for the measurements in the cleanroom (*objective iv*).

Physical properties of iodine oxide iodic acid clusters where studied in **Paper V**. Collision cross sections for iodine pentoxide iodic acid clusters was measured up to cluster containing seven iodine pentoxide clusters and compared to computationally derived CCSs. The comparison resulted a remarkably good agreement using the diffused scattering model without any tweaks in the model parameters. Together with prior studies (e.g. Oberreit et al., 2015; Rawat et al., 2015), this strengthens the confidence to the use of modelled CSS values when measured values are not available. It can be used to predict mobilities for molecules or molecular clusters of interest and derive quantities that are not directly measurable. In **Paper V,** this was utilized to examine the hydration of iodine pentoxide iodic acid clusters. The studied clusters were produced and analyzed in a background gas containing varying amount of water. The shift in the CSS due to the added water molecules in the clusters was modelled and compared against the measured shift. Because the extent of hydration was not directly

measurable, the modelled CCS of the hydrated clusters were necessary. Based on a simple Langmuir-like model, clusters were observed to be only moderately hydrated (*objective i*). These iodine oxide iodic acid clusters proved to be quite stable against the fragmentation in API, suggesting that they can be relatively stable also in ambient air. This may be a contributor to the rapid cluster growth by sequential addition of iodic acid molecules that is observed in Sipilä et al. (2016) to take place in the coastal marine site.

6 References

Aalto, P., Hämeri, K., Becker, E., Weber, R., Salm, J., Mäkelä, J. M., Hoell, C., O'Dowd, C. D., Hansson, H.-C., Väkevä, M., Koponen, I. K., Buzorius, G., and Kulmala, M. (2001). Physical characterization of aerosol particles during nucleation events. *Tellus B: Chemical and Physical Meteorology, 53*(4), 344-358. doi:10.3402/tellusb.v53i4.17127

Aitken, J. (1888). On the Number of Dust Particles in the Atmosphere. *37*(957), 428-430. doi:10.1038/037428a0

Alanen, J., Saukko, E., Lehtoranta, K., Murtonen, T., Timonen, H., Hillamo, R., Karjalainen, P., Kuuluvainen, H., Harra, J., Keskinen, J., and Rönkkö, T. (2015). The formation and physical properties of the particle emissions from a natural gas engine. *162*, 155-161. doi:10.1016/j.fuel.2015.09.003

Alanen, J., Simonen, P., Saarikoski, S., Timonen, H., Kangasniemi, O., Saukko, E., Hillamo, R., Lehtoranta, K., Murtonen, T., Vesala, H., Keskinen, J., and Rönkkö, T. (2017). Comparison of primary and secondary particle formation from natural gas engine exhaust and of their volatility characteristics. *Atmos. Chem. Phys., 17*(14), 8739-8755. doi:10.5194/acp-17-8739-2017

Albrecht, B. A. (1989). Aerosols, Cloud Microphysics, and Fractional Cloudiness. *Science, 245*(4923), 1227-1230. doi:10.1126/science.245.4923.1227

Alenius, H., Catalán, J., Lindberg, H., Norppa, H., Palomäki, J., and Savolainen, K. (2014). Nanomaterials and Human Health. In (eds (pp. 59-133): Elsevier. doi:10.1016/b978-0-12-416604-2.00003-2

Amo-González, M., and Pérez, S. (2018). Planar Differential Mobility Analyzer with a Resolving Power of 110. *Analytical Chemistry, 90*(11), 6735-6741. doi:10.1021/acs.analchem.8b00579

ANSI/IEST/ISO. (1999). ANSI/IEST/ISO 14644-1: 1999. Cleanrooms and Associated Controlled Environments—Part 1: Classification of Air Cleanliness.

Bianchi, F., Kurten, T., Riva, M., Mohr, C., Rissanen, M. P., Roldin, P., Berndt, T., Crounse, J. D., Wennberg, P. O., Mentel, T. F., Wildt, J., Junninen, H., Jokinen, T., Kulmala, M., Worsnop, D. R., Thornton, J. A., Donahue, N., Kjaergaard, H. G., and Ehn, M. (2019). Highly Oxygenated Organic Molecules (HOM) from Gas-Phase Autoxidation Involving Peroxy Radicals: A Key Contributor to Atmospheric Aerosol. *Chemical Reviews, 119*(6), 3472-3509. doi:10.1021/acs.chemrev.8b00395

Bianchi, F., Trostl, J., Junninen, H., Frege, C., Henne, S., Hoyle, C. R., Molteni, U., Herrmann, E., Adamov, A., Bukowiecki, N., Chen, X., Duplissy, J., Gysel, M., Hutterli, M., Kangasluoma, J., Kontkanen, J., Kurten, A., Manninen, H. E., Munch, S., Perakylä, O., Petäjä, T., Rondo, L., Williamson, C., Weingartner, E., Curtius, J., Worsnop, D. R., Kulmala, M., Dommen, J., and Baltensperger, U. (2016). New particle formation in the free troposphere: A question of chemistry and timing. *Science, 352*(6289), 1109-1112. doi:10.1126/science.aad5456

Bocksell, T. L., and Loth, E. (2001). Random walk models for particle diffusion in free-shear flows. *Aiaa Journal, 39*(6), 1086-1096. doi:Doi 10.2514/2.1421

Boucher, O., Randall, D., Artaxo, P., Bretherton, C., Feingold, G., Forster, P., Kerminen, V. M., Kondo, Y., Liao, H., Lohmann, U., Rasch, P., Satheesh, S. K., Sherwood, S., Stevens, B., and Zhang, X. Y. (2013). Clouds and aerosols. In Climate Change 2013: The Physical Science Basis. Contribution of Working Group I to the Fifth Assessment Report of the Intergovernmental Panel on Climate Change (eds T. F. Stocker, D. Qin, G. K. Plattner, M. Tignor, S. K. Allen, J. Doschung, A. Nauels, Y. Xia, V. Bex, & P. M. Midgley) (pp. 571-657). Cambridge, UK: Cambridge University Press. doi:10.1017/CBO9781107415324.016

Brunekreef, B., and Holgate, S. T. (2002). Air pollution and health. *The Lancet, 360*(9341), 1233-1242. doi:https://doi.org/10.1016/S0140-6736(02)11274-8

Bustamante-Marin, X. M., and Ostrowski, L. E. (2017). Cilia and Mucociliary Clearance. *Cold Spring Harbor Perspectives in Biology, 9*(4), a028241. doi:10.1101/cshperspect.a028241

Cai, R., Attoui, M., Jiang, J., Korhonen, F., Hao, J., Petäjä, T., and Kangasluoma, J. (2018a). Characterization of a high-resolution supercritical differential mobility analyzer at reduced flow rates. *Aerosol Science and Technology, 52*(11), 1332-1343. doi:10.1080/02786826.2018.1520964

Cai, R., Jiang, J. K., Mirme, S., and Kangasluoma, J. (2019). Parameters governing the performance of electrical mobility spectrometers for measuring sub-3 nm particles. *Journal of Aerosol Science, 127*, 102-115. doi:10.1016/j.jaerosci.2018.11.002

Cai, R., Yang, D., Ahonen, L. R., Shi, L., Korhonen, F., Ma, Y., Hao, J., Petäjä, T., Zheng, J., Kangasluoma, J., and Jiang, J. (2018b). Data inversion methods to determine sub-3 nm aerosol size distributions using the Particle Size Magnifier. *Atmos. Meas. Tech. Discuss., 2018*, 1-32. doi:10.5194/amt-2018-35

Cheng, Y.-S. (2011). Condensation Particle Counters. In Aerosol Measurement. In Aerosol Measurement (eds P. Kulkarni, P. A. Baron, & K. Willeke) (3rd ed.). doi:doi:10.1002/9781118001684.ch17

Chu, B. W., Kerminen, V. M., Bianchi, F., Yan, C., Petäjä, T., and Kulmala, M. (2019). Atmospheric new particle formation in China. *Atmospheric Chemistry and Physics, 19*(1), 115-138. doi:10.5194/acp-19-115-2019

Dahneke, B. (1971). The capture of aerosol particles by surfaces. *Journal of Colloid and Interface Science, 37*(2), 342-353. doi:https://doi.org/10.1016/0021-9797(71)90302-X

Debevec, C., Sauvage, S., Gros, V., Sellegri, K., Sciare, J., Pikridas, M., Stavroulas, I., Leonardis, T., Gaudion, V., Depelchin, L., Fronval, I., Sarda-Esteve, R., Baisnee, D., Bonsang, B., Savvides, C., Vrekoussis, M., and Locoge, N. (2018). Driving parameters of biogenic volatile organic compounds and consequences on new particle formation observed at an eastern Mediterranean background site. *Atmospheric Chemistry and Physics, 18*(19), 14297-14325. doi:10.5194/acp-18-14297-2018

Dong, J., Shang, Y., Inthavong, K., Chan, H.-K., and Tu, J. (2018). Numerical Comparison of Nasal Aerosol Administration Systems for Efficient Nose-to-Brain Drug Delivery. *Pharmaceutical Research, 35*(1). doi:10.1007/s11095-017-2280-6

Ehn, M., Thornton, J. A., Kleist, E., Sipilä, M., Junninen, H., Pullinen, I., Springer, M., Rubach, F., Tillmann, R., Lee, B., Lopez-Hilfiker, F., Andres, S., Acir, I.-H., Rissanen, M., Jokinen, T., Schobesberger, S., Kangasluoma, J., Kontkanen, J., Nieminen, T., Kurtén, T., Nielsen, L. B., Jørgensen, S., Kjaergaard, H. G., Canagaratna, M., Maso, M. D., Berndt, T., Petäjä, T., Wahner, A., Kerminen, V.-M., Kulmala, M., Worsnop, D. R., Wildt, J., and Mentel, T. F. (2014). A large source of low-volatility secondary organic aerosol. *Nature, 506*(7489), 476-479. doi:10.1038/nature13032

Eiceman, G. A., Hill, H. H., and Karpas, Z. (2013). *Ion Mobility Spectrometry* (Vol. Third edition). Boca Raton: CRC Press.

Elsaesser, A., and Howard, C. V. (2012). Toxicology of nanoparticles. *Advanced Drug Delivery Reviews, 64*(2), 129-137. doi:10.1016/j.addr.2011.09.001

Fernández de la Mora, J., Borrajo-Pelaez, R., and Zurita-Gotor, M. (2012). Capillary and Coulombic Effects on the Gas Phase Structure of Electrosprayed Concanavalin A Ions and Its Clusters C-n(+z) (n=1-6). *Journal of Physical Chemistry B, 116*(33), 9882-9898. doi:10.1021/jp210693z

Fernández de la Mora, J., and Kozlowski, J. (2013). Hand-held differential mobility analyzers of high resolution for 1–30nm particles: Design and fabrication considerations. *Journal of Aerosol Science, 57*, 45-53. doi:10.1016/j.jaerosci.2012.10.009

Fernández de la Mora, J., Ude, S., and Thomson, B. A. (2006). The potential of differential mobility analysis coupled to MS for the study of very large singly and multiply charged proteins and protein complexes in the gas phase. *Biotechnology Journal, 1*(9), 988-997. doi:10.1002/biot.200600070

Flagan, R. C. (1998). History of Electrical Aerosol Measurements. *28*(4), 301-380. doi:10.1080/02786829808965530

Flagan, R. C. (2011). Electrical Mobility Methods for Submicrometer Particle Characterization. In Aerosol Measurement (eds P. Kulkarni, P. A. Baron, & K. Willeke). doi:10.1002/9781118001684.ch15

Fletcher, N. H. (1958). Size Effect in Heterogeneous Nucleation. *The Journal of Chemical Physics, 29*(3), 572-576. doi:10.1063/1.1744540

Fu, Y., Xue, M., Cai, R., Kangasluoma, J., and Jiang, J. (2019). Theoretical and experimental analysis of the core sampling method: Reducing diffusional losses in aerosol sampling line. *Aerosol Science and Technology, 53*(7), 793-801. doi:10.1080/02786826.2019.1608354

Fuchs, N. A., and Sutugin, A. G. (1965). Coagulation rate of highly dispersed aerosols. *20*(6), 492-500. doi:10.1016/0095-8522(65)90031-0

Gabelica, V., Shvartsburg, A. A., Afonso, C., Barran, P., Benesch, J. L. P., Bleiholder, C., Bowers, M. T., Bilbao, A., Bush, M. F., Campbell, J. L., Campuzano, I. D. G., Causon, T., Clowers, B. H., Creaser, C. S., De Pauw, E., Far, J., Fernandez-Lima, F., Fjeldsted, J. C., Giles, K., Groessl, M., Hogan, C. J., Hann, S., Kim, H. I., Kurulugama, R. T., May, J. C., McLean, J. A., Pagel, K., Richardson, K., Ridgeway, M. E., Rosu, F., Sobott, F., Thalassinos, K., Valentine, S. J., and Wyttenbach, T. (2019). Recommendations for reporting ion mobility Mass Spectrometry

measurements. *Mass Spectrometry Reviews, 38*(3), 291-320. doi:10.1002/mas.21585

Gamero-Castaño, M., and Fernández de la Mora, J. (2000). A CONDENSATION NUCLEUS COUNTER (CNC) SENSITIVE TO SINGLY CHARGED SUB-NANOMETER PARTICLES. *Journal of Aerosol Science, 31*(7), 757-772. doi:https://doi.org/10.1016/S0021-8502(99)00555-8

Giechaskiel, B., Wang, X., Gilliland, D., and Drossinos, Y. (2011). The effect of particle chemical composition on the activation probability in n-butanol condensation particle counters. *42*(1), 20-37. doi:10.1016/j.jaerosci.2010.10.006

Giese, B., Laturnus, F., Adams, F. C., and Wiencke, C. (1999). Release of Volatile Iodinated C1−C4Hydrocarbons by Marine Macroalgae from Various Climate Zones. *Environmental Science & Technology, 33*(14), 2432-2439. doi:10.1021/es980731n

Givehchi, R., and Tan, Z. C. (2014). An Overview of Airborne Nanoparticle Filtration and Thermal Rebound Theory. *Aerosol and Air Quality Research, 14*(1), 45-63. doi:10.4209/aaqr.2013.07.0239

Gomez, A., and Deng, W. (2011). Fundamentals of Cone-Jet Electrospray. In Aerosol Measurement (eds P. Kulkarni, P. A. Baron, & K. Willeke) (3rd ed.). doi:10.1002/9781118001684.ch20

Gormley, P. G., and Kennedy, M. (1949). Diffusion from a Stream Flowing through a Cylindrical Tube. *Proceedings of the Royal Irish Academy. Section A: Mathematical and Physical Sciences, 52*, 163-169.

Griffiths, J. (2008). A Brief History of Mass Spectrometry. *Analytical Chemistry, 80*(15), 5678-5683. doi:10.1021/ac8013065

Guilhaus, M., Selby, D., and Mlynski, V. (2000). Orthogonal acceleration time-of-flight mass spectrometry. *Mass Spectrometry Reviews, 19*(2), 65-107. doi:10.1002/(sici)1098-2787(2000)19:2<65::aid-mas1>3.0.co;2-e

Halgren, T. A. (1996a). Merck molecular force field. I. Basis, form, scope, parameterization, and performance of MMFF94. *Journal of Computational Chemistry, 17*(5-6), 490-519. doi:doi:10.1002/(SICI)1096-987X(199604)17:5/6<490::AID-JCC1>3.0.CO;2-P

Halgren, T. A. (1996b). Merck molecular force field. II. MMFF94 van der Waals and electrostatic parameters for intermolecular interactions. *Journal of Computational Chemistry, 17*(5-6), 520-552. doi:doi:10.1002/(SICI)1096-987X(199604)17:5/6<520::AID-JCC2>3.0.CO;2-W

Halgren, T. A. (1996c). Merck molecular force field. III. Molecular geometries and vibrational frequencies for MMFF94. *Journal of Computational Chemistry, 17*(5-6), 553-586. doi:doi:10.1002/(SICI)1096-987X(199604)17:5/6<553::AID-JCC3>3.0.CO;2-T

Halgren, T. A., and Nachbar, R. B. (1996). Merck molecular force field. IV. conformational energies and geometries for MMFF94. *Journal of Computational Chemistry, 17*(5-6), 587-615. doi:doi:10.1002/(SICI)1096-987X(199604)17:5/6<587::AID-JCC4>3.0.CO;2-Q

Harrison, G., and Tammet, H. (2008). Ions in the Terrestrial Atmosphere and Other Solar System Atmospheres. In Planetary Atmospheric Electricity (eds M. B. Karen Aplin) (pp. 107-118). New York, NY, UNITED STATES: Springer.

Hering, S. V., and Stolzenburg, M. R. (2005). A Method for Particle Size Amplification by Water Condensation in a Laminar, Thermally Diffusive Flow. *39*(5), 428-436. doi:10.1080/027868290953416

Hinds, W. C., kirjoittaja. (1999). *Aerosol technology : properties, behavior, and measurement of airborne particles*. In. Retrieved from http://login.libproxy.helsinki.fi/login?url=http://search.ebscohost.com/login.aspx?direct=true&scope=site&db=nlebk&db=nlabk&AN=531512

https://helka.finna.fi/Record/helka.3171434

Hirsikko, A., Kulmala, M., Paatero, J., and Hatakka, J. (2007a). The 222Rn activity concentration, external radiation dose and air ion production rates in a boreal forest in Finland between March 2000 and June 2006. *Boreal Environment Research, 12*(3), 265-278.

Hirsikko, A., Yli-Juuti, T., Nieminen, T., Vartiainen, E., Laakso, L., Hussein, T., and Kulmala, M. (2007b). Indoor and outdoor air ions and aerosol particles in the urban atmosphere of Helsinki: characteristics, sources and formation. *Boreal Environment Research, 12*(3), 295-310.

Hoffmann, T., O'Dowd, C. D., and Seinfeld, J. H. (2001). Iodine oxide homogeneous nucleation: An explanation for coastal new particle production. *Geophysical Research Letters, 28*(10), 1949-1952. doi:Doi 10.1029/2000gl012399

Hogan, C. J., and de la Mora, J. F. (2009). Tandem ion mobility-mass spectrometry (IMS-MS) study of ion evaporation from ionic liquid-acetonitrile nanodrops. *Physical Chemistry Chemical Physics, 11*(36), 8079-8090. doi:10.1039/b904022f

Hogan, C. J., and de la Mora, J. F. (2010). Ion-Pair Evaporation from Ionic Liquid Clusters. *Journal of the American Society for Mass Spectrometry, 21*(8), 1382-1386. doi:10.1016/j.jasms.2010.03.044

Hopkins, L. E., Laing, E. A., Peake, J. L., Uyeminami, D., Mack, S. M., Li, X., Smiley-Jewell, S., and Pinkerton, K. E. (2018). Repeated Iron–Soot Exposure and Nose-to-brain Transport of Inhaled Ultrafine Particles. *46*(1), 75-84. doi:10.1177/0192623317729222

Iida, K., Stolzenburg, M. R., and McMurry, P. H. (2009). Effect of Working Fluid on Sub-2 nm Particle Detection with a Laminar Flow Ultrafine Condensation Particle Counter. *Aerosol Science and Technology, 43*(1), 81-96. doi:10.1080/02786820802488194

Jiang, J. K., Chen, M. D., Kuang, C. A., Attoui, M., and McMurry, P. H. (2011). Electrical Mobility Spectrometer Using a Diethylene Glycol Condensation Particle Counter for Measurement of Aerosol Size Distributions Down to 1 nm. *Aerosol Science and Technology, 45*(4), 510-521. doi:10.1080/02786826.2010.547538

Jokinen, T., Kontkanen, J., Lehtipalo, K., Manninen, H. E., Aalto, J., Porcar-Castell, A., Garmash, O., Nieminen, T., Ehn, M., Kangasluoma, J., Junninen, H., Levula, J., Duplissy, J., Ahonen, L. R., Rantala, P., Heikkinen, L., Yan, C., Sipilä, M., Worsnop, D. R., Back, J., Petäjä, T., Kerminen, V. M., and Kulmala, M. (2017).

Solar eclipse demonstrating the importance of photochemistry in new particle formation. *Scientific Reports, 7*. doi:ARTN 45707 10.1038/srep45707

Jokinen, T., Sipilä, M., Junninen, H., Ehn, M., Lönn, G., Hakala, J., Petäjä, T., Mauldin, R. L., Kulmala, M., and Worsnop, D. R. (2012). Atmospheric sulphuric acid and neutral cluster measurements using CI-APi-TOF. *Atmospheric Chemistry and Physics, 12*(9), 4117-4125. doi:10.5194/acp-12-4117-2012

Jokinen, V., and Mäkelä, J. M. (1997). Closed-loop arrangement with critical orifice for DMA sheath/excess flow system. *28*(4), 643-648. doi:10.1016/s0021-8502(96)00457-0

Junninen, H., Ehn, M., Petäjä, T., Luosujärvi, L., Kotiaho, T., Kostiainen, R., Rohner, U., Gonin, M., Fuhrer, K., Kulmala, M., and Worsnop, D. R. (2010). A high-resolution mass spectrometer to measure atmospheric ion composition. *Atmospheric Measurement Techniques, 3*(4), 1039-1053. doi:10.5194/amt-3-1039-2010

Järvinen, A., Keskinen, J., and Yli-Ojanperä, J. (2018). Extending the Faraday cup aerosol electrometer based calibration method up to 5 µm. *Aerosol Science and Technology*, 1-33. doi:10.1080/02786826.2018.1472742

Kangasluoma, J., Attoui, M., Junninen, H., Lehtipalo, K., Samodurov, A., Korhonen, F., Sarnela, N., Schmidt-Ott, A., Worsnop, D., Kulmala, M., and Petäjä, T. (2015). Sizing of neutral sub 3 nm tungsten oxide clusters using Airmodus Particle Size Magnifier. *Journal of Aerosol Science, 87*, 53-62. doi:10.1016/j.jaerosci.2015.05.007

Kangasluoma, J., Attoui, M., Korhonen, F., Ahonen, L., Siivola, E., and Petäjä, T. (2016a). Characterization of a Herrmann-type high-resolution differential mobility analyzer. *Aerosol Science and Technology, 50*(3), 222-229. doi:10.1080/02786826.2016.1142065

Kangasluoma, J., Franchin, A., Duplissy, J., Ahonen, L., Korhonen, F., Attoui, M., Mikkilä, J., Lehtipalo, K., Vanhanen, J., Kulmala, M., and Petäjä, T. (2016b). Operation of the Airmodus A11 nano Condensation Nucleus Counter at various inlet pressures and various operation temperatures, and design of a new inlet system. *Atmos. Meas. Tech., 9*(7), 2977-2988. doi:10.5194/amt-9-2977-2016

Kangasluoma, J., Hering, S., Picard, D., Lewis, G., Enroth, J., Korhonen, F., Kulmala, M., Sellegri, K., Attoui, M., and Petäjä, T. (2017). Characterization of three new condensation particle counters for sub-3 nm particle detection during the Helsinki CPC workshop: the ADI versatile water CPC, TSI 3777 nano enhancer and boosted TSI 3010. *Atmos. Meas. Tech., 10*(6), 2271-2281. doi:10.5194/amt-10-2271-2017

Kangasluoma, J., Junninen, H., Lehtipalo, K., Mikkilä, J., Vanhanen, J., Attoui, M., Sipilä, M., Worsnop, D., Kulmala, M., and Petäjä, T. (2013). Remarks on Ion Generation for CPC Detection Efficiency Studies in Sub-3-nm Size Range. *Aerosol Science and Technology, 47*(5), 556-563. doi:10.1080/02786826.2013.773393

Kangasluoma, J., Kuang, C., Wimmer, D., Rissanen, M. P., Lehtipalo, K., Ehn, M., Worsnop, D. R., Wang, J., Kulmala, M., and Petäjä, T. (2014). Sub-3 nm particle size and composition dependent response of a nano-CPC battery. *Atmospheric Measurement Techniques, 7*(3), 689-700. doi:10.5194/amt-7-689-2014

Kangasluoma, J., Samodurov, A., Attoui, M., Franchin, A., Junninen, H., Korhonen, F., Kurtén, T., Vehkamäki, H., Sipilä, M., Lehtipalo, K., Worsnop, D. R., Petäjä, T., and Kulmala, M. (2016c). Heterogeneous Nucleation onto Ions and Neutralized Ions: Insights into Sign-Preference. *The Journal of Physical Chemistry C, 120*(13), 7444-7450. doi:10.1021/acs.jpcc.6b01779

Kerminen, V.-M., and Kulmala, M. (2002). Analytical formulae connecting the "real" and the "apparent" nucleation rate and the nuclei number concentration for atmospheric nucleation events. *Journal of Aerosol Science, 33*(4), 609-622. doi:https://doi.org/10.1016/S0021-8502(01)00194-X

Kerminen, V. M., Chen, X. M., Vakkari, V., Petäjä, T., Kulmala, M., and Bianchi, F. (2018). Atmospheric new particle formation and growth: review of field observations. *Environmental Research Letters, 13*(10). doi:ARTN 103003 10.1088/1748-9326/aadf3c

Knutson, E. O., and Whitby, K. T. (1975). Aerosol classification by electric mobility: apparatus, theory, and applications. *Journal of Aerosol Science, 6*(6), 443-451. doi:10.1016/0021-8502(75)90060-9

Kousaka, Y., Niida, T., Okuyama, K., and Tanaka, H. (1982). Development of a Mixing Type Condensation Nucleus Counter. *Journal of Aerosol Science, 13*(3), 231-240. doi:Doi 10.1016/0021-8502(82)90064-7

Krechmer, J. E., Groessl, M., Zhang, X., Junninen, H., Massoli, P., Lambe, A. T., Kimmel, J. R., Cubison, M. J., Graf, S., Lin, Y.-H., Budisulistiorini, S. H., Zhang, H., Surratt, J. D., Knochenmuss, R., Jayne, J. T., Worsnop, D. R., Jimenez, J.-L., and Canagaratna, M. R. (2016). Ion mobility spectrometry–mass spectrometry (IMS–MS) for on- and offline analysis of atmospheric gas and aerosol species. *9*(7), 3245-3262. doi:10.5194/amt-9-3245-2016

Kuang, C., Chen, M., Zhao, J., Smith, J., McMurry, P. H., and Wang, J. (2012). Size and time-resolved growth rate measurements of 1 to 5 nm freshly formed atmospheric nuclei. *Atmospheric Chemistry and Physics, 12*(7), 3573-3589. doi:10.5194/acp-12-3573-2012

Kuang, C. A., Chen, M. D., McMurry, P. H., and Wang, J. (2012). Modification of Laminar Flow Ultrafine Condensation Particle Counters for the Enhanced Detection of 1 nm Condensation Nuclei. *Aerosol Science and Technology, 46*(3), 309-315. doi:10.1080/02786826.2011.626815

Kulkarni, P., Baron, P. A., and Willeke, K. (2011). *Aerosol measurement : principles, techniques, and applications* (Third edition ed.). Hoboken, N.J.: Wiley.

Kulmala, M. (2003). ATMOSPHERIC SCIENCE: How Particles Nucleate and Grow. *Science, 302*(5647), 1000-1001. doi:10.1126/science.1090848

Kulmala, M., and Kerminen, V.-M. (2008). On the formation and growth of atmospheric nanoparticles. *90*(2-4), 132-150. doi:10.1016/j.atmosres.2008.01.005

Kulmala, M., Kontkanen, J., Junninen, H., Lehtipalo, K., Manninen, H. E., Nieminen, T., Petäjä, T., Sipilä, M., Schobesberger, S., Rantala, P., Franchin, A., Jokinen, T., Järvinen, E., Äijala, M., Kangasluoma, J., Hakala, J., Aalto, P. P., Paasonen, P., Mikkilä, J., Vanhanen, J., Aalto, J., Hakola, H., Makkonen, U., Ruuskanen, T., Mauldin, R. L., Duplissy, J., Vehkamäki, H., Back, J., Kortelainen, A., Riipinen, I.,

Kurten, T., Johnston, M. V., Smith, J. N., Ehn, M., Mentel, T. F., Lehtinen, K. E. J., Laaksonen, A., Kerminen, V. M., and Worsnop, D. R. (2013). Direct Observations of Atmospheric Aerosol Nucleation. *Science, 339*(6122), 943-946. doi:10.1126/science.1227385

Kulmala, M., Petäjä, T., Ehn, M., Thornton, J., Sipilä, M., Worsnop, D. R., and Kerminen, V. M. (2014). Chemistry of Atmospheric Nucleation: On the Recent Advances on Precursor Characterization and Atmospheric Cluster Composition in Connection with Atmospheric New Particle Formation. *Annual Review of Physical Chemistry, 65*(1), 21-37. doi:10.1146/annurev-physchem-040412-110014

Kulmala, M., Petäjä, T., Kerminen, V. M., Kujansuu, J., Ruuskanen, T., Ding, A. J., Nie, W., Hu, M., Wang, Z. B., Wu, Z. J., Wang, L., and Worsnop, D. R. (2016). On secondary new particle formation in China. *Frontiers of Environmental Science & Engineering, 10*(5). doi:ARTN 08 10.1007/s11783-016-0850-1

Kulmala, M., Petäjä, T., Nieminen, T., Sipilä, M., Manninen, H. E., Lehtipalo, K., Dal Maso, M., Aalto, P. P., Junninen, H., Paasonen, P., Riipinen, I., Lehtinen, K. E. J., Laaksonen, A., and Kerminen, V. M. (2012). Measurement of the nucleation of atmospheric aerosol particles. *Nature Protocols, 7*(9), 1651-1667. doi:DOI 10.1038/nprot.2012.091

Kulmala, M., Riipinen, I., Sipilä, M., Manninen, H. E., Petäjä, T., Junninen, H., Dal Maso, M., Mordas, G., Mirme, A., Vana, M., Hirsikko, A., Laakso, L., Harrison, R. M., Hanson, I., Leung, C., Lehtinen, K. E. J., and Kerminen, V. M. (2007). Toward direct measurement of atmospheric nucleation. *Science, 318*(5847), 89-92. doi:10.1126/science.1144124

Kulmala, M., Suni, T., Lehtinen, K. E. J., Dal Maso, M., Boy, M., Reissell, A., Rannik, Ü., Aalto, P., Keronen, P., Hakola, H., Bäck, J., Hoffmann, T., Vesala, T., and Hari, P. (2004a). A new feedback mechanism linking forests, aerosols, and climate. *Atmos. Chem. Phys., 4*(2), 557-562. doi:10.5194/acp-4-557-2004

Kulmala, M., Vehkamäki, H., Petäjä, T., Dal Maso, M., Lauri, A., Kerminen, V. M., Birmili, W., and McMurry, P. H. (2004b). Formation and growth rates of ultrafine atmospheric particles: a review of observations. *Journal of Aerosol Science, 35*(2), 143-176. doi:10.1016/j.jaerosci.2003.10.003

Kurten, A., Curtius, J., Nillius, B., and Borrmann, S. (2005). Characterization of an automated, water-based expansion condensation nucleus counter for ultrafine particles. *Aerosol Science and Technology, 39*(12), 1174-1183. doi:10.1080/02786820500431355

Kwon, H. B., Yoo, S. J., Han, J. S., Lee, S. M., Hong, U. S., Hwang, J. H., and Kim, Y. J. (2018). Mems-Based Particle Size Magnifier for Measuring Ultra Low Nanoparticle Concentration. *2018 Ieee Micro Electro Mechanical Systems (Mems)*, 1286-1288.

Köhler, H. (1936). The nucleus in and the growth of hygroscopic droplets. *Trans. Faraday Soc., 32*(0), 1152-1161. doi:10.1039/tf9363201152

Larriba, C., and Hogan, C. J. (2013a). Free molecular collision cross section calculation methods for nanoparticles and complex ions with energy accommodation. *Journal of Computational Physics, 251*, 344-363. doi:10.1016/j.jcp.2013.05.038

Larriba, C., and Hogan, C. J. (2013b). Ion Mobilities in Diatomic Gases: Measurement versus Prediction with Non-Specular Scattering Models. *Journal of Physical Chemistry A, 117*(19), 3887-3901. doi:10.1021/jp312432z

Laturnus, F., Giese, B., Wiencke, C., and Adams, F. C. (2000). Low-molecular-weight organoiodine and organobromine compounds released by polar macroalgae - The influence of abiotic factors. *368*(2-3), 297-302. doi:10.1007/s002160000491

Lee, K. W., and Liu, B. Y. H. (1982). Theoretical Study of Aerosol Filtration by Fibrous Filters. *Aerosol Science and Technology, 1*(2), 147-161. doi:10.1080/02786828208958584

Lehtinen, K. E. J., Dal Maso, M., Kulmala, M., and Kerminen, V.-M. (2007). Estimating nucleation rates from apparent particle formation rates and vice versa: Revised formulation of the Kerminen–Kulmala equation. *Journal of Aerosol Science, 38*(9), 988-994. doi:10.1016/j.jaerosci.2007.06.009

Lehtipalo, K., Leppä, J., Kontkanen, J., Kangasluoma, J., Franchin, A., Wimnner, D., Schobesberger, S., Junninen, H., Petäjä, T., Sipilä, M., Mikkilä, J., Vanhanen, J., Worsnop, D. R., and Kulmala, M. (2014). Methods for determining particle size distribution and growth rates between 1 and 3 nm using the Particle Size Magnifier. *Boreal Environment Research, 19*, 215-236.

Lehtipalo, K., Yan, C., Dada, L., Bianchi, F., Xiao, M., Wagner, R., Stolzenburg, D., Ahonen, L. R., Amorim, A., Baccarini, A., Bauer, P. S., Baumgartner, B., Bergen, A., Bernhammer, A. K., Breitenlechner, M., Brilke, S., Buchholz, A., Mazon, S. B., Chen, D. X., Chen, X. M., Dias, A., Dommen, J., Draper, D. C., Duplissy, J., Ehn, M., Finkenzeller, H., Fischer, L., Frege, C., Fuchs, C., Garmash, O., Gordon, H., Hakala, J., He, X. C., Heikkinen, L., Heinritzi, M., Helm, J. C., Hofbauer, V., Hoyle, C. R., Jokinen, T., Kangasluoma, J., Kerminen, V. M., Kim, C., Kirkby, J., Kontkanen, J., Kurten, A., Lawler, M. J., Mai, H. J., Mathot, S., Mauldin, R. L., Molteni, U., Nichman, L., Nie, W., Nieminen, T., Ojdanic, A., Onnela, A., Passananti, M., Petäjä, T., Piel, F., Pospisilova, V., Quelever, L. L. J., Rissanen, M. P., Rose, C., Sarnela, N., Schallhart, S., Schuchmann, S., Sengupta, K., Simon, M., Sipilä, M., Tauber, C., Tome, A., Trostl, J., Vaisanen, O., Vogel, A. L., Volkamer, R., Wagner, A. C., Wang, M. Y., Weitz, L., Wimmer, D., Ye, P. L., Ylisirnio, A., Zha, Q. Z., Carslaw, K. S., Curtius, J., Donahue, N. M., Flagan, R. C., Hansel, A., Riipinen, I., Virtanen, A., Winkler, P. M., Baltensperger, U., Kulmala, M., and Worsnop, D. R. (2018). Multicomponent new particle formation from sulfuric acid, ammonia, and biogenic vapors. *Science Advances, 4*(12). doi:ARTN eaau5363

10.1126/sciadv.aau5363

Leino, K., Lampilahti, J., Poutanen, P., Väänänen, R., Manninen, A., Buenrostro Mazon, S., Dada, L., Franck, A., Wimmer, D., Aalto, P. P., Ahonen, L. R., Enroth, J., Kangasluoma, J., Keronen, P., Korhonen, F., Laakso, H., Matilainen, T., Siivola, E., Manninen, H. E., Lehtipalo, K., Kerminen, V. M., Petäjä, T., and Kulmala, M. (2019). Vertical profiles of sub-3nm particles over the boreal forest. *Atmos. Chem. Phys., 19*(6), 4127-4138. doi:10.5194/acp-19-4127-2019

Li, C. X., and Hogan, C. J. (2017). Vapor specific extents of uptake by nanometer scale charged particles. *Aerosol Science and Technology, 51*(5), 653-664. doi:10.1080/02786826.2017.1288285

Lopez-Hilfiker, F. D., Iyer, S., Mohr, C., Lee, B. H., Apos, Ambro, E. L., Kurtén, T., and Thornton, J. A. (2016). Constraining the sensitivity of iodide adduct chemical ionization mass spectrometry to multifunctional organic molecules using the collision limit and thermodynamic stability of iodide ion adducts. *9*(4), 1505-1512. doi:10.5194/amt-9-1505-2016

Makkonen, R., Asmi, A., Kerminen, V. M., Boy, M., Arneth, A., Hari, P., and Kulmala, M. (2012). Air pollution control and decreasing new particle formation lead to strong climate warming. *12*(3), 1515-1524. doi:10.5194/acp-12-1515-2012

Manninen, H. E. (2009). Long-term field measurements of charged and neutral clusters using Neutral cluster and Air Ion Spectrometer (NAIS). *Boreal Environment Research, 14*(4), 591-605.

Mason, E. A., Viehland, L. A., Ellis, H. W., James, D. R., and Mcdaniel, E. W. (1975). Mobilities of K+ Ions in Hot Gases. *Physics of Fluids, 18*(8), 1070-1071. doi:Doi 10.1063/1.861246

McDaniel, E. W., and Viehland, L. A. (1984). The transport of slow ions in gases: Experiment, theory, and applications. *110*(5-6), 333-367. doi:10.1016/0370-1573(84)90195-9

McFiggans, G., Bale, C. S. E., Ball, S. M., Beames, J. M., Bloss, W. J., Carpenter, L. J., Dorsey, J., Dunk, R., Flynn, M. J., Furneaux, K. L., Gallagher, M. W., Heard, D. E., Hollingsworth, A. M., Hornsby, K., Ingham, T., Jones, C. E., Jones, R. L., Kramer, L. J., Langridge, J. M., Leblanc, C., LeCrane, J. P., Lee, J. D., Leigh, R. J., Longley, I., Mahajan, A. S., Monks, P. S., Oetjen, H., Orr-Ewing, A. J., Plane, J. M. C., Potin, P., Shillings, A. J. L., Thomas, F., von Glasow, R., Wada, R., Whalley, L. K., and Whitehead, J. D. (2010). Iodine-mediated coastal particle formation: an overview of the Reactive Halogens in the Marine Boundary Layer (RHaMBLe) Roscoff coastal study. *Atmospheric Chemistry and Physics, 10*(6), 2975-2999. doi:10.5194/acp-10-2975-2010

McMurry, P. H. (2000). The history of condensation nucleus counters. *Aerosol Science and Technology, 33*(4), 297-322. doi:Doi 10.1080/02786820050121512

McMurry, P. H., and Friedlander, S. K. (1979). New Particle Formation in the Presence of an Aerosol. *Atmospheric Environment, 13*(12), 1635-1651. doi:Doi 10.1016/0004-6981(79)90322-6

McMurry, P. H., Kulmala, M., and Worsnop, D. R. (2011). Special Issue on Aerosol Measurements in the 1 nm Range. *Aerosol Science and Technology, 45*(4), i-i. doi:10.1080/02786826.2011.554922

Meng, X., Ma, Y., Chen, R., Zhou, Z., Chen, B., and Kan, H. (2013). Size-fractionated particle number concentrations and daily mortality in a Chinese city. *Environ Health Perspect, 121*(10), 1174-1178. doi:10.1289/ehp.1206398

Merikanto, J., Spracklen, D. V., Mann, G. W., Pickering, S. J., and Carslaw, K. S. (2009). Impact of nucleation on global CCN. *Atmospheric Chemistry and Physics, 9*(21), 8601-8616. doi:10.5194/acp-9-8601-2009

Mertes, S., Schröder, F., and Wiedensohler, A. (1995). The Particle Detection Efficiency Curve of the TSI-3010 CPC as a Function of the Temperature Difference between Saturator and Condenser. *23*(2), 257-261. doi:10.1080/02786829508965310

Mirme, A., Tamm, E., Mordas, G., Vana, M., Uin, J., Mirme, S., Bernotas, T., Laakso, L., Hirsikko, A., and Kulmala, M. (2007). A wide-range multi-channel air ion spectrometer. *Boreal Environment Research, 12*(3), 247-264.

Mirme, S., Mirme, A., Minikin, A., Petzold, A., Hõrrak, U., Kerminen, V. M., and Kulmala, M. (2010). Atmospheric sub-3 nm particles at high altitudes. *Atmos. Chem. Phys., 10*(2), 437-451. doi:10.5194/acp-10-437-2010

Mäkelä, J. M., Aalto, P., Jokinen, V., Pohja, T., Nissinen, A., Palmroth, S., Markkanen, T., Seitsonen, K., Lihavainen, H., and Kulmala, M. (1997). Observations of ultrafine aerosol particle formation and growth in boreal forest. *24*(10), 1219-1222. doi:10.1029/97gl00920

Mäkelä, J. M., Hoffmann, T., Holzke, C., Väkevä, M., Suni, T., Mattila, T., Aalto, P. P., Tapper, U., Kauppinen, E. I., and O'Dowd, C. D. (2002). Biogenic iodine emissions and identification of end-products in coastal ultrafine particles during nucleation bursts. *107*(D19), PAR 14-11-PAR 14-14. doi:10.1029/2001jd000580

Nieminen, T., Kerminen, V.-M., Petäjä, T., Aalto, P. P., Arshinov, M., Asmi, E., Baltensperger, U., Beddows, D. C. S., Beukes, J. P., Collins, D., Ding, A., Harrison, R. M., Henzing, B., Hooda, R., Hu, M., Hõrrak, U., Kivekäs, N., Komsaare, K., Krejci, R., Kristensson, A., Laakso, L., Laaksonen, A., Leaitch, W. R., Lihavainen, H., Mihalopoulos, N., Németh, Z., Nie, W., Amp, Apos, Dowd, C., Salma, I., Sellegri, K., Svenningsson, B., Swietlicki, E., Tunved, P., Ulevicius, V., Vakkari, V., Vana, M., Wiedensohler, A., Wu, Z., Virtanen, A., and Kulmala, M. (2018). Global analysis of continental boundary layer new particle formation based on long-term measurements. *Atmospheric Chemistry and Physics, 18*(19), 14737-14756. doi:10.5194/acp-18-14737-2018

O'Dowd, C. D., Aalto, P. P., Yoon, Y. J., and Hämeri, K. (2004). The use of the pulse height analyser ultrafine condensation particle counter (PHA-UCPC) technique applied to sizing of nucleation mode particles of differing chemical composition. *Journal of Aerosol Science, 35*(2), 205-216. doi:10.1016/j.jaerosci.2003.08.003

O'Dowd, C. D., and Hoffmann, T. (2005). Coastal new particle formation: A review of the current state-of-the-art. *Environmental Chemistry, 2*(4), 245-255. doi:10.1071/En05077

O'Dowd, C. D., Jimenez, J. L., Bahreini, R., Flagan, R. C., Seinfeld, J. H., Hämeri, K., Pirjola, L., Kulmala, M., Jennings, S. G., and Hoffmann, T. (2002). Marine aerosol formation from biogenic iodine emissions. *Nature, 417*(6889), 632-636. doi:DOI 10.1038/nature00775

Oberdorster, G., Oberdorster, E., and Oberdorster, J. (2005). Nanotoxicology: An emerging discipline evolving from studies of ultrafine particles. *Environmental Health Perspectives, 113*(7), 823-839. doi:Doi 10.1289/Ehp.7339

Oberdörster, G., Sharp, Z., Atudorei, V., Elder, A., Gelein, R., Kreyling, W., and Cox, C. (2004). Translocation of Inhaled Ultrafine Particles to the Brain. *Inhalation Toxicology, 16*(6/7), 437-445. doi:10.1080/08958370490439597

Oberreit, D., Rawat, V. K., Larriba-Andaluz, C., Ouyang, H., McMurry, P. H., and Hogan, C. J. (2015). Analysis of heterogeneous water vapor uptake by metal iodide cluster ions via differential mobility analysis-mass spectrometry. *Journal of Chemical Physics, 143*(10). doi:Artn 10420410.1063/1.4930278

Okuyama, K., Kousaka, Y., and Motouchi, T. (1984). Condensational Growth of Ultrafine Aerosol Particles in a New Particle Size Magnifier. *Aerosol Science and Technology, 3*(4), 353-366. doi:10.1080/02786828408959024

Passananti, M., Zapadinsky, E., Zanca, T., Kangasluoma, J., Myllys, N., Rissanen, M. P., Kurten, T., Ehn, M., Attoui, M., and Vehkamaki, H. (2019). How well can we predict cluster fragmentation inside a mass spectrometer? *Chemical Communications, 55*(42), 5946-5949. doi:10.1039/c9cc02896j

Pawar, K., and Kaul, G. (2014). Toxicity of titanium oxide nanoparticles causes functionality and DNA damage in buffalo (Bubalus bubalis) sperm in vitro. *Toxicology and Industrial Health, 30*(6), 520-533. doi:Doi 10.1177/0748233712462475

Petäjä, T., Mordas, G., Manninen, H., Aalto, P. P., Hämeri, K., and Kulmala, M. (2006). Detection efficiency of a water-based TSI Condensation Particle Counter 3785. *Aerosol Science and Technology, 40*(12), 1090-1097.

Pope, C. A., Ezzati, M., and Dockery, D. W. (2009). Fine-Particulate Air Pollution and Life Expectancy in the United States. *New England Journal of Medicine, 360*(4), 376-386. doi:10.1056/nejmsa0805646

Pruppacher, H. R. (2010). *Microphysics of clouds and precipitation*. In J. D. Klett (Ed.), *Atmospheric and oceanographic sciences library*. Retrieved from http://login.libproxy.helsinki.fi/login?url=http://dx.doi.org/10.1007/978-0-306-48100-0

Pui, D. Y. H., Romay-Novas, F., and Liu, B. Y. H. (1987). Experimental Study of Particle Deposition in Bends of Circular Cross Section. *Aerosol Science and Technology, 7*(3), 301-315. doi:10.1080/02786828708959166

Pye, H. O. T., D'Ambro, E. L., Lee, B. H., Schobesberger, S., Takeuchi, M., Zhao, Y., Lopez-Hilfiker, F., Liu, J., Shilling, J. E., Xing, J., Mathur, R., Middlebrook, A. M., Liao, J., Welti, A., Graus, M., Warneke, C., de Gouw, J. A., Holloway, J. S., Ryerson, T. B., Pollack, I. B., and Thornton, J. A. (2019). Anthropogenic enhancements to production of highly oxygenated molecules from autoxidation. *116*(14), 6641-6646. doi:10.1073/pnas.1810774116 %J Proceedings of the National Academy of Sciences

Rantala, P., Aalto, J., Taipale, R., Ruuskanen, T. M., and Rinne, J. (2015). Annual cycle of volatile organic compound exchange between a boreal pine forest and the atmosphere. *12*(19), 5753-5770. doi:10.5194/bg-12-5753-2015

Rawat, V. K., Vidal-de-Miguel, G., and Hogan, C. J. (2015). Modeling vapor uptake induced mobility shifts in peptide ions observed with transversal modulation ion mobility spectrometry-mass spectrometry. *Analyst, 14*(20), 6945-6954.

Revercomb, H. E., and Mason, E. A. (1975). Theory of plasma chromatography/gaseous electrophoresis. Review. *Analytical Chemistry, 47*(7), 970-983. doi:10.1021/ac60357a043

Rose, C., Sellegri, K., Asmi, E., Hervo, M., Freney, E., Colomb, A., Junninen, H., Duplissy, J., Sipilä, M., Kontkanen, J., Lehtipalo, K., and Kulmala, M. (2015). Major contribution of neutral clusters to new particle formation at the interface between the

boundary layer and the free troposphere. *15*(6), 3413-3428. doi:10.5194/acp-15-3413-2015

Rus, J., Moro, D., Sillero, J. A., Royuela, J., Casado, A., Estevez-Molinero, F., and Fernández de la Mora, J. (2010). IMS–MS studies based on coupling a differential mobility analyzer (DMA) to commercial API–MS systems. *International Journal of Mass Spectrometry, 298*(1), 30-40. doi:https://doi.org/10.1016/j.ijms.2010.05.008

Russell, L. M., Zhang, S.-H., Flagan, R. C., Seinfeld, J. H., Stolzenburg, M. R., and Caldow, R. (1996). Radially Classified Aerosol Detector for Aircraft-Based Submicron Aerosol Measurements. *13*(3), 598-609. doi:10.1175/1520-0426(1996)013<0598:rcadfa>2.0.co;2

Rönkkö, T., Kuuluvainen, H., Karjalainen, P., Keskinen, J., Hillamo, R., Niemi, J. V., Pirjola, L., Timonen, H. J., Saarikoski, S., Saukko, E., Järvinen, A., Silvennoinen, H., Rostedt, A., Olin, M., Yli-Ojanperä, J., Nousiainen, P., Kousa, A., and Dal Maso, M. (2017). Traffic is a major source of atmospheric nanocluster aerosol. *Proceedings of the National Academy of Sciences, 114*(29), 7549-7554. doi:10.1073/pnas.1700830114

Saiz-Lopez, A., and Plane, J. M. C. (2004). Novel iodine chemistry in the marine boundary layer. *Geophysical Research Letters, 31*(4). doi:Artn L04112 10.1029/2003gl019215

Saunders, R. (2006). Formation Pathways and Composition of Iodine Oxide Ultra-Fine Particles %J Environmental Chemistry. *2*(4), 299-303. http://search.proquest.com/docview/20418855/?pq-origsite=primo

Saunders, R. (2010). Studies of the Formation and Growth of Aerosol from Molecular Iodine Precursor %J Zeitschrift Fur Physikalische Chemie-International Journal Of Research In P. *224*(7-8), 1095-1117. http://gateway.webofknowledge.com/gateway/Gateway.cgi?&GWVersion=2&SrcAuth=ExLibris&SrcApp=Primo1&DestLinkType=FullRecord&KeyUT=000285161400010&DestApp=WOS

Sgro, L., and Fernández de la Mora, J. (2004). A Simple Turbulent Mixing CNC for Charged Particle Detection Down to 1.2 nm. *38*(1), 1-11. doi:10.1080/02786820490247560

Shrivastav, V., Nahin, M., Hogan, C. J., and Larriba-Andaluz, C. (2017). Benchmark Comparison for a Multi-Processing Ion Mobility Calculator in the Free Molecular Regime. *Journal of the American Society for Mass Spectrometry, 28*(8), 1540-1551. doi:10.1007/s13361-017-1661-8

Sipilä, M., Lehtipalo, K., Attoui, M., Neitola, K., Petäjä, T., Aalto, P. P., O'Dowd, C. D., and Kulmala, M. (2009). Laboratory Verification of PH-CPC's Ability to Monitor Atmospheric Sub-3 nm Clusters. *Aerosol Science and Technology, 43*(2), 126-135. doi:10.1080/02786820802506227

Sipilä, M., Sarnela, N., Jokinen, T., Henschel, H., Junninen, H., Kontkanen, J., Richters, S., Kangasluoma, J., Franchin, A., Peräkylä, O., Rissanen, M. P., Ehn, M., Vehkamäki, H., Kurten, T., Berndt, T., Petäjä, T., Worsnop, D., Ceburnis, D., Kerminen, V.-M., Kulmala, M., and O'Dowd, C. (2016). Molecular-scale evidence of aerosol particle formation via sequential addition of HIO3. *537*(7621), 532-534. doi:10.1038/nature19314

Smith, D. K., Pantoya, M. L., Parkey, J. S., and Kesmez, M. (2017). The water-iodine oxide system: a revised mechanism for hydration and dehydration. *Rsc Advances, 7*(17), 10183-10191. doi:10.1039/c6ra27854j

Spracklen, D. V., Carslaw, K. S., Kulmala, M., Kerminen, V. M., Mann, G. W., and Sihto, S. L. (2006). The contribution of boundary layer nucleation events to total particle concentrations on regional and global scales. *6*(4), 7323-7368. doi:10.5194/acpd-6-7323-2006

Stolzenburg, D., Steiner, G., and Winkler, P. M. (2017). A DMA-train for precision measurement of sub-10 nm aerosol dynamics. *Atmos. Meas. Tech., 10*(4), 1639-1651. doi:10.5194/amt-10-1639-2017

Stolzenburg, M. R. (1988). An Ultrafine Aerosol Size Distribution Measuring System. *Ph.D. Thesis, Department of Mechanical Engineering, University of Minnesota*.

Stolzenburg, M. R., and McMurry, P. H. (1991). An Ultrafine Aerosol Condensation Nucleus Counter. *Aerosol Science and Technology, 14*(1), 48-65. doi:Doi 10.1080/02786829108959470

Stolzenburg, M. R., and McMurry, P. H. (2008). Equations governing single and tandem DMA configurations and a new lognormal approximation to the transfer function. *Aerosol Science and Technology, 42*(6), 421-432. doi:10.1080/02786820802157823

Strak, M., Janssen, N. A. H., Godri, K. J., Gosens, I., Mudway, I. S., Cassee, F. R., Lebret, E., Kelly, F. J., Harrison, R. M., Brunekreef, B., Steenhof, M., and Hoek, G. (2012). Respiratory Health Effects of Airborne Particulate Matter: The Role of Particle Size, Composition, and Oxidative Potential-The RAPTES Project. *Environmental Health Perspectives, 120*(8), 1183-1189. doi:10.1289/ehp.1104389

Sunder, S., and Vikis, A. C. (1987). Raman-Spectra of Iodine Oxyacids Produced by the Gas-Phase Reaction of Iodine with Ozone in the Presence of Water-Vapor. *Canadian Journal of Spectroscopy, 32*(2), 45-48.

Swietlicki, E., Hansson, H. C., Hämeri, K., Svenningsson, B., Massling, A., McFiggans, G., McMurry, P. H., Petäjä, T., Tunved, P., Gysel, M., Topping, D., Weingartner, E., Baltensperger, U., Rissler, J., Wiedensohler, A., and Kulmala, M. (2008). Hygroscopic properties of submicrometer atmospheric aerosol particles measured with H-TDMA instruments in various environments—a review. *Tellus B: Chemical and Physical Meteorology, 60*(3), 432-469. doi:10.1111/j.1600-0889.2008.00350.x

Tammet, H. (1995). Size and mobility of nanometer particles, clusters and ions. *Journal of Aerosol Science, 26*(3), 459-475. doi:https://doi.org/10.1016/0021-8502(94)00121-E

Tammet, H. (2006). Continuous scanning of the mobility and size distribution of charged clusters and nanometer particles in atmospheric air and the Balanced Scanning Mobility Analyzer BSMA. *Atmospheric Research, 82*(3-4), 523-535. doi:10.1016/j.atmosres.2006.02.009

Tammet, H. F. (1970). *The Aspiration Method for the Determination of Atmospheric-ion Spectra*: ISRAEL PROGRAM F. SCIENTIFIC TRANSLATIONS.

Tenbrink, H. M., Plomp, A., Spoelstra, H., and Vandevate, J. F. (1983). A High-Resolution Electrical Mobility Aerosol Spectrometer (Mas). *Journal of Aerosol Science, 14*(5), 589-597. doi:Doi 10.1016/0021-8502(83)90064-2

Thomas, J. M., Chen, X., Maißer, A., and Hogan, C. J. (2018). Differential heat and mass transfer rate influences on the activation efficiency of laminar flow condensation particle counters. *International Journal of Heat and Mass Transfer, 127*, 740-750. doi:10.1016/j.ijheatmasstransfer.2018.07.002

Tröstl, J., Chuang, W. K., Gordon, H., Heinritzi, M., Yan, C., Molteni, U., Ahlm, L., Frege, C., Bianchi, F., Wagner, R., Simon, M., Lehtipalo, K., Williamson, C., Craven, J. S., Duplissy, J., Adamov, A., Almeida, J., Bernhammer, A.-K., Breitenlechner, M., Brilke, S., Dias, A., Ehrhart, S., Flagan, R. C., Franchin, A., Fuchs, C., Guida, R., Gysel, M., Hansel, A., Hoyle, C. R., Jokinen, T., Junninen, H., Kangasluoma, J., Keskinen, H., Kim, J., Krapf, M., Kürten, A., Laaksonen, A., Lawler, M., Leiminger, M., Mathot, S., Möhler, O., Nieminen, T., Onnela, A., Petäjä, T., Piel, F. M., Miettinen, P., Rissanen, M. P., Rondo, L., Sarnela, N., Schobesberger, S., Sengupta, K., Sipilä, M., Smith, J. N., Steiner, G., Tomè, A., Virtanen, A., Wagner, A. C., Weingartner, E., Wimmer, D., Winkler, P. M., Ye, P., Carslaw, K. S., Curtius, J., Dommen, J., Kirkby, J., Kulmala, M., Riipinen, I., Worsnop, D. R., Donahue, N. M., and Baltensperger, U. (2016). The role of low-volatility organic compounds in initial particle growth in the atmosphere. *Nature, 533*(7604), 527-531. doi:10.1038/nature18271

Tuch, T. M., Haudek, A., Müller, T., Nowak, A., Wex, H., and Wiedensohler, A. (2009). Design and performance of an automatic regenerating adsorption aerosol dryer for continuous operation at monitoring sites. *2*(2), 417-422. doi:10.5194/amt-2-417-2009

Twomey, S. A., Piepgrass, M., and Wolfe, T. L. (1984). An assessment of the impact of pollution on global cloud albedo. *Tellus Series B-Chemical and Physical Meteorology, 36B*(5), 356-366. doi:10.1111/j.1600-0889.1984.tb00254.x

Ude, S., and de la Mora, J. F. (2005). Molecular monodisperse mobility and mass standards from electrosprays of tetra-alkyl ammonium halides. *Journal of Aerosol Science, 36*(10), 1224-1237. doi:10.1016/j.jaerosci.2005.02.009

Ude, S., Fernández De La Mora, J., and Thomson, B. A. (2004). Charge-Induced Unfolding of Multiply Charged Polyethylene Glycol Ions. *Journal of the American Chemical Society, 126*(38), 12184-12190. doi:10.1021/ja0381306

Wagner, R., Manninen, H. E., Franchin, A., Lehtipalo, K., Mirme, S., Steiner, G., Petäjä, T., and Kulmala, M. (2016). On the accuracy of ion measurements using a Neutral cluster and Air Ion Spectrometer. *Boreal Environment Research, 21*(3-4), 230-241.

Wang, H.-C., and Kasper, G. (1991). Filtration efficiency of nanometer-size aerosol particles. *Journal of Aerosol Science, 22*(1), 31-41. doi:https://doi.org/10.1016/0021-8502(91)90091-U

Wang, J., Flagan, R. C., and Seinfeld, J. H. (2002). Diffusional losses in particle sampling systems containing bends and elbows. *Journal of Aerosol Science, 33*(6), 843-857.

Wang, M., and Penner, J. E. (2009). Aerosol indirect forcing in a global model with particle nucleation. *9*(1), 239-260. doi:10.5194/acp-9-239-2009

Wang, S. C., and Flagan, R. C. (1990). Scanning Electrical Mobility Spectrometer. *Aerosol Science and Technology, 13*(2), 230-240.

Vanhanen, J., Mikkilä, J., Lehtipalo, K., Sipilä, M., Manninen, H. E., Siivola, E., Petäjä, T., and Kulmala, M. (2011). Particle Size Magnifier for Nano-CN Detection. *Aerosol Science and Technology, 45*(4), 533-542. doi:10.1080/02786826.2010.547889

Vanommeslaeghe, K., Hatcher, E., Acharya, C., Kundu, S., Zhong, S., Shim, J., Darian, E., Guvench, O., Lopes, P., Vorobyov, I., and MacKerell, A. D. (2010). CHARMM General Force Field: A Force Field for Drug-Like Molecules Compatible with the CHARMM All-Atom Additive Biological Force Fields. *Journal of Computational Chemistry, 31*(4), 671-690. doi:10.1002/jcc.21367

Vehkamäki, H. (2006). *Classical nucleation theory in multicomponent systems*. Berlin: Springer.

Vehkamäki, H., and Riipinen, I. (2012). Thermodynamics and kinetics of atmospheric aerosol particle formation and growth. *Chemical Society Reviews, 41*(15), 5160-5173. doi:10.1039/c2cs00002d

Wiedensohler, A. (1988). An Approximation of the Bipolar Charge-Distribution for Particles in the Sub-Micron Size Range. *Journal of Aerosol Science, 19*(3), 387-389.

Wiedensohler, A., Birmili, W., Nowak, A., Sonntag, A., Weinhold, K., Merkel, M., Wehner, B., Tuch, T., Pfeifer, S., Fiebig, M., Fjaraa, A. M., Asmi, E., Sellegri, K., Depuy, R., Venzac, H., Villani, P., Laj, P., Aalto, P., Ogren, J. A., Swietlicki, E., Williams, P., Roldin, P., Quincey, P., Huglin, C., Fierz-Schmidhauser, R., Gysel, M., Weingartner, E., Riccobono, F., Santos, S., Gruning, C., Faloon, K., Beddows, D., Harrison, R. M., Monahan, C., Jennings, S. G., O'Dowd, C. D., Marinoni, A., Horn, H. G., Keck, L., Jiang, J., Scheckman, J., McMurry, P. H., Deng, Z., Zhao, C. S., Moerman, M., Henzing, B., de Leeuw, G., Loschau, G., and Bastian, S. (2012). Mobility particle size spectrometers: harmonization of technical standards and data structure to facilitate high quality long-term observations of atmospheric particle number size distributions. *Atmospheric Measurement Techniques, 5*(3), 657-685. doi:10.5194/amt-5-657-2012

Wiedensohler, A., Orsini, D., Covert, D. S., Coffmann, D., Cantrell, W., Havlicek, M., Brechtel, F. J., Russell, L. M., Weber, R. J., Gras, J., Hudson, J. G., and Litchy, M. (1997). Intercomparison Study of the Size-Dependent Counting Efficiency of 26 Condensation Particle Counters. *27*(2), 224-242. doi:10.1080/02786829708965469

Wiley, W. C., and McLaren, I. H. (1955). Time-of-Flight Mass Spectrometer with Improved Resolution. *Review of Scientific Instruments, 26*(12), 1150-1157. doi:10.1063/1.1715212

Wilson, J. C., Blackshear, E. D., and Hyun, J. H. (1983). An Improved Continuous-Flow Condensation Nucleus Counter for Use in the Stratosphere. *Journal of Aerosol Science, 14*(3), 387-391. doi:Doi 10.1016/0021-8502(83)90143-X

Winkler, P. M., Steiner, G., Vrtala, A., Vehkamaki, H., Noppel, M., Lehtinen, K. E. J., Reischl, G. P., Wagner, P. E., and Kulmala, M. (2008). Heterogeneous Nucleation Experiments Bridging the Scale from Molecular Ion Clusters to Nanoparticles. *Science, 319*(5868), 1374-1377. doi:10.1126/science.1149034

Winklmayr, W., Reischl, G. P., Lindner, A. O., and Berner, A. (1991). A new electromobility spectrometer for the measurement of aerosol size distributions in the size range from 1 to 1000 nm. *Journal of Aerosol Science, 22*(3), 289-296. doi:10.1016/s0021-8502(05)80007-2

Volckens, J., and Leith, D. (2003). Effects of sampling bias on gas–particle partitioning of semi-volatile compounds. *Atmospheric Environment, 37*(24), 3385-3393. doi:https://doi.org/10.1016/S1352-2310(03)00356-X

von Klot, S., Peters, A., Aalto, P., Bellander, T., Berglind, N., D'Ippoliti, D., Elosua, R., Hörmann, A., Kulmala, M., Lanki, T., Löwel, H., Pekkanen, J., Picciotto, S., Sunyer, J., and Forastiere, F. (2005). Ambient Air Pollution Is Associated With Increased Risk of Hospital Cardiac Readmissions of Myocardial Infarction Survivors in Five European Cities. *Circulation, 112*(20), 3073-3079. doi:10.1161/CIRCULATIONAHA.105.548743

Xiao, S., Wang, M. Y., Yao, L., Kulmala, M., Zhou, B., Yang, X., Chen, J. M., Wang, D. F., Fu, Q. Y., Worsnop, D. R., and Wang, L. (2015). Strong atmospheric new particle formation in winter in urban Shanghai, China. *15*(4), 1769-1781. doi:10.5194/acp-15-1769-2015

Yan, C., Dada, L., Rose, C., Jokinen, T., Nie, W., Schobesberger, S., Junninen, H., Lehtipalo, K., Sarnela, N., Makkonen, U., Garmash, O., Wang, Y., Zha, Q., Paasonen, P., Bianchi, F., Sipilä, M., Ehn, M., Petäjä, T., Kerminen, V. M., Worsnop, D. R., and Kulmala, M. (2018). The role of H2SO4-NH3 anion clusters in ion-induced aerosol nucleation mechanisms in the boreal forest. *Atmos. Chem. Phys., 18*(17), 13231-13243. doi:10.5194/acp-18-13231-2018

Yli-Ojanpera, J., Makela, J. M., Marjamaki, M., Rostedt, A., and Keskinen, J. (2010). Towards traceable particle number concentration standard: Single charged aerosol reference (SCAR). *Journal of Aerosol Science, 41*(8), 719-728. doi:10.1016/j.jaerosci.2010.04.012

Yli-Ojanperä, J., Sakurai, H., Iida, K., Mäkelä, J. M., Ehara, K., and Keskinen, J. (2012). Comparison of Three Particle Number Concentration Calibration Standards Through Calibration of a Single CPC in a Wide Particle Size Range. *46*(11), 1163-1173. doi:10.1080/02786826.2012.701023

Yu, F., and Luo, G. (2009). Simulation of particle size distribution with a global aerosol model: contribution of nucleation to aerosol and CCN number concentrations. *9*(20), 7691-7710. doi:10.5194/acp-9-7691-2009

Yu, H., Hallar, A. G., You, Y., Sedlacek, A., Springston, S., Kanawade, V. P., Lee, Y. N., Wang, J., Kuang, C. G., McGraw, R. L., McCubbin, I., Mikkila, J., and Lee, S. H. (2014). Sub-3nm particles observed at the coastal and continental sites in the United States. *Journal of Geophysical Research-Atmospheres, 119*(2), 860-879. doi:10.1002/2013jd020841

Yu, H., Zhou, L. Y., Dai, L., Shen, W. C., Zheng, J., Ma, Y., and Chen, M. D. (2016). Nucleation and growth of sub-3 nm particles in the polluted urban atmosphere of a megacity in China. *15*(13), 18653-18690. doi:10.5194/acpd-15-18653-2015

Yu, W. B., He, X. B., Vanommeslaeghe, K., and MacKerell, A. D. (2012). Extension of the CHARMM general force field to sulfonyl-containing compounds and its utility in biomolecular simulations. *Journal of Computational Chemistry, 33*(31), 2451-2468. doi:10.1002/jcc.23067

Zapadinsky, E., Passananti, M., Myllys, N., Kurtén, T., and Vehkamäki, H. (2019). Modeling on Fragmentation of Clusters inside a Mass Spectrometer. *The Journal of Physical Chemistry A*. doi:10.1021/acs.jpca.8b10744

Zhang, Z. Q., and Liu, B. Y. H. (1990). Dependence of the Performance of TSI 3020 Condensation Nucleus Counter on Pressure, Flow Rate, and Temperature. *13*(4), 493-504. doi:10.1080/02786829008959464

References

(1) Thomas, J. M.; He, S.; Larriba-Andaluz, C.; DePalma, J. W.; Johnston, M. V.; Hogan, C. J. Ion Mobility Spectrometry-Mass Spectrometry Examination of the Structures, Stabilities, and Extents of Hydration of Dimethylamine-Sulfuric Acid Clusters. *Phys. Chem. Chem.Phys.* **2016,** *18*, 22962-22972.

(2) Rus, J.; Moro, D.; Sillero, J. A.; Royuela, J.; Casado, A.; Estevez-Molinero, F.; Fernandez de la Mora, J. IMS–MS Studies Based on Coupling a Differential Mobility Analyzer (DMA) to Commercial API–MS Systems. *Int. J. Mass Spectrom.* **2010,** *298*, 30-40.

(3) Oberreit, D.; Rawat, V. K.; Larriba-Andaluz, C.; Ouyang, H.; McMurry, P. H.; Hogan, C. J. Analysis of Heterogeneous Water Vapor Uptake by Metal Iodide Cluster Ions via Differential Mobility Analysis-Mass Spectrometry. *J. Chem. Phys.* **2015,** *143*, 104204.

(4) Fernandez de la Mora, J.; Borrajo, R.; M., Z.-G. Capillary and Coulombic Effects on the Gas Phase Structure of Electrosprayed Concanavalin A Ions and Its Clusters C_n^{+z} (n = 1−6). *J. Phys. Chem. B* **2012,** *116*, 9882-9898.

(5) Vanommeslaeghe, K.; *et al*. CHARMM General Force Field: A Force Field for Drug-Like Molecules Compatible with the CHARMM All-Atom Additive Biological Force Fields. *J. Comput. Chem.* **2010,** *31*, 671-690.

(6) Halgren, T. A. Merck Molecular Force Field. I. Basis, Form, Scope, Parameterization, and Performance of MMFF94. *J. Comput. Chem.***1996,** *17*, 490-519.

(7) Yu, W.; He, X.; Vanommeslaeghe, K.; MacKerell Jr., A. D. Extension of the CHARMM General Force Field to Sulfonyl-Containing Compounds and its Utility in Biomolecular Simulations. *J. Comput. Chem.* **2012,** *33*, 2451-2468.

(8) Halgren, T. A. Merck Molecular Force Field. II. MMFF94 van der Waals and Electrostatic Parameters for Intermolecular Interactions. *J. Comput. Chem.***1996,** *17*, 520-552.

(9) Halgren, T. A. Merck Molecular Force Field. III. Molecular Geometries and Vibrational Frequencies for MMFF94. *J. Comput. Chem.* **1996,** *17*, 553-586.

(10) Halgren, T. A.; Nachbar, R. B. Merck Molecular Force Field. IV. Conformational Energies and Geometries for MMFF94. *J. Comput. Chem.***1996,** *17*, 587-615.

(11) Chai, J.-D.; Head-Gordon, M. Long-Range Corrected Hybrid Density Functionals with Damped Atom–Atom Dispersion Corrections. *Phys. Chem. Chem.Phys.* **2008,** *10*, 6615-6620.

(12) Iyer, S.; Lopez-Hilfiker, F.; Lee, B. H.; Thornton, J. A.; Kurtén, T. Modeling the Detection of Organic and Inorganic Compounds Using Iodide-Based Chemical Ionization. *J. Phys. Chem. A* **2016,** *120*, 576-587.

(13) Kendall, R. A.; Dunning, T. H.; Harrison, R. J. Electron Affinities of the First-Row Atoms Revisited. Systematic Basis Sets and Wave Functions. *J. Chem. Phys.* **1992,** *96*, 6796-6806.

(14) Dunning, T. H. Gaussian Basis Sets for Use in Correlated Molecular Calculations. I. The Atoms Boron through Neon and Hydrogen. *J. Chem. Phys.* **1989,** *90*, 1007-1023.

(15) Feller, D. The Role of Databases in Support of Computational Chemistry Calculations. *J. Comput. Chem.* **1996,** *17*, 1571-1586.

(16) Zhang, J.; Dolg, M. ABCluster: the Artificial Bee Colony Algorithm for Cluster Global Optimization. *Phys. Chem. Chem.Phys.* **2015,** *17*, 24173-24181.

(17) Weigend, F.; Ahlrichs, R. Balanced Basis Sets of Split Valence, Triple Zeta Valence and Quadruple Zeta Valence Quality for H to Rn: Design and Assessment of Accuracy. *Phys. Chem. Chem.Phys.* **2005,** *7*, 3297-3305.
(18) Larriba, C.; Hogan, C. J. Ion Mobilities in Diatomic Gases: Measurement versus Prediction with Non-Specular Scattering Models. *J. Phys. Chem. A* **2013,** *117*, 3887-3901.
(19) Larriba, C.; Hogan, C. J. Free Molecular Collision Cross Section Calculation Methods for Nanoparticles and Complex Ions with Energy Accommodation. *J. Comput. Phys.* **2013,** *251*, 344-363.
(20) Mason, E. A.; McDaniel, E. W. *Transport Properties of Ions in Gases*. Wiley: New York, 1988.